

UNCLASSIFIED

AD NUMBER
ADB281574
NEW LIMITATION CHANGE
TO Approved for public release, distribution unlimited
FROM Distribution authorized to U.S. Gov't. agencies only; Proprietary Info.; Oct 2001. Other requests shall be referred to US Army Medical Research and Materiel Comd., 504 Scott St., Fort Detrick, MD 21702-5012.
AUTHORITY
USAMRMC Ltr, 30 Sep 2002

THIS PAGE IS UNCLASSIFIED

AD _____

Award Number: DAMD17-98-1-8186

TITLE: Measurements of Breast Tissue Optical Properties

PRINCIPAL INVESTIGATOR: Albert Cerussi, Ph.D.

CONTRACTING ORGANIZATION: University of California
Irvine, California 92697-1875

REPORT DATE: October 2001

TYPE OF REPORT: Annual Summary

PREPARED FOR: U.S. Army Medical Research and Materiel Command
Fort Detrick, Maryland 21702-5012

DISTRIBUTION STATEMENT: Distribution authorized to U.S. Government agencies only (proprietary information, Oct 01). Other requests for this document shall be referred to U.S. Army Medical Research and Materiel Command, 504 Scott Street, Fort Detrick, Maryland 21702-5012.

The views, opinions and/or findings contained in this report are those of the author(s) and should not be construed as an official Department of the Army position, policy or decision unless so designated by other documentation.

20020814 203

NOTICE

USING GOVERNMENT DRAWINGS, SPECIFICATIONS, OR OTHER DATA INCLUDED IN THIS DOCUMENT FOR ANY PURPOSE OTHER THAN GOVERNMENT PROCUREMENT DOES NOT IN ANY WAY OBLIGATE THE U.S. GOVERNMENT. THE FACT THAT THE GOVERNMENT FORMULATED OR SUPPLIED THE DRAWINGS, SPECIFICATIONS, OR OTHER DATA DOES NOT LICENSE THE HOLDER OR ANY OTHER PERSON OR CORPORATION; OR CONVEY ANY RIGHTS OR PERMISSION TO MANUFACTURE, USE, OR SELL ANY PATENTED INVENTION THAT MAY RELATE TO THEM.

LIMITED RIGHTS LEGEND

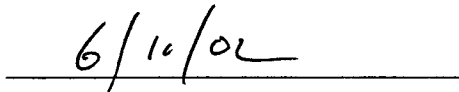
Award Number: DAMD17-98-1-8186

Organization: University of California, Irvine

Those portions of the technical data contained in this report marked as limited rights data shall not, without the written permission of the above contractor, be (a) released or disclosed outside the government, (b) used by the Government for manufacture or, in the case of computer software documentation, for preparing the same or similar computer software, or (c) used by a party other than the Government, except that the Government may release or disclose technical data to persons outside the Government, or permit the use of technical data by such persons, if (i) such release, disclosure, or use is necessary for emergency repair or overhaul or (ii) is a release or disclosure of technical data (other than detailed manufacturing or process data) to, or use of such data by, a foreign government that is in the interest of the Government and is required for evaluational or informational purposes, provided in either case that such release, disclosure or use is made subject to a prohibition that the person to whom the data is released or disclosed may not further use, release or disclose such data, and the contractor or subcontractor or subcontractor asserting the restriction is notified of such release, disclosure or use. This legend, together with the indications of the portions of this data which are subject to such limitations, shall be included on any reproduction hereof which includes any part of the portions subject to such limitations.

THIS TECHNICAL REPORT HAS BEEN REVIEWED AND IS APPROVED FOR PUBLICATION.





REPORT DOCUMENTATION PAGEForm Approved
OMB No. 074-0188

Public reporting burden for this collection of information is estimated to average 1 hour per response, including the time for reviewing instructions, searching existing data sources, gathering and maintaining the data needed, and completing and reviewing this collection of information. Send comments regarding this burden estimate or any other aspect of this collection of information, including suggestions for reducing this burden to Washington Headquarters Services, Directorate for Information Operations and Reports, 1215 Jefferson Davis Highway, Suite 1204, Arlington, VA 22202-4302, and to the Office of Management and Budget, Paperwork Reduction Project (0704-0188), Washington, DC 20503

1. AGENCY USE ONLY (Leave blank)		2. REPORT DATE October 2001	3. REPORT TYPE AND DATES COVERED Annual Summary (30 Sep 98 - 29 Sep 01)	
4. TITLE AND SUBTITLE Measurements of Breast Tissue Optical Properties			5. FUNDING NUMBERS DAMD17-98-1-8186	
6. AUTHOR(S) Albert Cerussi, Ph.D.				
7. PERFORMING ORGANIZATION NAME(S) AND ADDRESS(ES) University of California Irvine, California 92697-1875 E-mail: acerussi@bli.uci.edu			8. PERFORMING ORGANIZATION REPORT NUMBER	
9. SPONSORING / MONITORING AGENCY NAME(S) AND ADDRESS(ES) U.S. Army Medical Research and Materiel Command Fort Detrick, Maryland 21702-5012			10. SPONSORING / MONITORING AGENCY REPORT NUMBER	
11. SUPPLEMENTARY NOTES				
12a. DISTRIBUTION / AVAILABILITY STATEMENT Distribution authorized to U.S. Government agencies only (proprietary information, Oct 01). Other requests for this document shall be referred to U.S. Army Medical Research and Materiel Command, 504 Scott Street, Fort Detrick, Maryland 21702-5012.				12b. DISTRIBUTION CODE
13. ABSTRACT (Maximum 200 Words) Near-infrared (NIR) optical spectroscopy demonstrates unique possibilities for non-invasively monitoring tissue physiology. A bedside-capable instrument using low levels of non-ionizing near-infrared light measured both absorption and scattering properties of tissues. A diffusive model quantified oxygenated and deoxygenated hemoglobin, water, and lipid by their absorption signatures. Cellular density, fat, and collagen content were inferred from measured light-scattering spectra. This quantitative functional information cannot be obtained with other non-invasive radiological techniques. Measurements revealed physiological breast changes consistent with age-dependent histological alterations in over 30 healthy female volunteers. Measurements of several cancer patients demonstrated significant changes in tumor water and hemoglobin saturation values relative to normal tissue. A detailed measurement demonstrated water, hemoglobin saturation, and hemoglobin concentration changes in a breast tumor in direct response to chemotherapy, demonstrating a direct non-invasive measure of tumor angiogenesis. After 3 cycles of chemotherapy, the final tumor was not palpable (5 mm size) but detectible using our technique. Potential applications based upon these findings include monitoring the effectiveness of treatments affecting breast composition (i.e., hormone replacement and chemotherapy), tumor characterization, and evaluating physiologic changes affecting breast cancer risk. The prototype instrument is comparable in cost to commercialized ultrasound.				
14. SUBJECT TERMS Breast Cancer			15. NUMBER OF PAGES 58	
			16. PRICE CODE	
17. SECURITY CLASSIFICATION OF REPORT Unclassified	18. SECURITY CLASSIFICATION OF THIS PAGE Unclassified	19. SECURITY CLASSIFICATION OF ABSTRACT Unclassified	20. LIMITATION OF ABSTRACT Unlimited	

NSN 7540-01-280-5500

Standard Form 298 (Rev. 2-89)
Prescribed by ANSI Std. Z39-18
298-102

Table of Contents

Cover.....	
SF 298.....	2
I. Introduction.....	4
II. Body.....	4
II.a Items in the Original Specific Aims.....	4
II.b Progress on Statement of Work.....	4
III. Progress Summaries.....	5
III.a Clinical Summary.....	5
III.b Instrumentation Summary.....	7
III.c Protocol Design/ Clinical Exposure Summary.....	7
III.d Clinical Collaboration.....	7
III.e Student Supervision.....	8
IV Conclusions.....	8
V. Appendix.....	8
V.a Reportable Outcomes: Peer-Reviewed Publications.....	8
V.b Reportable Outcomes: Non-Peer-Reviewed Publications.....	9
V.c Reportable Outcomes: Conferences.....	9
V.d Reportable Outcomes: Additional Support.....	9
Enclosures:	
Attached publications (5)	
Human Subjects List	

I. INTRODUCTION

Near-infrared light offers unique possibilities for detecting physiological information from deep within biological tissues without injections, surgery, dangerous radiation, or great expense. Although it has been known for some time that non-ionizing near-infrared (NIR) light penetrates a few centimeters into biological tissues, recent modeling advances have promised hope for clinical applications. NIR light provides the concentrations and oxygenation state of hemoglobin, as well as the scattering properties of the tissue and thus provide criteria to characterize breast lesions *in vivo*. Optically monitoring physiological changes in breast tissue provides a new way to look at both disease progression and prevention. Our prototype NIR instrument has observed changes in tissue physiology that are characteristic of disease progression and treatment. We have also observed changes in breast tissue physiology resulting from hormone replacement therapy, menopausal status, menstrual cycle stage and chemotherapeutic intervention. Because our technique is safe, non-invasive and comparable in cost to ultrasound, patients can be studied as often as necessary without risk.

II. BODY

II.a Items in the Original Specific Aims

The original specific aims of this project are:

- (1) *Optimize* the instrumentation and theory currently used to extract the absolute optical absorption and reduced scattering parameters.
- (2) *Perform clinical measurements* of breast tissue optical properties in order to determine exact absorption and scattering factors in different tissue regions.
- (3) *Compare* optical property measurements to gross pathology, histopathology, ultrasound, and mammography results in order to determine absorption and scattering factors characteristic of tumor and normal tissue.

Items, 1 & 2 have been given sufficient attention to warrant several publications over the cycle of this grant. The third item is being written in another publication as a detailed case report describing the monitoring of chemotherapy in a breast tumor.

II.b Progress on Statement of Work

Below I list progress on each of the items listed in the 3-year statement of work as originally described by Dr. Joshua Fishkin (page 10 of original proposal). After taking over his original grant in 1999, new opportunities arose that allowed me to place a greater emphasis on clinical measurements as opposed to developing more sophisticated computational models. Given the scarcity of clinical data available, I elected to pursue this option at the expense of the computational options.

- 1.a *Selection and addition of new laser diodes, modification of instrument software.* completed. We have constructed 2 more instruments that feature 10 laser diodes

(upgraded from 4). The new systems also feature a method providing continuous coverage from 650 to 1000 nm (Paper #4). The instrument software has been completely re-written to include these new features.

- 1.b *Clinical measurements: completed*. Initial clinical studies were conducted at BLI. Only non-invasive measurements were performed (see clinical summary).
- 1.c *Accuracy studies of one and two chromophores systems: completed*. The FDPM technique reproduced the absorption and scattering properties of a tissue-like water-based phantom. For higher absorption phantoms, the FDPM technique was less accurate. However, the SFDPM technique (Paper #4) greatly enhanced our accuracy, and reduced errors from instrument calibration.
- 1.d *Spherical & cylindrical phantom studies: not completed*. Constructing solid phantoms proved difficult. A company (Medlite) was contracted to construct these phantoms.
- 2.a *Clinical measurements: completed*. See clinical summary for details.
- 2.b *Studies with inhomogeneous phantoms: completed*. In order to assess the accuracy of the physiological measurements, I elected to compare my measurements against known normal breast physiology (as opposed to tissue phantoms). This comparison is more useful than phantom studies because a phantom can never reproduce exact human physiological conditions (see clinical summary).
- 2.c *Accuracy study of 3 & 4 chromophore systems: completed*. Using the SSFDPM technique, we reproduced the spectra of a 4 chromophore system. Details of this work were reported (Paper #4).
- 3a. *Construction of tissue simulating phantoms: not completed*. Heterogeneous phantoms were not constructed (see 1.d).
- 3b. *Clinical measurements: completed*. A clinical system now resides permanently at UCIMC. Our clinical systems have been used in normal, cancer, and chemotherapeutic monitoring studies. Results of these measurements have been the subject of three peer-reviewed papers (paper #1-3), with more planned. The results of these measurements have shown that the FDPM technique can measure subtle physiological changes in the breast that are indicative of disease and recovery from disease.

III. PROGRESS SUMMARIES

III.a Clinical Summary

I have quantified the concentrations of blood, water, fat and scattering in the breasts of over 35 healthy volunteers. The addition of fat and the spectral scattering dependence has provided some unique insights into breast physiology. Current data have demonstrated :

- NIR absorption and scattering in the pre-menopausal breast is significantly higher than in the post-menopausal breast (Paper #3, Figures 2 & 3).
- Blood and water decreases as age increases (Paper #3, Figures 4& 5).
- There is a general increase in lipids as age increases (Paper #1, Figure 4).
- Increased scattering in the pre-menopausal breast is likely due to higher collagen density and lower amounts of fat (the components of mammographic density) (Paper #1, Figure 6).
- Measurements of tissue scattering spectra and lipids correlate with expected breast composition from body-mass-index (Paper #1, Figures 5 & 6).
- Hemoglobin saturation (S_tO_2) measurements of pre-menopausal women are statistically lower than those of post-menopausal women. Post-menopausal women on hormone replacement therapy (HRT) show S_tO_2 values closer to the pre-menopausal breast than the post-menopausal breast. (The S_tO_2 measures of the arterial and venous hemoglobin saturation in tissue) (Paper #3, Table 2).
- Optical assessment of tissue physiology is sensitive to menstrual cycle (Paper #2, Table 1).

All of the findings are not surprising, but until now, none of these compositional breast properties of the tissue could be measured non-invasively in a safe manner. *These measurements provided a control to which we could compare our measurements against known physiology.* At present, they represent the *most complete set of data available* on the NIR optical properties of breast tissue. The normal subjects provided a continuous stream of patients from which we drew considerable clinical experience. Detailed studies of cancer patients did not commence until early 2001 when the new instrument arrived at the UCI medical center. I will now discuss the results of several exciting measurements performed on diseased patients.

One published measurement clearly demonstrates our ability to measure important physiological changes brought on by the progression of disease (Paper #1, Figures 11,12, &13). Measurements of a fibroadenoma show significant increases in water (Figure 11) and hemoglobin (Figure 12). Traditional optical measures of tumors have relied on only relative measurements (i.e., S_tO_2), which was slightly lower in the fibroadenoma (Figure 13). These increases in water and hemoglobin have also been seen in 3 cancer patients (unpublished data). Interestingly, the S_tO_2 was significantly lower in tumors vs. normal compared to benign lesions vs. normal (unpublished results). The small number of subjects involved does not provide enough statistical power to claim this will always be the case, but produces a physiological basis on which to proceed for continued studies.

Monitors of therapeutic intervention are of significant interest to the medical community. We have measured what is believed to be the first optical measurement of the effects of chemotherapy in a human subject (to be published). Our results demonstrate :

- For a responder, tumor water and hemoglobin concentrations *decreased significantly* over the course of the first chemotherapy cycle, and in subsequent cycles as well.
- For a responder, normal tissue hemoglobin concentrations also *decreased* to a lesser degree over the course of therapy. Independent measurements of hematocrit (part of patient's clinical treatment, and not our trial) also decreased.
- For a responder, fat increased and tumor oxygen metabolism (S_tO_2) decreased over the course of therapy, indicating *decreases in angiogenic activity of the tumor*.
- The final lesion prior to surgery was not palpable but was detectible by our optical method.
- Measurements on a non-responder showed *no significant changes* in water or hemoglobin.

These preliminary measurements suggest that it may be possible to monitor the effectiveness of chemotherapy using a non-invasive technique. Most importantly, it is clear that our technique was measuring changes in tumor angiogenesis resulting from chemotherapy.

III.b Instrumentation Summary

Two technical improvements have forwarded the achievement of the initial specific aims. We have incorporated a steady-state spectrometer into the FDPM instrument. The application of a simple model then transforms a seven-wavelength instrument to a hundreds of wavelengths instrument. The spectrometer added previously unimaginable precision in determining the physiological makeup of tissues.

I have also completed a second FDPM instrument that resides in the Breast Center at the Chao Comprehensive Cancer Center. This instrument represents significant technical advances, including higher spectral content and faster measurement times. This new system was used in the chemotherapy measurements listed above and has generated physician interest in the project. The success of this instrument led us to complete a third system.

III.c Protocol Design/ Clinical Exposure Summary

I have designed and managed two UCI research protocols (#95-563 & #99-2183). I have added some modifications to these protocols have helped us gain further insight into the optics of breast tissue. No difficulties or complications have occurred during the course of these trials. Exposure to this aspect of clinical research has taught me how to work with review committees and how to design and implement clinical research protocols, thus improving my translational research skills.

III.d Clinical Collaboration

The close connection between basic and clinical research was one of the primary reasons for coming to the Beckman Laser Institute. Interactions with clinicians at UCI have been very fruitful. My primary physician collaborators have been Drs. John Butler and David Hsiang, both

surgical oncologists. Both physicians have recruited cancer patients and provided important medical insight into our analysis. In addition, our work has enabled collaboration with physicians at other universities (see IV.d). Their interest in research has proven invaluable to my development as a breast cancer researcher.

III.e Student Supervision

I have also benefited from working with Dr. Tromberg's students. I have been partially responsible for training and guiding them in their studies of biomedical optics. Ryan Lanning has contributed to the project by helping construct and refine instrumentation used in our breast studies, and has now graduated and gone on to Harvard Medical School. Natasha Shah has been very important in performing clinical measurements. She has graduated with a Master's in chemistry, and is now a staff researcher in Dr. Tromberg's lab. Dorota Jakubowski, an MD/PhD student, has been instrumental as a programmer, and has done a significant amount of work in the chemotherapy measurements listed above.

IV CONCLUSIONS

Two carefully-designed experiments demonstrated that the FDPM technique measures functionally relevant physiological changes in breast tissue. One experiment on normal women demonstrated that NIR-derived physiology correlates nicely with known histology. The other measurement succeeded in monitoring changes in tumor angiogenesis. Both measurements were performed non-invasively. These results now form a foundation upon which we will further refine the technique and push focused translational research applications into clinical practice.

V. APPENDIX

V.a Reportable Outcomes: Peer-Reviewed Publications

- [1] A. E. Cerussi, D. Jakubowski, N. Shah, F. Bevilacqua, R. Lanning, A. J. Berger, D. Hsiang, J. Butler, R. F. Holcombe, and B. J. Tromberg, "Spectroscopy enhances the information content of optical mammography," *Journal of Biomedical Optics*, accepted for publication.
- [2] N. Shah, A. Cerussi, C. Eker, J. Espinoza, J. Butler, J. Fishkin, R. Hornung, and B. Tromberg, "Non-Invasive functional optical spectroscopy of human breast tissue," *Proceedings of the National Academy of Sciences* **98**(8) 4420-4425 (2001).
- [3] A. E. Cerussi, A. J. Berger, F. Bevilacqua, N. Shah, D. Jakubowski, J. Butler, R. F. Holcombe, and B. J. Tromberg, "Sources of absorption and scattering contrast for non-invasive optical mammography," *Academic Radiology*, **8**, 211-218 (2001).
- [4] F. Bevilacqua, A. Berger, A. Cerussi, D. Jakubowski, and B. Tromberg, "Broadband absorption spectroscopy in turbid media by combining frequency-domain and steady-state methods," *Applied Optics*, **39**, 6498-6507 (2000).
- [5] B. J. Tromberg, N. Shah, R. Lanning, A. Cerussi, J. Espinoza, T. Pham, L. Svaasand, J. Butler, 'Non-Invasive in vivo characterization of breast tumors using photon migration spectroscopy,' *Neoplasia* **2**, 1-15 (2000).

V.b Reportable Outcomes: Non-Peer-Reviewed Publications

- [1] A. E. Cerussi, F. Bevilacqua, N. Shah, D. Jakubowski, A. J. Berger, R. Lanning, and B. J. Tromberg "The Effects of water and lipids on NIR optical breast measurements, " *Proceedings of SPIE* **4250**, 419-428 (2001).
- [2] A. J. Berger, F. Bevilacqua, D. B. Jakubowski, A. E. Cerussi, J. Butler, D. Hsiang, and B. J. Tromberg, "Broadband absorption spectroscopy by combining frequency-domain and steady-state techniques," *Proceedings of SPIE* **4250**, 437-442 (2001).

V.c Reportable Outcomes: Conferences

- [1] A. E. Cerussi, F. Bevilacqua, N. Shah, D. Jakubowski, A. J. Berger, R. Lanning, and B. J. Tromberg "The Effects of water and lipids on NIR optical breast measurements, " *BiOS 2000, International Society for Optical Engineering*, Optical Tomography and Spectroscopy of Tissue: Theory, Instrumentation, Model, and Human Studies, San Jose, CA, Presentation 4250-72 (January 2001).
- [2] A. E. Cerussi, A. J. Berger, F. Bevilacqua, D. Jakubowski, N. Shah, and B. J. Tromberg, "Non-Invasive quantification of breast tissue physiology; Optical measurements of blood, water, and lipids," Biomedical Engineering Society 2000 Meeting, Seattle, WA, Presentation 14794, (October 2000).
- [3] A. E. Cerussi, A. J. Berger, F. Bevilacqua, N. Shah, D. Jakubowski, J. Butler, R. F. Holcombe, and B. J. Tromberg, "Quantitative non-invasive optical spectroscopy of breast tissue physiology," Optical Imaging Workshop: From Bench to Bedside at the NIH, Bethesda, MD, P-23, (September 2000).
- [4] A. E. Cerussi, N. Shah, A. J. Berger, D. Jakubowski, J. B. Fishkin, J. Butler, and B. J. Tromberg, "Quantitative near-infrared spectroscopy of normal and cancerous breast tissue: uses in detection and prevention," DOD Breast Cancer Research Program: Era of Hope, Atlanta, GA, E-14 (June 2000).

V.d Reportable Outcomes: Additional Support

- We have received funding based upon this work from the California Breast Cancer Research Program, a 3 year, \$500,000 collaborative effort with Dr. Laura Esserman at University of California at San Francisco.
- The Chao Comprehensive Cancer Center has also received a gift from Avon for being a cancer center for excellence. From this gift, \$250,000 was appropriated to the optical breast cancer detection program because of our contributions to the field.

Sources of Absorption and Scattering Contrast for Near-Infrared Optical Mammography¹

Albert E. Cerussi, PhD, Andrew J. Berger, PhD,² Frederic Bevilacqua, PhD, Natasha Shah, BS, Dorota Jakubowski, MS
John Butler, MD, Randall F. Holcombe, MD, Bruce J. Tromberg, PhD

Rationale and Objectives. Near-infrared (NIR) diffuse optical spectroscopy and imaging may enhance existing technologies for breast cancer screening, diagnosis, and treatment. NIR techniques are based on sensitive, quantitative measurements of functional contrast between healthy and diseased tissue. In this study, the authors quantified the origins of this contrast in healthy breasts.

Materials and Methods. A seven-wavelength frequency-domain photon migration probe was used to perform noninvasive NIR measurements in the breasts of 28 healthy women, both pre- and postmenopausal, aged 18–64 years. A diffusive model of light transport quantified oxygenated and deoxygenated hemoglobin, water, and lipid by their absorption signatures. Changes in the measured light-scattering spectra were quantified by means of a “scatter power” parameter.

Results. Substantial quantitative differences were observed in both absorption and scattering spectra of breast as a function of subject age. These physiologic changes were consistent with long-term hormone-dependent transformations that occur in breast. Instrument response was not adversely affected by subject age or menopausal status.

Conclusion. These measurements provide new insight into endogenous optical absorption and scattering contrast mechanisms and have important implications for the development of optical mammography. NIR spectroscopy yields quantitative functional information that cannot be obtained with other noninvasive radiologic techniques.

Key Words. Breast, parenchymal pattern; breast radiography, technology; optical imaging.

This article describes the application of a new class of near-infrared (NIR) spectroscopy tools for noninvasive, quantitative characterization of breast tissue physiology.

Acad Radiol 2001; 8:211–218

¹ From the Beckman Laser Institute and Medical Clinic, University of California, Irvine, 1002 Health Sciences Rd, Irvine, CA 92612 (A.E.C., A.J.B., F.B., N.S., D.J., B.J.T.); and the Department of Oncological Surgery (J.B.) and the Division of Hematology/Oncology (R.F.H.), University of California, Irvine Medical Center, Orange, Calif. Received November 2, 2000; revision requested November 11; revision received and accepted November 16. Supported by grants and gifts from the National Institutes of Health (NIH) Laser Microbeam and Medical Program (RR-01192), the NIH (R29-GM50958), the Department of Energy (DOE DE-FG03-91ER61227), the Office of Naval Research (ONR N00014-91-C-0134), the California Breast Cancer Research Program, Avon, the U.S. Army Medical Research and Material Command (DAMD17-98-1-8186) (A.E.C.), the George E. Hewitt Foundation (A.J.B.), and the Swiss National Science Foundation (F.B.). **Address correspondence to B.J.T.**

² Current address: Institute of Optics, University of Rochester, NY.

© AUR, 2001

Diagnostic methods currently in use, such as mammography, magnetic resonance imaging, and ultrasound (US), offer excellent anatomic lesion-detection capabilities but generally cannot provide quantitative information regarding tissue function and composition (1). Positron emission tomography shows great promise in evaluating the metabolic demands of tissue but requires exogenous radionuclides and is insensitive to tissue hemodynamics. NIR optical spectroscopy is intrinsically sensitive to the principal components of breast: blood, water, and adipose, as well as epithelial and connective tissues. Results of preliminary studies suggest that the fractional contribution of each component to NIR signals depends strongly on factors such as age, menopausal status, and the progression of disease. Thus, NIR optical spectroscopy provides an opportunity for revealing physiologic information that cannot otherwise be obtained noninvasively.

As optical diagnostic methods become more clinically applicable, there is a growing need to identify and quantify sources of endogenous contrast in breast (2–11). This article presents the results of quantitative NIR spectroscopic studies in 28 subjects ranging in age from 18 to 64 years. We provide evidence that NIR tissue spectroscopy is inherently sensitive to long-term age and hormone-dependent dynamics. Similar studies have been initiated (12–14) but in only a few subjects or with limited sensitivity to physiologic parameters. These data are expected to play an important role in characterizing the sensitivity of NIR optical spectroscopy and imaging for applications such as tumor detection, therapeutic monitoring, and risk assessment.

NIR photons (600–1,000 nm) are nonionizing and weakly absorbed by tissue. Many investigators have used them to explore brain, breast, and muscle tissue, exploiting their enhanced penetrance relative to that of visible or ultraviolet radiation (1). In breast tissue, the principal NIR absorbers are assumed to be reduced hemoglobin (Hb-R), oxygenated hemoglobin (Hb-O₂), water (H₂O), and lipids (15). NIR tissue spectroscopy offers a safe way to quantify these components and to view unique functional information with low-cost “point-of-care” devices. Multiple light scattering complicates quantitative measurements of light absorption in the NIR range. The process of using frequency-domain photon migration (FDPM) techniques to separate the effects of absorption from scattering has been described in detail (16,17). FDPM enables the use of quantitative spectroscopic analysis tools to determine the composition and structure of tissue noninvasively (18).

The application of FDPM techniques to NIR tissue spectroscopy differs substantially from conventional bulk NIR methods, such as diaphanography (19). FDPM employs computational models that allow the quantitative separation of the effects of absorption and scattering (20). Thus, within the limits of applicability of the light transport models to the breast, all parameters measured in this study are absolute values.

MATERIALS AND METHODS

Patient Selection

All volunteers enrolled in this study competently provided informed consent to participate in one of two trials (nos. 95-563 and 99-2183) under the guidelines of an Institutional Review Board. The 28 women ranged in age from 18 to 64 years. Fifteen of them were premenopausal (average age, 28 years \pm 9), and seven were postmenopausal

(average age, 56 years \pm 2). The remaining six women (average age, 56 years \pm 5) were taking some form of hormone replacement therapy (HRT); three of the six classified themselves as perimenopausal. None of the women had any known cancerous lesions or other known forms of breast disease.

Measurement Technique

Each subject rested in a supine position during the measurement. The instrument probe, slightly larger than a US probe (Fig 1), was the only item placed in contact with the subject. It consisted of a sealed APD module and an optical fiber placed 22 mm from the APD. All measurements were performed in a reflection-style geometry. The probe was placed on the breast with minimal pressure and only the force of gravity; no compression was used. In this configuration, we estimate that the mean sampling depth was approximately 1 cm below the skin. We report data only on measurements performed in the center of the left upper outer quadrant (measurements on the right upper quadrant yielded similar results). Error bars in the figures and tables represent the standard deviations (SDs) of repeated measurements.

Instruments

A schematic of our 1-GHz, portable FDPM device is shown in Figure 1. This FDPM instrument has been described in detail elsewhere (21). It employs multiple diode lasers that provide visible and NIR light at seven wavelengths (672, 800, 806, 852, 896, 913, and 978 nm). A hand-held probe has been designed to house an APD that records the modulated diffuse light signals after propagation through the tissue. This probe has a plastic attachment on the casing to position a source optical fiber a fixed distance from the APD. A 100- μ m-diameter graded index optical fiber positioned 22 mm from the APD detector was used to deliver the diode laser outputs to the tissue surface. A network analyzer (8753c; Agilent, Palo Alto, Calif), measured the phase and amplitude of the detected electronic signal from the APD over a range of source modulation frequencies. A steady-state current source was mixed with radiofrequency power provided by the network analyzer in a bias network. This bias network serially distributed power to each laser diode and produced intensity-modulated light. An optical switch delivered light serially from each diode to the tissue via the single optical fiber described above. The optical power-launched into the tissue ranged from 5 to 25 mW for each wavelength.

A sweep over all seven wavelengths took approximately 35–60 seconds. The system acquired data in less than 3 sec-

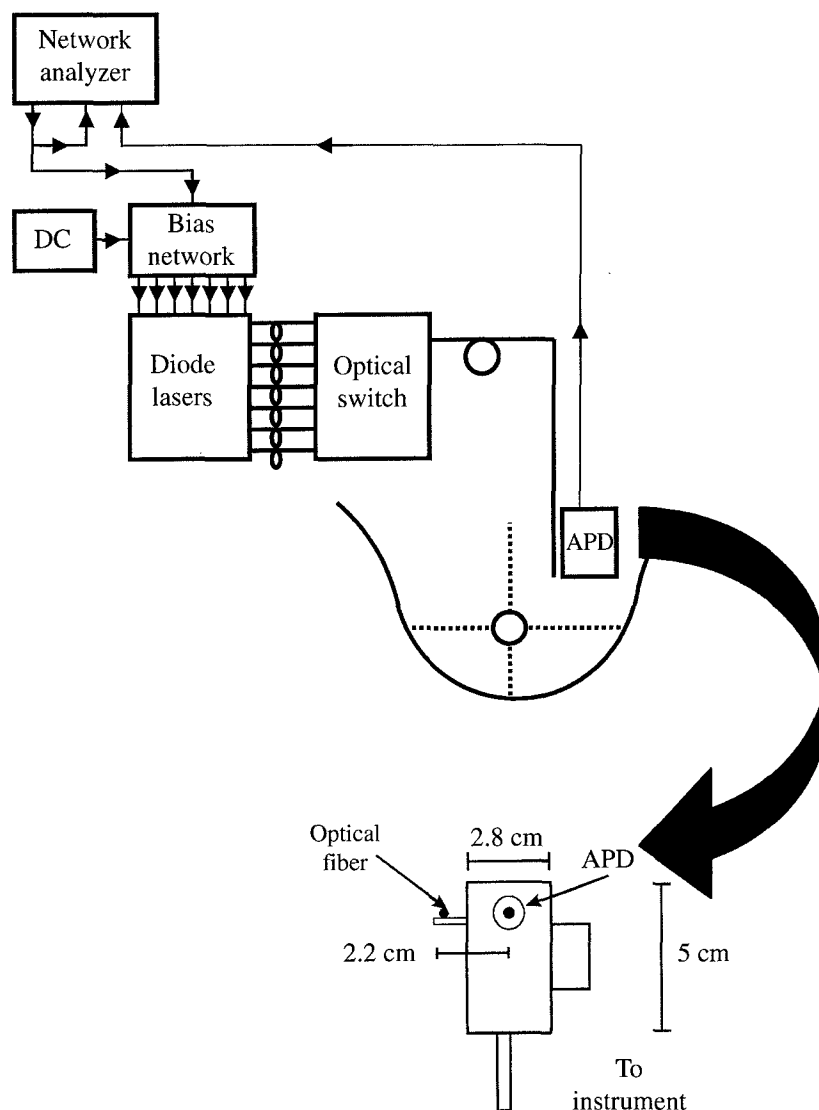


Figure 1. Schematic drawing of FDPM instrument, hand-held probe, and measurement map. The components of the instrument are the diode lasers, avalanche photodiode (APD), network analyzer, steady-state current source (DC), bias network, and optical switch. Measurements were performed with a hand-held probe (close-up at bottom of Figure) that contained the APD and a source optical fiber. The measurement location was in the center of the left upper outer quadrant of the breast, as indicated.

onds per wavelength, with a 2-second delay between each laser diode in the system because of switching considerations. The system was wheeled into a medical clinic for each measurement. Instrumental artifacts were removed by means of calibration on a tissue-simulating phantom with known absorption and scattering properties.

Measured Parameters and Data Analysis

The amplitude and phase of a NIR diffusive light wave demodulates and retards, respectively, as the wave propa-

gates through multiple-scattering media such as tissue. The real and imaginary parts of this diffuse wave were fit simultaneously to a light-diffusion model (the P_1 approximation to the Boltzmann transport equation) (22,23) by minimizing the χ^2 surface with a Marquardt-Levenberg algorithm. This fit determined the absolute optical absorption coefficient μ_a and the absolute optical reduced scattering coefficient μ'_s at each wavelength. Typical μ_a and μ'_s uncertainties, determined from the χ^2 distribution of the fits, are 3% to 1% of their mean values. Precision

errors in actual tissue measurements were determined by performing multiple network analyzer sweeps and multiple probe placements on a given location and were found to be less than 10% for μ_a and 5% for μ_s' .

When the optical properties μ_s' and μ_a are recovered for the seven wavelengths, the spectral dependence of the absorption may be combined with known values of molecular extinction coefficients to calculate physiologically relevant parameters. We assume that bulk breast tissue is composed principally of four NIR absorbers: Hb-R, Hb-O₂, H₂O, and lipids. The concentrations of these absorbers (c) were quantified by solving the equation $\bar{\mu}_a = E\bar{c}$, where E is a 7×4 matrix that contains the molar extinction coefficients of the four chromophores at the seven source wavelengths (24–26).

For each measurement, we report four hemoglobin parameters: [Hb-R], [Hb-O₂], the total hemoglobin concentration (THC = [Hb-R] + [Hb-O₂]), and the tissue hemoglobin saturation ($S_{O_2} = [\text{Hb-O}_2]/\text{THC} \times 100\%$), where the characters in square brackets denote concentration in moles per liter. Values for water and lipid content are reported as percentages. The water percentage is the concentration of measured tissue water divided by the concentration of pure water (55.6 mol/L). The lipid percentage indicates the kilograms per liter of lipid measured relative to an assumed "pure" lipid density of 0.9 kg/L. Thus, the water and lipid percentages we report are relative figures of merit compared with pure solutions of the substance and are not strict volume or mass fractions.

The scattering properties of the tissue also yield important physiologic information. NIR scattering in tissue has the following dependence: $\mu_s' = A\lambda^{-SP}$, where A is a constant, λ is the wavelength (in nanometers), and SP is the scatter power. Scatter power is related to the scattering center size (d) compared with the optical wavelength. As an example, scatter power is 4 in the case of Rayleigh scattering ($d \ll \lambda$) and is approximately 1 for large Mie-like scatterers ($d \sim \lambda$).

RESULTS

Sensitivity: Pre- versus Postmenopausal Subjects

Both Figures 2 and 3 present a typical series of measurements of seven absorption and scattering coefficients, respectively. The points represent an average of several measurements in the center of the left upper outer breast quadrants in two subjects, a 32-year-old premenopausal woman and a 54-year-old postmenopausal woman. Error bars indicate the SDs of repeated measurements. There are vast absorption and scattering differences between

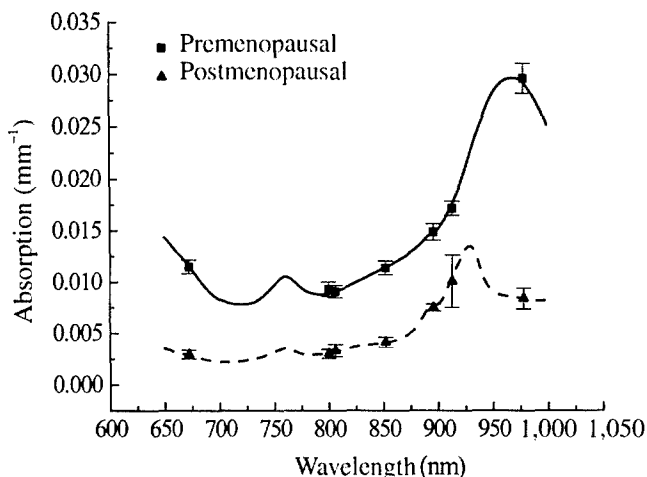


Figure 2. Measured absorption spectra for a 32-year-old premenopausal subject (■, solid line) and a 54-year-old postmenopausal subject (▲, dashed line). Points represent the average of several measurements, and lines represent a least-squares fit (extrapolated to all wavelengths) based on the assumption that breast absorption is due only to Hb-R, Hb-O₂, H₂O, and lipids. Error bars show the SDs of repeated measurements. Concentrations of chromophores from this measurement are listed in Table 1.

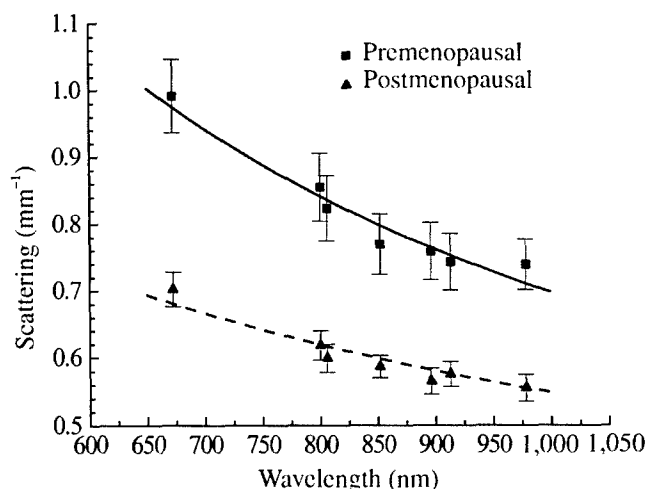


Figure 3. Measured scattering spectra for the same subjects as in Figure 2. The lines represent a fit to $\mu_s' = A\lambda^{-SP}$, where μ_s' is the reduced scattering coefficient (per millimeter), A is a constant, λ is the wavelength (in nanometers) and SP is the scatter power. Results of the fit from this measurement are listed in Table 1. Error bars show the SDs of repeated measurements.

pre- and postmenopausal breast tissue. The solid lines in Figure 2 represent a weighted least-squares fit of the seven absorption coefficients, with published extinction coefficients used for Hb-R, Hb-O₂, H₂O, and lipids (24–26). Lines between the measured points have been interpolated. The solid lines of Figure 3 represent a fit of the scattering coefficients to the equation $\mu_s' = A\lambda^{-SP}$.

Table 1
Measured Physiologic Properties in Breasts of a Premenopausal and a Postmenopausal Subject

Subject	[Hb-R] ($\mu\text{mol/L}$)	[Hb-O ₂] ($\mu\text{mol/L}$)	S _t O ₂ (%)	THC ($\mu\text{mol/L}$)	[H ₂ O]* (%)	Lipid† (%)	Scatter Power
Premenopausal	12.6 \pm 0.7	27.9 \pm 2.7	68.9 \pm 1.3	40.4 \pm 2.7	45.1 \pm 3.6	29.8 \pm 5.6	0.864 \pm 0.068
Postmenopausal	2.4 \pm 0.5	12.2 \pm 1.6	83.7 \pm 2.5	14.4 \pm 1.9	10.3 \pm 0.8	67.5 \pm 3.7	0.555 \pm 0.036

Note.—Measurements are given as individual means \pm SDs for the two subjects represented in Figures 2 and 3.

* Measured concentration relative to pure water.

† Measured mass density relative to pure lipid.

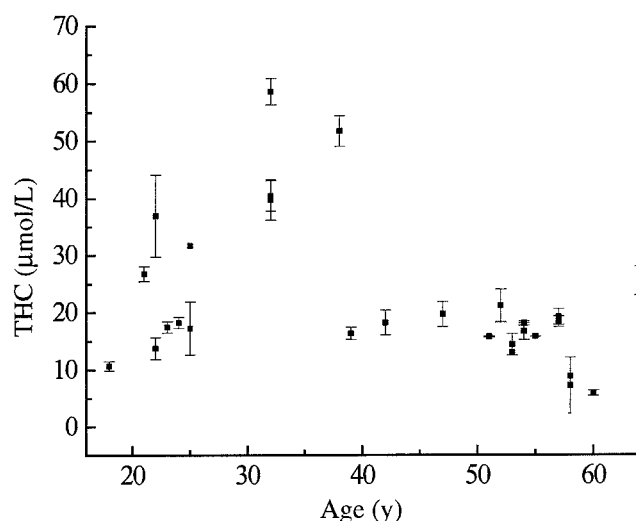


Figure 4. Plot of the THC versus subject age. Premenopausal subjects (<50 years, $n = 15$) show considerable variation with age because of intersubject variations, such as menstrual cycle variations and differences in overall hormone production. Postmenopausal subjects (>50 years, $n = 13$) appear to show a decrease in THC. Error bars show the SDs of repeated measurements.

These optical spectra provide insight into breast tissue composition. There are higher concentrations of hemoglobin (ie, both Hb-R and Hb-O₂) in the premenopausal subject, as evidenced by the overall higher absorption in the 670–850-nm range. There is also more water relative to lipids in the premenopausal subject, as revealed by the large water absorption peak at 980 nm. Recovery of the absorption spectra allows calculations of the tissue concentrations of Hb-R, Hb-O₂, H₂O, and lipids. In addition, the light scattering intensity is substantially lower in the postmenopausal breast. Table 1 summarizes the fitted physiologic properties for the two subjects represented in Figures 2 and 3.

Quantities versus Age

The next three figures present FDPM-measured quantities as a function of subject age. Figure 4 shows the

THC, Figure 5 shows the tissue water percentage (referenced to the concentration of pure water), and Figure 6 shows the scatter power. Premenopausal subjects (ie, aged younger than 50 years) display a variety of values in all three plots. This spread is the result of intersubject variations, including, but not limited to, menstrual cycle differences and gynecologic age. The THC, and to a lesser extent the water, seemed to increase in premenopausal subjects (aged 18–39 years), perhaps reaching a peak value near age 30 years. Between the ages of 40 and 49 years, the THC appears to level off, while water and scatter power seem to decline. After age 50 years (predominantly postmenopausal subjects), there is a general decrease with age in THC, water, and scatter power.

The late decrease in THC and water correlates well with previous histologic studies showing both atrophy in well-vascularized lobular tissue and an increase in the fat-to-collagen ratio after menopause (15). This decrease is consistent with compositional analysis data showing lower blood and water content for fat versus glandular tissue (27). Scatter power also declines with age after age 50 years. Compared with fat, collagen and glandular tissue scatter light with a higher intensity and a steeper spectral dependence (28). Thus, smaller scatter powers are expected in fatty tissue. Exact knowledge of the weighted biologic contributions to optical tissue scattering is a matter of debate.

Correlation between Absorption and Scattering Information

Figure 7 displays a correlation plot of the measured water and lipid percentages versus scatter power. The lipid percentage is the mass density of lipids in the tissue referenced to the mass density of soybean oil. Note that neither the water nor the lipid percentage represents a strict mass or volume fraction for the tissue (ie, not all components are normalized to 100%). Lines represent fits of water (solid line) and lipids (dashed line) as functions of scatter power.

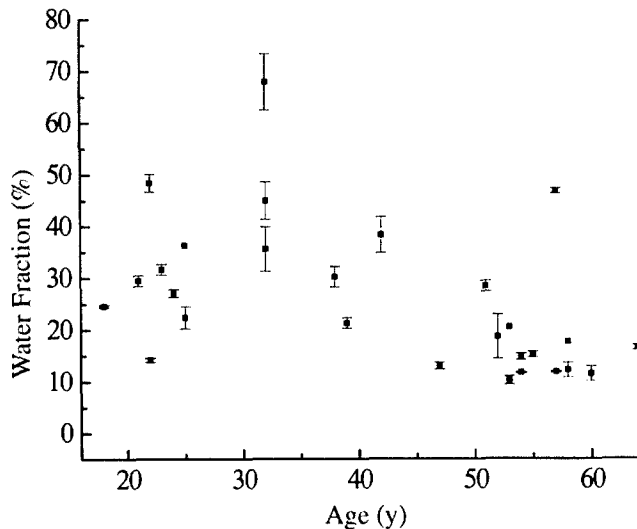


Figure 5. Plot of the measured tissue water percentage versus subject age. Premenopausal subjects show considerable variation over age because of intersubject variations such as menstrual cycle variations and differences in overall hormone production. Postmenopausal and perimenopausal subjects appear to show a decrease in water content. The percentages are water concentrations normalized to the concentration of pure water. Error bars show the SDs of repeated measurements.

Tissue scattering correlates well with the parenchymal composition measured via absorption. As scatter power increases, the lipid percentage decreases ($R^2 = -0.841$, $P < .001$) and the water percentage increases ($R^2 = +0.850$, $P < .001$). The absorption spectra of water and lipids overlap, which can lead to errors in measuring these chromophores. Figure 7, however, clearly shows that both scattering and absorption provide complementary information regarding breast composition, indicating that such errors do not substantially distort our findings.

Tissue Metabolism and Menopause

The S_tO_2 is the percentage fraction of arterial and venous Hb- O_2 that contributes to the tissue THC, and it should not be confused with arterial saturation, which is measured with pulse oximetry. Table 2 presents the measured S_tO_2 in all subjects with a body-mass index less than 40. The average S_tO_2 was approximately 76% for both the premenopausal subjects and those receiving HRT; their means were not significantly different. The S_tO_2 values for the postmenopausal women not receiving HRT, however, were significantly higher, averaging $81.9\% \pm 8.8$ ($P = .062$).

Decreases in S_tO_2 are associated with increased metabolism (ie, extraction of O_2 from the blood). Tumors, for

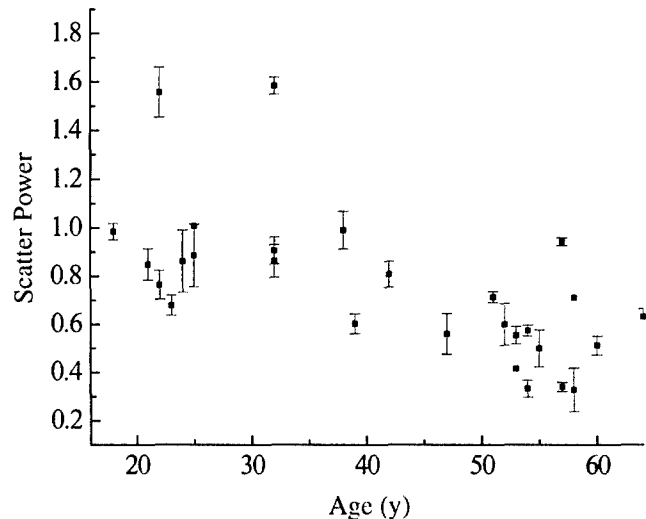


Figure 6. Plot of the measured optical scatter power (in arbitrary units) versus subject age. Optical scatter power refers to the magnitude of the slope of the scattering versus wavelength curve. Premenopausal subjects show considerably higher scatter power than postmenopausal subjects. This general pattern is the same for mammographic density. Error bars show the SDs of repeated measurements.

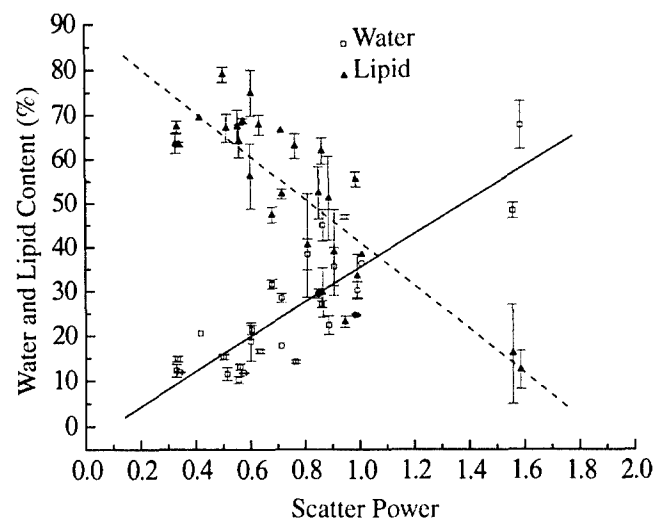


Figure 7. Correlation plots for water percentage (□, solid line) and lipid percentage (▲, dashed line) versus scatter power. Percentages are referenced to the concentration of pure water and the mass density of pure fat. Scatter power correlates with water ($R^2 = +0.850$, $P < .001$) and correlates negatively with lipids ($R^2 = -0.841$, $P < .001$). Error bars show the SDs of repeated measurements.

example, have been shown in vivo to have lower S_tO_2 values than nontumor tissue (6,18,29). The postmenopausal increase in S_tO_2 relative to the premenopausal women and those receiving HRT is plausible, because general tissue metabolism in the breast should decrease

Table 2
Comparison of S_tO_2 Measurements

Subjects	S_tO_2 (%)
Premenopausal ($n = 15$)	76.3 ± 6.4
Receiving HRT ($n = 6$)	76.9 ± 9.2
Postmenopausal ($n = 6$)	81.9 ± 8.8

Note.—Measurements are given as means \pm SDs and are provided for all subjects with a body-mass index of less than 40.

after menopause as the tissue begins to atrophy. The similarity between S_tO_2 values in premenopausal and HRT women suggests that their metabolisms are similar because of the effects of both endogenous and exogenous hormones.

DISCUSSION

Although it is difficult to validate noninvasive *in vivo* measurements directly, our initial results indicate that the sensitivity of NIR spectroscopy is a reasonable reflection of long-term hormone-controlled breast remodeling. Additional work in the field has demonstrated that short-term menstrual cycle changes are detectable with a similar NIR technique (30). Our results indirectly validate the general accuracy of NIR breast spectroscopy. This quantitative physiologic information is not obtainable with any other noninvasive radiologic method.

An important feature of NIR methods is the ability to characterize quantitatively the breast tissue of women regardless of age, hormonal status, or mammographic density. Increased mammographic density contributes to a 22% false-negative rate and a high false-positive rate (56.2% cumulative risk after 10 examinations) in women less than 50 years of age (31,32). A recent study found that routine initial mammography was not clinically advantageous for women less than 35 years of age (33). Furthermore, the use of HRT in postmenopausal women is known to increase mammographic density (34) and has been recently shown to impede the efficacy of mammographic screening (35,36). The sensitivity of NIR spectroscopy to known biologic processes suggests that optical methods may reveal important new information complementing that provided by conventional diagnostic techniques, particularly in the case of radiographically dense breast tissue.

In general, premenopausal breast tissue is more optically attenuating than postmenopausal breast tissue, in

both absorption and scattering. It is important to note that this trend, particularly in scattering, is also true for mammographic density. Radiographically dense breast tissue is due to differing amounts of fat, collagen, epithelium, and water (37). Although x rays are inherently sensitive to dense electron structures in tissue, such as microcalcifications, NIR photons are naturally sensitive to tissue constituents. Thus, NIR spectroscopy has a unique potential for quantifying the elements of breast tissue that contribute to mammographic density. This observation may be important in screening, since it may identify breast tissue at physiologic risk for malignant transformation, and the technique can be performed easily in all women.

In addition to scattering contrast, we report age-dependent variations in THC, H_2O , and lipids, as well as changes in S_tO_2 for pre- and postmenopausal subjects. Knowledge of the "normal" values of these chromophores will help in evaluating the usefulness of optical methods for detecting and characterizing lesions in the breast. Several investigators have reported a two- to fourfold THC contrast between normal and tumor structures. *In vivo* tumor S_tO_2 values are also typically lower than those of normal tissue (6,18,29). Thus, detailed studies of normal tissue are essential for determining the sensitivity required of optical instrumentation for detecting lesions in women of varying age and hormonal status. Furthermore, as baseline levels are characterized, data on an individual's absorption and scattering variations could provide important insight into disease appearance and progression. When applied to patients receiving chemotherapy and/or HRT, this information could also be used to generate feedback that would permit customized treatment planning based on individual physiologic response.

REFERENCES

- Philos Trans R Soc Lond B. 1997; vol 352.
- Alfano RR, ed. Advances in optical biopsy and optical mammography. Ann NY Acad Sci 1998; vol 838.
- Heusmann H, Kölzer J, Mitic G. Characterization of female breasts *in vivo* by time-resolved and spectroscopic measurements in near infrared spectroscopy. J Biomed Opt 1996; 1:425-434.
- Franceschini MA, Moesta KT, Fantini S, et al. Frequency-domain techniques enhance optical mammography: initial clinical results. Proc Natl Acad Sci U S A 1997; 94:6468-6473.
- Moesta KT, Fantini S, Jess H, et al. Contrast features of breast cancer in frequency-domain laser scanning mammography. J Biomed Opt 1998; 3:129-136.
- McBride TO, Pogue BW, Gerety ED, Poplack SB, Osterberg UL, Paulsen KD. Spectroscopic diffuse optical tomography for the quantitative assessment of hemoglobin concentration and oxygen saturation in breast tissue. Appl Opt 1999; 38:5480-5490.
- Grosenick D, Wabnitz H, Rinneberg HH, Moesta KT, Schlag PM. Development of a time-domain optical mammograph and first *in vivo* applications. Appl Opt 1999; 38:2927-2943.

8. Colak SB, van der Mark MB, Hooft GW 't, Hoogenraad JH, van der Linden ES, Kuipers FA. Clinical optical tomography and NIR spectroscopy for breast cancer detection. *IEEE J Sel Top Quant* 1999; 5:1143-1158.
9. Tromberg BJ, Shah N, Lanning R, et al. Non-invasive in vivo characterization of breast tumors using photon migration spectroscopy. *Neoplasia* 2000; 2:1-15.
10. Holboke MJ, Tromberg BJ, Li X, et al. Three-dimensional diffuse optical mammography with ultrasound localization in a human subject. *J Biomed Opt* 2000; 5:237-247.
11. Ntziachristos V, Yodh AG, Schnall M, Chance B. Concurrent MRI and diffuse optical tomography of breast after indocyanine green enhancement. *Proc Natl Acad Sci U S A* 2000; 97:2767-2772.
12. Suzuki K, Yamashita Y, Ohta K, Kaneko M, Yoshida M, Chance B. Quantitative measurement of optical parameters in normal breasts using time-resolved spectroscopy: in vivo results of 30 Japanese women. *J Biomed Opt* 1996; 1:330-334.
13. Quaresima V, Matcher SJ, Ferrari M. Identification and quantification of intrinsic optical contrast for near-infrared mammography. *Photochem Photobiol* 1998; 67:4-14.
14. Cubeddu R, Pifferi A, Taroni P, Torricelli A, Valentini G. Noninvasive absorption and scattering spectroscopy of bulk diffusive media: an application to the optical characterization of human breast. *Appl Phys Lett* 1999; 74:874-876.
15. Thomsen S, Tatman D. Physiological and pathological factors of human breast disease that can influence optical diagnosis. *Ann N Y Acad Sci* 1998; 838:171-193.
16. Fishkin JB, Gratton E. Propagation of photon-density waves in strongly scattering media containing an absorbing semi-infinite plane bounded by a straight edge. *J Opt Soc Am A Opt Image Sci Vision* 1993; 10:127-140.
17. Yodh A, Chance B. Spectroscopy and imaging with diffusing light. *Phys Today* 1996; 48:34-40.
18. Fishkin JB, Coquoz O, Anderson ER, Brenner M, Tromberg BJ. Frequency-domain photon migration measurements of normal and malignant tissue optical properties in a human subject. *Appl Opt* 1997; 36:10-20.
19. Cutler M. Transillumination as an aid in the diagnosis of breast lesions. *Surg Gynecol Obstet* 1929; 48:721-728.
20. Patterson MS, Chance B, Wilson BC. Time resolved reflectance and transmittance for the non-invasive measurement of tissue optical properties. *Appl Opt* 1989; 28:2331-2336.
21. Pham T, Coquoz O, Fishkin J, Anderson EA, Tromberg BJ. A broad bandwidth frequency domain instrument for quantitative tissue optical spectroscopy. *Rev Sci Instrum* 2000; 71:1-14.
22. Kaltenbach JM, Kaschke M. Frequency- and time-domain modeling of light transport in random media. In: Müller GJ, Chance B, Alfano RR, et al, eds. *Medical optical tomography: functional imaging and monitoring*, series IS11. Bellingham, Wash: Society of Photo-Optical Instrumentation Engineers, 1993; 65-86.
23. Fishkin JB, Fantini S, vandeVen MJ, Gratton E. Gigahertz photon density waves in a turbid medium: theory and experiments. *Phys Rev E* 1996; 53:2307-2319.
24. Wray S, Cope M, Delpy DT, Wyatt JS, Reynolds EO. Characterization of the near infrared absorption spectra of cytochrome aa3 and haemoglobin for the non-invasive monitoring of cerebral oxygenation. *Biochim Biophys Acta* 1988; 933:184-192.
25. Hale GM, Querry MR. Optical constants of water in the 200-nm to 200- μ m wavelength region. *Appl Opt* 1973; 12:555-563.
26. Eker C. Optical characterization of tissue for medical diagnostics. Lund, Sweden: Lund Institute of Technology, 1999.
27. Duck FA. *Physical properties of tissue*. London, England: Academic Press, 1990; 320-328.
28. Peters VG, Wyman DR, Patterson MS, Frank GL. Optical properties of normal and diseased human breast tissues in the visible and near infrared. *Phys Med Biol* 1990; 35:1317-1334.
29. Fantini S, Walker SA, Franceschini MA, Kaschke M, Schlag PM, Moesta KT. Assessment of the size, position, and optical properties of breast tumors in vivo by noninvasive optical methods. *Appl Opt* 1998; 37:1982-1989.
30. Cubeddu R, D'Andrea C, Pifferi A, Taroni P, Torricelli A, Valentini G. Effects of the menstrual cycle on the red and near-infrared optical properties of the human breast. *Photochem Photobiol* 2000; 72:383-391.
31. Kerlikowske K, Barclay J. Outcomes of modern screening mammography. *J Natl Cancer Inst Monogr* 1997; 169:105-111.
32. Elmore JG, Barton MB, Mocer VM, Polk S, Arena PJ, Fletcher SW. Ten-year risk of false positive screening mammograms and clinical breast examinations. *N Engl J Med* 1998; 338:1089-1096.
33. Hindle WH, Davis L, Wright D. Clinical value of mammography for symptomatic women 35 years of age and younger. *Am J Obstet Gynecol* 1999; 180:1484-1490.
34. Baines CJ, Dayan R. A tangled web: factors likely to affect the efficacy of screening mammography. *J Natl Cancer Inst* 1999; 91:833-838.
35. Laya MB, Larson EB, Taplin SH, White E. Effect of estrogen replacement therapy on the specificity and sensitivity of screening mammography. *J Natl Cancer Inst* 1996; 88:643-649.
36. Litherland JC, Stallard S, Hole D, Cordiner C. The effect of hormone replacement therapy on the sensitivity of screening mammograms. *Clin Radiol* 1999; 54:285-288.
37. Oza AM, Boyd NF. Mammographic parenchymal patterns: a marker of breast cancer risk. *Epidemiol Rev* 1993; 15:196-208.

Noninvasive functional optical spectroscopy of human breast tissue

Natasha Shah^{*†}, Albert Cerussi^{*}, Charlotta Eker[‡], Jenny Espinoza^{*}, John Butler[§], Joshua Fishkin^{*}, Rene Hornung^{*¶}, and Bruce Tromberg^{*¶}

^{*}Laser Microbeam and Medical Program, Beckman Laser Institute and Medical Clinic, University of California, Irvine, CA 92612; [†]Department of Chemistry, University of California, 516 Rowland Hall, Irvine, CA 92697-2025; [‡]Department of Physics, Lund Institute of Technology, P.O. Box 118, S-221 00 Lund, Sweden; [§]Department of Surgery, Division of Surgical Oncology, Chao Cancer Center, University of California, Orange, CA 92665; and [¶]Department of Obstetrics and Gynecology, University Hospital, 8091 Zurich, Switzerland

Edited by Britton Chance, University of Pennsylvania, Philadelphia, PA, and approved February 6, 2001 (received for review October 26, 2000)

Near infrared diffuse optical spectroscopy and diffuse optical imaging are promising methods that eventually may enhance or replace existing technologies for breast cancer screening and diagnosis. These techniques are based on highly sensitive, quantitative measurements of optical and functional contrast between healthy and diseased tissue. In this study, we examine whether changes in breast physiology caused by exogenous hormones, aging, and fluctuations during the menstrual cycle result in significant alterations in breast tissue optical contrast. A noninvasive quantitative diffuse optical spectroscopy technique, frequency-domain photon migration, was used. Measurements were performed on 14 volunteer subjects by using a hand-held probe. Intrinsic tissue absorption and reduced scattering parameters were calculated from frequency-domain photon migration data. Wavelength-dependent absorption (at 674, 803, 849, and 956 nm) was used to determine tissue concentration of oxyhemoglobin, deoxyhemoglobin, total hemoglobin, tissue hemoglobin oxygen saturation, and bulk water content. Results show significant and dramatic differences in optical properties between menopausal states. Average premenopausal intrinsic tissue absorption and reduced scattering values at each wavelength are 2.5- to 3-fold higher and 16–28% greater, respectively, than absorption and scattering for postmenopausal subjects. Absorption and scattering properties for women using hormone replacement therapy are intermediate between premenopausal and postmenopausal populations. Physiological properties show differences in mean total hemoglobin (7.0 μ M, 11.8 μ M, and 19.2 μ M) and water concentration relative to pure water (10.9%, 15.3%, and 27.3%) for postmenopausal, hormone replacement therapy, and premenopausal subjects, respectively. Because of their unique, quantitative information content, diffuse optical methods may play an important role in breast diagnostics and improving our understanding of breast disease.

X-ray mammography is widely used for screening breast cancer, the most common form of cancer in women. Because of uncertainties associated with radiographic density, mammography has up to a 22% false-negative rate as well as a high false-positive rate (56.2% cumulative risk after 10 exams) in women under 50 years of age (1, 2). A recent study found that routine initial mammography was not clinically advantageous for women under 35 years of age (3). Furthermore, the use of hormone replacement therapy (HRT) in postmenopausal women is known to increase mammographic density (4) and has been shown recently to impede the efficacy of mammographic screening (5, 6). Techniques such as MRI and ultrasound (US) are used only as secondary procedures because of factors such as high cost and poor specificity (MRI) or low sensitivity (US).

Currently, invasive procedures such as fine-needle aspiration or surgical biopsy are implemented to provide a definitive diagnosis. Given the suboptimal performance of x-ray mammography in premenopausal and perimenopausal women, the majority of invasive follow-up procedures are performed on normal or benign tissue that present no malignant disease (7). As a result, the use of noninvasive, near-infrared (NIR) optical

methods as a supplement to present techniques for diagnosing and detecting breast cancer has generated considerable interest.

Optical methods are advantageous, because they are noninvasive, quantitative, and relatively inexpensive; do not require compression; and pose no risk of ionizing radiation. A promising NIR optical technique currently under development is frequency domain photon migration (FDPM). FDPM methods have detected successfully the presence of small palpable breast lesions *in vivo* in women with previously diagnosed breast abnormalities (8–10).

FDPM employs intensity-modulated NIR light to characterize tissue quantitatively in terms of its optical parameters, i.e., the reduced-scattering coefficient (μ_s') and the absorption coefficient (μ_a). The concentration of significant NIR absorbers [deoxyhemoglobin (Hb), oxyhemoglobin (HbO₂), water, and adipose] can be calculated by using measured μ_a values (11, 12). Multiple scattering of light in breast tissue occurs as a consequence of spatial variations in refractive index, which are influenced by cellular and extracellular matrix density (13, 14). Both μ_a and μ_s' provide an understanding of changes in tissue cellularity, metabolic activity, physiology, and host response to cancer. Detection of lesions is based on the functional contrast between normal and diseased tissue in the same patient. However, the physiology of healthy breast tissue is complex, influenced by multiple internal and external factors such as menstrual-cycle phase, menopausal status, exogenous hormones, lactation, and pregnancy. Consequently, to establish a better basis for optical detection and diagnosis based on differential functional contrast, the optical properties of normal breast tissue must be carefully examined and characterized.

There has been increasing attention paid to the study of normal breast tissue optical properties and changes that occur with age, menopausal status, and HRT (15–17). During the reproductive years, the breast is comprised mostly of glandular tissue. With menopause, there is a progressive atrophy of glandular tissue; mitotic activity slows down; and vascular requirements decrease. Some of these changes have been monitored qualitatively by mammography and MRI (3, 18–20). Involution of breast glandular tissue can be impeded by the use of exogenous hormones, such as estrogen and progesterone (21). Presently, up to 20% of U.S. women use HRT to alleviate symptoms of menopause. However, long-term use has been

This paper was submitted directly (Track II) to the PNAS office.

Abbreviations: FDPM, frequency-domain photon migration; HRT, hormone replacement therapy; μ_a , absorption coefficient; μ_s' , reduced scattering coefficient; Hb, deoxyhemoglobin; HbO₂, oxyhemoglobin; NIR, near infrared; Pren, premenopausal subject *n*; Postn, postmenopausal subject *n*.

To whom reprint requests should be addressed at: Laser Microbeam and Medical Program, Beckman Laser Institute and Medical Clinic, University of California, 1002 Health Sciences Road East, Irvine, CA 92612. E-mail: tromberg@blli.uci.edu.

The publication costs of this article were defrayed in part by page charge payment. This article must therefore be hereby marked "advertisement" in accordance with 18 U.S.C. §1734 solely to indicate this fact.

linked with increased risk for breast cancer (22). MRI studies further suggest that fluctuations in endogenous hormones may alter menstrual cycle patterns and impact breast cancer risk (23–26). In addition, the phase of the menstrual cycle has been shown to influence mammographic accuracy and survival rates after tumor resection (27, 28).

In this article, we provide initial results examining differences in both optical and physiological properties of healthy breast tissue of 14 women. Our results show that the population studied can be well differentiated on the basis of quantitative NIR spectroscopic measurements. Optical contrast is based on physiological changes accompanying menstrual cycle variations, exogenous hormone levels, and menopausal status. We believe this study is particularly important, because standard-of-care screening with x-ray mammography has diminished efficacy in two of the populations we examine, i.e., premenopausal and HRT subjects. The sensitivity of our technique to known biological processes suggests our methods may provide important information complementary to conventional diagnostic techniques, particularly in the case of radiographically dense breast tissue. Ultimately, this technique may enhance our understanding of pathophysiological changes that accompany malignant transformation and provide insight into processes associated with increased disease risk.

Materials and Methods

FDPM Instrument. A portable, multiwavelength, high-bandwidth FDPM instrument has been designed and optimized for clinical optical property studies (Fig. 1, quadrant a). The instrument employs multiple diode lasers (box 1) to provide visible and NIR light at six wavelengths (674, 803, 849, 894, 947, and 956 or 980 nm). The FDPM instrument is described in detail by Tromberg *et al.* (10) and Pham *et al.* (29). A hand-held probe has been designed to house an avalanche photodiode (APD) that records the diffuse light signals after propagation through the tissue (box 2). This probe has multiple grooves on the casing to position source optical fibers a fixed distance from the APD. A 100- μ m-diameter graded index optical fiber positioned 25 mm from the APD detector delivers the diode laser output to the tissue surface. The network analyzer (box 3) measures the phase and amplitude of the electronic signal. A dc source (box 4) is mixed with rf power provided by the network analyzer in a bias network (box 5), which distributes power to each laser diode and produces amplitude modulated light. An optical switch (box 6) delivers light serially from each diode to the tissue. The optical power launched into the subject ranged from 10 to 20 MW for each wavelength.

Measurement Technique. Subjects were measured in the supine position. Measurements were made in reflectance geometry by placing the hand-held probe on the skin surface with light pressure. The phase shift and amplitude of the photon density wave was measured at each wavelength for 201 modulation frequencies between 50 MHz and 1,000 MHz at a source-detector separation of 25 mm. The range of modulation frequencies was swept repetitively such that each amplitude and phase value represents up to 12 measurements. Four to six wavelengths were used for the measurements.

Subjects. A total of 14 subjects was studied: Pre subjects (Pre, premenopausal) 1–6 were premenopausal subjects aged 18 to 33 years. Pre subject 4 (29 years old) was measured during the proliferative phase of her menstrual cycle; Pre subject 1 (27 years old) was measured around ovulation; and Pre subjects 2, 3, and 5 (aged 22, 26, and 32 years, respectively) were measured during the secretory phase. Pre subject 6 (18 years old) was studied at two different points in her menstrual cycle. One measurement was performed near ovulation (day 14) of the subject's regular

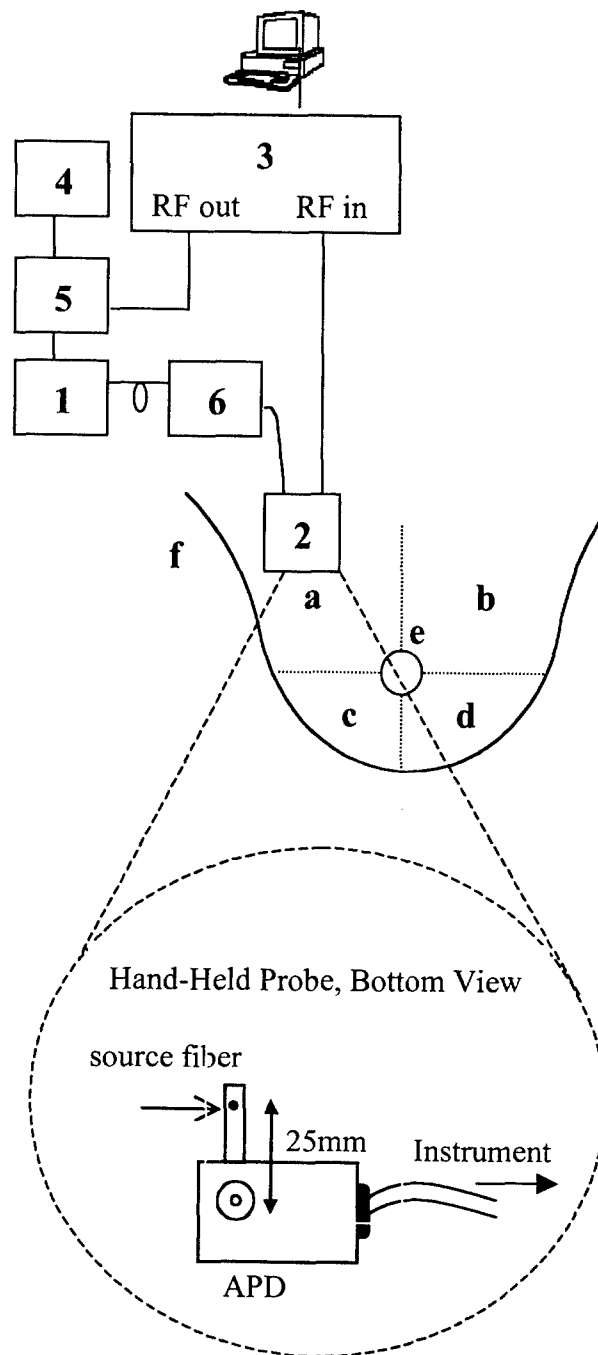


Fig. 1. Schematic drawing of FDPM instrument, hand-held probe, and measurement map of healthy subjects. The components of the instrument are: diode lasers (box 1), avalanche photodiode (box 2), network analyzer (box 3), DC current source (box 4), bias T (box 5), and optical switch (box 6). See text for detailed description. The breast is divided into four quadrants: upper outer (a), upper inner (b), lower outer (c), and lower inner (d). FDPM measurements are made in each quadrant, on the areolar border (e), and on the glandular tail (f) that extends into the axilla.

28-day cycle, and another measurement was performed during the luteal phase (day 25) of the menstrual cycle. Post subjects (Post, postmenopausal) 1–3 were postmenopausal women aged 57 to 67 years. The remaining five subjects were postmenopausal women 51–60 years of age who were using HRT. HRT subjects 1 and 5 were on combination HRT (progesterone and estrogen), and HRT subjects 2–4 were taking estrogen-only HRT. All HRT

subjects have been taking exogenous hormone for at least 2 years. Experiments were conducted in adherence to University of California, Irvine, Institutional Review Board-approved protocols 95-563 and 99-2183. The subjects were healthy with no known breast diseases. After providing informed consent, subjects filled out a brief questionnaire that surveyed pertinent medical history.

When using four wavelengths, the time required for a single measurement was approximately 90 seconds. A total of 12 sites, six per breast, for each subject was measured during subject visits. The measurement map is shown in Fig. 1. Measurements were made in each of the four quadrants, approximately halfway from the center of the breast to the edge of the breast, laterally (a–d). Additional measurements were made on the superior areolar border (e) and the axillary tail (f). Calibration measurements were made approximately every 10 minutes on a tissue phantom of known optical properties.

Model. The P_1 approximation to the Boltzmann transport equation (30) was used to analyze the frequency-domain data and is valid when probing homogeneous turbid media at source-detector separations greater than 1 cm and modulation frequencies less than a few GHz. The model uses an extrapolated boundary condition for a semiinfinite geometry (31). The solution to the P_1 approximation relates the frequency-dependent phase and amplitude to the μ_a and μ_s' coefficients (32). To determine the optical properties from a given set of frequency-dependent data, a Marquardt–Levenburg χ^2 minimization algorithm was used to fit simultaneously the amplitude $A(\omega)$ and phase $\Phi(\omega)$ by minimizing the difference between the measured values and those predicted by the P_1 approximation.

Physiological properties were calculated from the determined μ_a values assuming principal chromophores in breast tissue for the NIR wavelengths used are Hb, HbO₂, and water. The concentrations in tissue of the three components were calculated by using μ_a at four wavelengths: 674, 803, 849, and 956 nm. The contribution of each component to the total μ_a at a given wavelength is represented by the equation $2.303(\epsilon_i c_i) = \mu_{ai}$, where ϵ_i is the extinction coefficient in units of cm²/mol of a particular chromophore at a given wavelength (λ) and c_i is the concentration of the chromophore. The total absorption at a given wavelength from the tissue chromophores is

$$\epsilon_{(Hb)}^{(\lambda)}[Hb] + \epsilon_{(HbO_2)}^{(\lambda)}[HbO_2] + \epsilon_{(H_2O)}^{(\lambda)}[H_2O] = \mu_a^{(\lambda)}, \quad [1]$$

where the brackets ($[]$) indicate concentration. The matrix representation of the four equations is (11)

$$\begin{bmatrix} 6.578 \times 10^6 & 0.740 \times 10^6 & 0.748 \\ 1.897 \times 10^6 & 2.037 \times 10^6 & 0.34 \\ 1.809 \times 10^6 & 2.659 \times 10^6 & 0.781 \\ 1.570 \times 10^6 & 3.049 \times 10^6 & 0.74 \end{bmatrix} \begin{bmatrix} [Hb] \\ [HbO_2] \\ [H_2O] \end{bmatrix} = \begin{bmatrix} \mu_a^{674} \\ \mu_a^{803} \\ \mu_a^{849} \\ \mu_a^{956} \end{bmatrix}. \quad [2]$$

Given that there are more wavelengths than principle chromophores, we have four equations, and three unknowns, and no general solution for c_i . The chromophore concentrations are determined by using a least-squares solution to $Ec = \mu_a$. In matrix representation, the chromophore concentration is given by using $c = (E^T E)^{-1} E^T \mu_a$, where E^T and E^{-1} denote the transpose and inverse of the matrix E , respectively.

Calibration. A measurement of the phase shift of intensity-modulated light at source wavelength λ propagating through a turbid medium at a given source-detector separation can be expressed as follows:

$$\Phi_{\text{meas}} = \Phi_{\text{medium}} + \Phi_{\text{instrument}}. \quad [3]$$

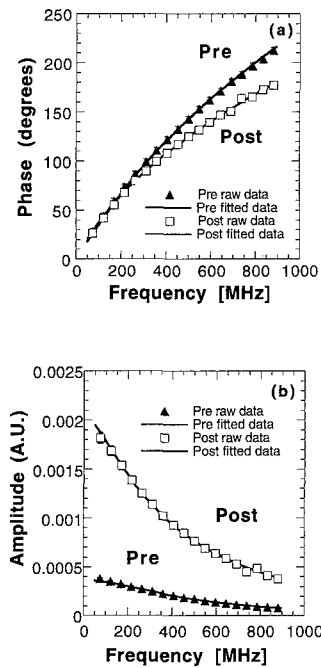


Fig. 2. FDPM measurements of phase lag (a) and amplitude vs. modulation frequency (b) for Pre 1 and Post 1. Source-detector separation, 2.5 cm; wavelength, 849 nm. Solid lines represent best diffusion-model function fits to phase and amplitude data for each subject. Error bars are on the order of the marker size.

To extract Φ_{medium} from Φ_{meas} at a single source-detector separation, $\Phi_{\text{instrument}}$ must be explicitly evaluated (Eq. 3). Similar arguments can be made for amplitude data (A); however, A_{medium} is determined by evaluating measured- and instrument-response ratios. The instrument response was calculated by making a measurement on a homogenous phantom with known optical properties. A siloxane phantom cast from flexible silicone (RTV 615/700, General Electric) and titanium diode in a 400-ml mold was used to calibrate the instrument response in phase and amplitude measurements. Optical properties of the phantom were determined by the two-distance technique described by Fantini *et al.* (33). Reference measurements were made on the phantom at the given source-detector separation during the time of the subject measurement. Calibrations were made at approximately 10-min intervals to account for amplitude drift.

Results and Discussion

The results of raw data and simultaneous fits to the P_1 approximation for Pre subject 1 and Post subject 1 are shown in Fig. 2. Clear differences are detected between the two subjects in both amplitude and phase data.

To establish the range of optical property values characteristic of normal menopausal states, we examined nine subjects (six premenopausal) not receiving exogenous hormone therapy. Fig. 3 shows a scatter plot of μ_a versus μ_s' at all four wavelengths for each subject. For comparative purposes, data from the right upper-outer quadrant measurements are shown. Glandular tissue is concentrated in the upper-outer quadrant of the breast, and consequently, more lesions appear in this region than any other (34). Fig. 3 shows that, in general, postmenopausal women have substantially lower μ_a and μ_s' values compared with premenopausal women. Average premenopausal μ_a values at each wavelength (0.0048–0.015 mm⁻¹) are 2.3- to 3-fold higher than postmenopausal absorption (average $\mu_a = 0.0016$ –0.0064 mm⁻¹). Furthermore, all postmenopausal μ_a values are less than

Absorption vs. Scattering for Post and Pre subjects

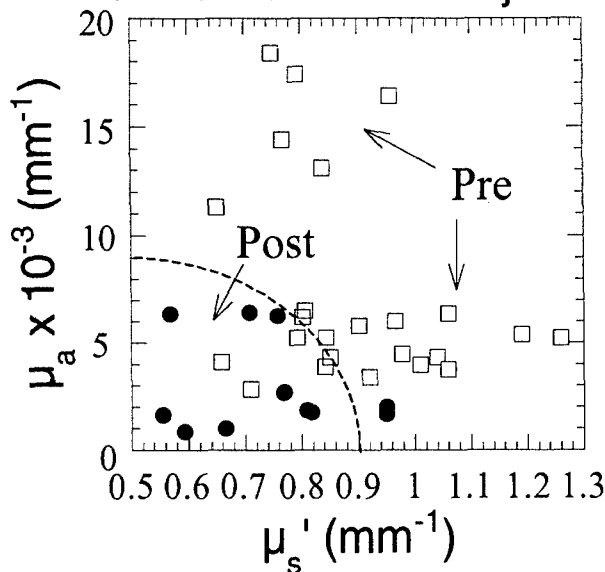


Fig. 3. μ_a vs. μ_s' for six pre- and three postmenopausal subjects at all wavelengths. Values are calculated from best diffusion-model fits to phase and amplitude data

0.007 mm⁻¹. Premenopausal women have 16–22% higher scattering values at each wavelength (average $\mu_s' = 0.83$ – 1.1 mm⁻¹) than postmenopausal subjects (average $\mu_s' = 0.67$ – 0.86 mm⁻¹). Because measurement uncertainties are less than 5% of the optical property value (29), these values constitute significant and dramatic differences between menopausal states.

A deeper understanding of the underlying physiological reasons for optical property contrast can be obtained by examining μ_s' spectra (i.e., μ_s' vs. λ) for three individuals. Results shown in Fig. 4 highlight the impact of estrogen on breast structure. The 29-year-old premenopausal subject displays μ_s' values that are consistently greater than the 67-year-old postmenopausal subject's values. Interestingly, μ_s' values for the 52-year-old postmenopausal subject receiving estrogen-only HRT fall directly between premenopausal and postmenopausal data. The elevated HRT values may be caused by the fact that estrogen increases the rate of mitosis within ductal tissue. Thus, optical property differences between HRT and postmenopausal subjects could be a consequence of epithelial tissue proliferation. Scattering contrast between premenopausal and postmenopausal subjects is probably caused by a combined effect of the loss of glandular epithelium as well as extracellular matrix remodeling. The more gradual μ_s' vs. λ slope shown for the postmenopausal subjects reflects large particle scattering consistent with a high percentage of fatty parenchyma found in this age group. In younger women, the relatively steep μ_s' vs. λ slope is likely to be influenced by the presence of extracellular collagen in addition to cellular/epithelial factors.

These concepts are substantiated further by Fig. 5, which illustrates an inverse correlation between μ_s' and age for subjects over 50. Whether the trend indicating increased scattering for HRT women is caused by exogenous hormone use is not yet clear. Premenopausal μ_s' values seem to be independent of age, most likely because of the timing of the measurements. The six premenopausal subjects were measured at different points of their menstrual cycles, which can significantly affect optical properties.

μ_s' vs. Wavelength

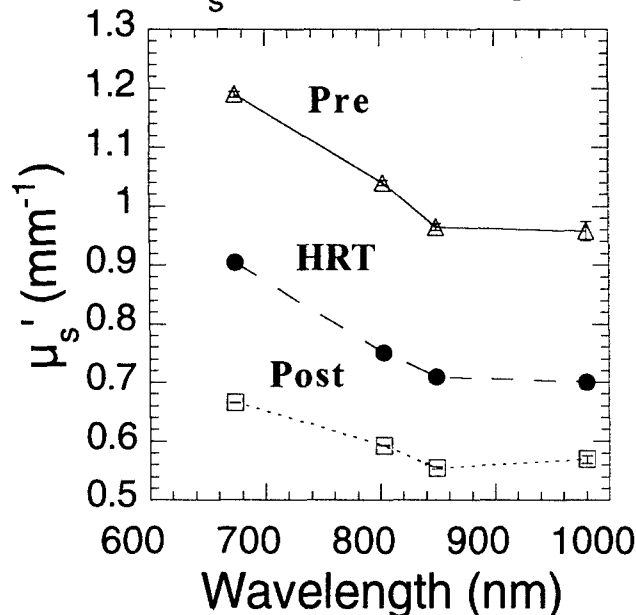


Fig. 4. μ_s' vs. wavelength for three subjects of varied hormonal and menopausal status. Some values at 980 nm represent values extrapolated from $\lambda\lambda^{-8}$ linear regression analysis of the data.

Average tissue hemoglobin concentrations (HbO₂, deoxy, and total) and tissue water concentration are shown in Fig. 6. The concentration of blood vessels and blood flow, indicated by total hemoglobin concentration (THC) (THC = [Hb] + [HbO₂]), is greatest in premenopausal breast because of the high vascular demands of the tissue. Blood vessel density and blood flow decrease as a result of menopausal involution of glandular tissue. This effect can be detected from the significant total hemoglobin concentration difference between premenopausal and postmenopausal subject groups.

Scattering vs. Age

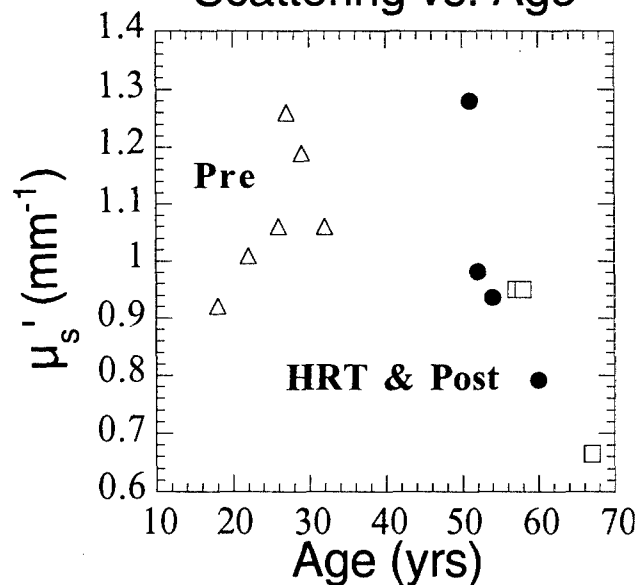


Fig. 5. μ_s' at 674 nm vs. age for all subjects. Pre 6 (age 18) is represented as an average of two points corresponding to two separate measurement dates.

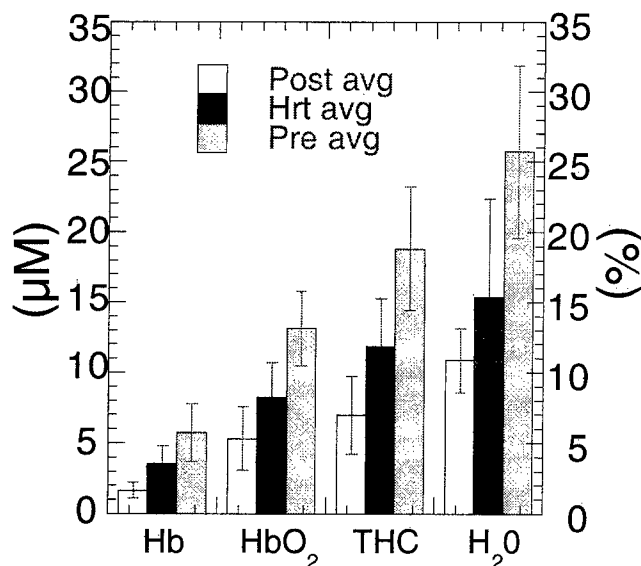


Fig. 6. Mean Hb concentrations [μM , HbO_2 , deoxy, and total (THC)] and water (H_2O) concentration relative to pure water (%) for each subject group. Values are determined from wavelength-dependent absorption values at 674, 803, 849, and 956 or 980 nm. Error bars represent the normalized standard deviation to the mean for six premenopausal, five HRT, and three postmenopausal subjects. Confidence values are $\approx 99\%$ for Hb, HbO_2 , THC, and H_2O .

Women using HRT exhibit Hb concentration values that are intermediate between premenopausal and postmenopausal subjects. Thus, FDPM measurements may be sensitive to subtle HRT effects, including elevations in blood flow, fibroglandular volume, and epithelial cell proliferation (35–38). The general decrease in total Hb concentration with age after 50 (Fig. 7) suggests that it is difficult to determine from limited existing data whether the measured HRT Hb effect is real or simply a consequence of age-related optical property changes.

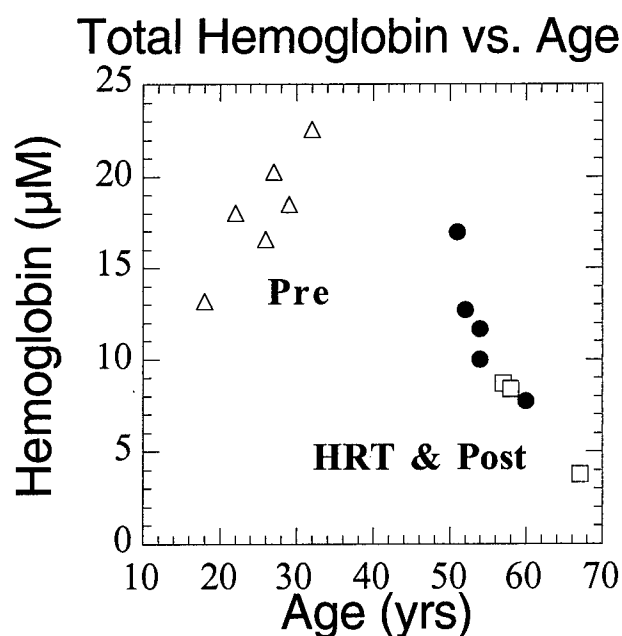


Fig. 7. Total Hb concentration vs. age for all subjects. Pre 6 (age 18) is represented as an average of two points corresponding to two separate measurement dates.

Table 1. Variation in physiological properties during the menstrual cycle

Parameter	Day 14	Day 25
Hb, μM	3.07 ± 0.04	4.72 ± 0.05
HbO_2 , μM	7.56 ± 0.04	11.04 ± 0.06
Total Hb, μM	10.63 ± 0.05	15.76 ± 0.08
S_tO_2 , %	71.12 ± 0.53	70.06 ± 0.53
Water, %	16.49 ± 0.11	21.12 ± 0.15

Calculated physiological properties, Hb concentration (μM , HbO_2 , deoxy, and total Hb), blood oxygen saturation (S_tO_2), and water concentration relative to pure water (%) for a premenopausal subject at Days 14 and 25 of a 28-day menstrual cycle.

Fig. 6 data show that the average water concentration for premenopausal women ($26 \pm 6\%$) is more than a factor of two greater than the mean tissue water concentration for postmenopausal women ($11 \pm 2\%$). These differences reflect the high water content of epithelial connective-tissue compartments in premenopausal tissue, whereas the postmenopausal breast is dominated by low water-content adipose. Water concentration in HRT subjects is slightly greater than the postmenopausal group's concentration ($15 \pm 7\%$). Differences may be caused by hormone-induced accumulation of fluids, a commonly occurring side effect from HRT (38).

Investigating positional variations in optical properties between pre- (Pre 1) and postmenopausal (Post 1) subjects reveals a higher degree of variation in scattering for post- ($\approx 8\%$ for all wavelengths) vs. premenopausal women ($\approx 4\%$). These values were calculated by normalizing the standard deviation of the values from measurements in each of the four quadrants ($n = 4$) to the mean (data not shown). This difference may represent the nonuniform glandular involution of breast tissue that accompanies menopause and results in palpable differences in density in the breast tissue of postmenopausal subjects (39). The positional variation in the μ_a is greater for wavelengths corresponding to hemoglobin absorption (674–849 nm) for the postmenopausal subjects (23–33% vs. 17–20% for Pre). However, wavelengths corresponding to fat and water concentrations (894, 947, and 956 nm) show a higher variability in premenopausal (13–16%) vs. only 7–8% in postmenopausal subjects.

Figs. 3–7 strongly suggest that physiological changes caused by hormonal fluctuations that occur over a period of many years can be detected and quantified. Previous studies (40) show these effects also are detectable within the menstrual cycle of premenopausal women. To test FDPM sensitivity to menstrual-cycle variations, we examined a premenopausal subject during ovulation and before the onset of menses. Table 1 data summarizing these results show that μ_a and μ_s are higher for the latter part of the cycle (Day 25) than in mid-cycle (Day 14). Absorption differences correspond to the calculated physiological properties. Our results show a 48.3% increase in Hb and 28.1% increase in water concentration during the luteal phase, changes that are consistent with the physiological effects caused by ovarian hormone fluctuations during the menstrual cycle. After ovulation, blood flow to the breast can increase by up to 50%; there is an increase in breast volume; and parenchymal water content changes by an average of 25% during the latter half cycle (24, 25). Changes in scattering were 3–5% and not statistically significant.

Conclusions

A hand-held photon migration probe has been developed that can detect significant differences in absorption and scattering properties occurring with changes in age and menstrual-cycle phase. The sensitivity of quantitative NIR spectroscopy to breast biology is unique among radiological methods. Consequently, optical techniques may eventually provide a practical, noninva-

sive means for enhancing the accuracy of tumor diagnostics in premenopausal and perimenopausal subjects and for increasing our understanding breast pathophysiology.

A.E.C., R.H., and C.E. acknowledge support from the U.S. Army Medical Research and Materiel Command (DAMD17-98-1-8186), the

Swiss National Science Foundation, and the American Cancer Society, respectively. This work was supported by the National Institutes of Health Laser Microbeam and Medical Program (RR-01192), the National Institutes of Health (GM-50958), the Avon Foundation, the Chao Family Comprehensive Cancer Center (CA-62203), and the Department of Energy (DOE DE-FG03-91ER61227).

1. Kerlikowske, K. & Barclay, J. (1997) *J. Natl. Cancer Inst. Monogr.* **22**, 105–110.
2. Elmore, J. G., Barton, M. B., Moceri, V. M., Polk, S., Arena, P. J. & Fletcher, S. W. (1998) *N. Engl. J. Med.* **338**, 1089–1096.
3. Hindle, W. H., Davis, L. & Wright, D. (1999) *Am. J. Obstet. Gynecol.* **180**, 1484–1490.
4. Baines, C. J. & Dayan, R. (1999) *J. Natl. Cancer Inst.* **91**, 833–838.
5. Laya, M. B., Larson, E. B., Taplin, S. H. & White, E. (1996) *J. Natl. Cancer Inst.* **88**, 643–649.
6. Litherland, J. C., Stallard, S., Hole, D. & Cordiner, C. (1999) *Clin. Radiol.* **54**, 285–288.
7. Fletcher, S. W. (1997) *J. Natl. Cancer Inst. Monogr.* **22**, 5–9.
8. Fantini, S., Walker, S. A., Franceschini, M. A., Kaschke, M., Selg, P. M. & Moesta, T. K. (1998) *Appl. Opt.* **37**, 1982–1989.
9. Franceschini, M. A., Moesta, K. T., Fantini, S., Gaida, G., Gratton, E., Jess, H., Mantulin, W. W., Seeber, M., Schlag, P. M. & Kaschke, M. (1997) *Proc. Natl. Acad. Sci. USA* **94**, 6468–6473.
10. Tromberg, B. J., Coquoz, O., Fishkin, J. B., Pham, T., Anderson, E. R., Butler, J., Cahn, M., Gross, J. D., Venugopalan, V. & Pham, D. (1997) *Philos. Trans. R. Soc. London B* **352**, 661–668.
11. Cope, M. (1991) Ph.D. thesis (University of London).
12. Sevcik, E. M., Chance, B., Leigh, J. & Nioka, S. (1991) *Anal. Biochem.* **195**, 330–351.
13. Beauvoit, B., Kitai, T. & Chance, B. (1994) *Biophys. J.* **67**, 2501–2510.
14. Thomsen, S. & Tatman, D. (1998) *Ann. N.Y. Acad. Sci.* **838**, 171–193.
15. Suzuki, K., Yamashita, Y., Ohta, K. & Chance, B. (1994) *Invest. Radiol.* **29**, 410–414.
16. Suzuki, K., Yamashita, Y., Ohta, K., Kaneko, M., Yoshida, M. & Chance, B. (1996) *J. Biomed. Opt.* **1**, 330–334.
17. Cubeddu, R., Pifferi, A., Taroni, P., Torricelli, A. & Valentini, G. (1999) *Appl. Phys. Lett.* **74**, 874–876.
18. Brisson, J., Morrison, A. S. & Khalid, N. (1998) *J. Natl. Cancer Inst.* **80**, 1534–1540.
19. Boyd, N. F., Greenberg, C., Lockwood, G., Little, L., Martin, L., Byng, J., Yaffe, M. & Tritchler, D. (1997) *J. Natl. Cancer Inst.* **89**, 488–496.
20. Lee, N. A., Rusinek, H., Weinreb, J., Chandra, R., Toth, H., Singer, C. & Newstead, G. (1997) *Am. J. Roentgenol.* **168**, 501–506.
21. Kaufman, Z., Garstin, W. I. H., Hayes, R. & Michell, M. J. (1991) *Clin. Radiol.* **43**, 385–388.
22. Colditz, G. A. (1997) *Ann. N.Y. Acad. Sci.* **833**, 129–136.
23. Drife, J. O. (1989) *Int. J. Gynecol. Obstet. Suppl.* **1**, 19–24.
24. Fowler, P. A., Casey, C. E., Cameron, G. G., Foster, M. A. & Knight, C. H. (1990) *Br. J. Obstet. Gynaecol.* **97**, 595–602.
25. Graham, S. J., Stanchev, P. L., Lloydsmith, J. O. A., Bronskill, M. J. & Plewes, D. B. (1995) *J. Magn. Reson.* **5**, 695–701.
26. Whelan, E. A., Sandler, D. P., Root, J. L., Smith, K. R. & Weinberg, C. R. (1994) *Am. J. Epidemiol.* **140**, 1081–1090.
27. White, E., Velentgas, P., Mandelson, M. T. & Lehman, C. D. (1998) *J. Natl. Cancer Inst.* **90**, 906–910.
28. Hrushesky, W. J. M. (1993) *J. Surg. Oncol.* **53**, 1–3.
29. Pham, T. H., Coquoz, O., Fishkin, J. B., Anderson, E. & Tromberg, B. J. (2000) *Rev. Sci. Instrum.* **71**, 2500–2513.
30. Fishkin, J. B., Fantini, S., Vandeven, M. J. & Gratton, E. (1996) *Phys. Rev. E Stat. Phys. Plasmas Fluids Relat. Interdiscip. Top.* **53**, 2307–2319.
31. Haskell, R. C., Svaasand, L. O., Tsay, T. T., Feng, T. C., McAdams, M. S. & Tromberg, B. J. (1994) *J. Opt. Soc. Am. A* **11**, 2727–2741.
32. Fishkin, J. B. & Gratton, E. (1993) *J. Opt. Soc. Am. A* **10**, 127–140.
33. Fantini, S., Franceschini, M. A. & Gratton, E. (1994) *J. Opt. Soc. Am. B* **11**, 2128–2138.
34. Reichart, C. M., Moshiri, S., Austin, R. M. & Norris, H. J. (1988) in *Diagnosis and Management of Breast Cancer*, eds. Lippman, M. E., Lichter, A. S. & Danforth, D. N., Jr. (Saunders, Philadelphia), pp. 22–26.
35. Bourne, T., Hillard, T. C., Whitehead, M. I., Crook, D. & Campbell S. (1990) *Lancet* **335**, 1470–1471.
36. Pines, A., Fisman, E. Z., Levo, Y., Averbuch, M., Lidor, A., Drory, Y., Finkelstein, A., Hetman-Peri, M., Moshkowitz, M., Ben-Ari, E. & Ayalon, D. (1991) *Am. J. Obstet. Gynecol.* **164**, 806–812.
37. Berkowitz, J. E., Gatewood, O. M., Goldblum, L. E. & Gayler B. W. (1990) *Radiology (Easton, Pa.)* **174**, 199–201.
38. Key, T. J. A. (1995) *Mutat. Res.* **333**, 59–67.
39. Wren, B. G. (1996) *Baillieres Clin. Obstet. Gynaecol.* **10**, 433–447.
40. Cubeddu, R., D'Andrea, C., Pifferi, A., Taroni, P., Torricelli, A. & Valentino, G. (2000) *Photochem. Photobiol.* **72**, 383–391.

Broadband absorption spectroscopy in turbid media by combined frequency-domain and steady-state methods

Frédéric Bevilacqua, Andrew J. Berger, Albert E. Cerussi, Dorota Jakubowski, and Bruce J. Tromberg

A technique for measuring broadband near-infrared absorption spectra of turbid media that uses a combination of frequency-domain (FD) and steady-state (SS) reflectance methods is presented. Most of the wavelength coverage is provided by a white-light SS measurement, whereas the FD data are acquired at a few selected wavelengths. Coefficients of absorption (μ_a) and reduced scattering (μ'_s) derived from the FD data are used to calibrate the intensity of the SS measurements and to estimate μ'_s at all wavelengths in the spectral window of interest. After these steps are performed, one can determine μ_a by comparing the SS reflectance values with the predictions of diffusion theory, wavelength by wavelength. Absorption spectra of a turbid phantom and of human breast tissue *in vivo*, derived with the combined SSFD technique, agree well with expected reference values. All measurements can be performed at a single source-detector separation distance, reducing the variations in sampling volume that exist in multidistance methods. The technique uses relatively inexpensive light sources and detectors and is easily implemented on an existing multiwavelength FD system. © 2000 Optical Society of America

OCIS codes: 170.1470, 170.4090, 170.5280, 170.7050.

1. Introduction

Reflectance spectroscopy is a technique for characterizing turbid media that has become widely used in medical diagnostics. In many cases the quantification of chromophore concentrations is desired, and this requires the ability to separate the effects of absorption from those of scattering. Fundamentally, the coefficients of absorption μ_a and of reduced scattering μ'_s can be determined by a series of reflectance measurements performed in one of three domains, namely, time¹⁻³ (with a fast pulse of light), frequency⁴⁻⁷ (with a sinusoidally modulated source of light), and steady state⁸⁻¹⁵ (with a source of constant intensity but multiple detectors at different distances). Unsurprisingly, these three techniques have

different merits and limitations. Spatially resolved steady-state techniques are relatively inexpensive and are more readily suited for the determination of μ_a and μ'_s over large, continuous ranges of wavelengths than are the other methods. However, the steady-state approach works best when measurements are performed with a combination of short (~ 1 transport mean free path) and long (many transport mean free paths) source-detector separations.¹¹ Ideally, the optical properties of the sample should not vary over the ranges of volumes probed by the various measurements. The larger the spread of distances probed, the more likely that heterogeneities, such as those found in biological tissue, will distort the data from the predictions of the model. One approach to limiting this effect, given that the shortest separations provide great stability for the calculation of μ'_s , is to use relatively short (< 10 -mm) source-detector separations.^{12,13} Inasmuch as the mean probing depth scales with the source-detector separation, with this approach such measurements are sensitive to superficial components (to depths of less than 5 mm for typical biological tissues).

Time- and frequency-domain techniques are well suited for deeper (> 1 cm for biological tissue) inves-

When this research was performed, all authors were with the Beckman Laser Institute, University of California, Irvine, Irvine, California 92612. A. J. Berger is now with The Institute of Optics, University of Rochester, Rochester, New York 14627. B. J. Tromberg's e-mail address is tromberg@bli.uci.edu.

Received 26 April 2000; revised manuscript received 18 August 2000.

0003-6935/00/346498-10\$15.00/0

© 2000 Optical Society of America

tigations. Moreover, they can be performed with only one or a few source-detector separations, which makes them more robust for use in studying heterogeneous samples. Because such techniques require sources that can be pulsed or modulated rapidly, covering a large wavelength range requires a tunable laser or an extensive collection of laser diodes, both of which can be expensive, difficult to maintain, and slow to cover the entire spectrum. This is an important drawback, because, as discussed by Hull *et al.*,¹⁴ the quantification of chromophore concentrations can be significantly affected by use of a limited number of wavelengths.

In this paper we suggest a way to use steady-state (SS) and frequency-domain (FD) reflectance measurements in tandem to obtain broad wavelength coverage with increased penetration depth. This method is especially promising for near-infrared spectroscopy of tissue, e.g., to characterize breast physiology. For such applications, the method proposed here permits rapid data acquisition, deep tissue probing, and robust resolution of the contributions from the four major near-infrared tissue absorbers: oxyhemoglobin, deoxyhemoglobin, water, and fat. The central innovations are using FD-derived μ_a and μ_s' values to convert the SS measurements into units of absolute reflectance and using the power-law wavelength dependence of μ_s' to obtain interpolated and extrapolated values at non-laser wavelengths. FD measurements are made at a handful of diode laser wavelengths spanning the range of interest (650–1000 nm), whereas the SS measurements are made continuously across the entire range. Unlike for spatially resolved SS, however, here only a single, large source-detector separation is used, preferably the same one as for the FD measurements. The instrumentation is straightforward and particularly easy to add to an existing FD system.

After describing our method of combining the SS and FD methods (SSFD), we test the SSFD technique by using it to measure the absorption spectra of turbid samples. First, we analyze a liquid tissue phantom whose absorption spectrum is known (by direct spectrophotometry of the absorbing component before mixing) and with which the SSFD result can be compared. We also measure locations on the breasts of two human female volunteers, demonstrating that data can be gathered *in vivo* and analyzed to provide pertinent physiological parameters. Differences among the measured breast spectra can be interpreted in terms of different relative levels of water, fat, and hemoglobin present in the explored tissue volumes. In addition, estimates of absolute concentrations are comparable with those reported in other recent broadband *in vivo* studies. Finally, we discuss possible reasons for imperfect spectral fits and compare concentration predictions derived from SSFD analysis with those derived from FD data alone.

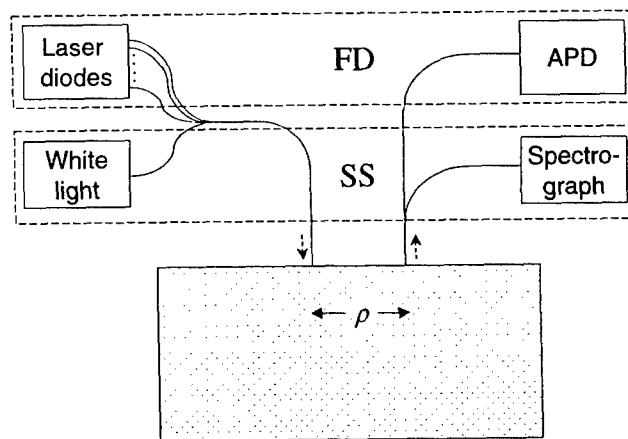


Fig. 1. Configuration of light sources, optical fibers, and detectors: APD, avalanche photodiode. The dashed rectangles denote components that belong to the FD and SS systems.

2. Experimental Methods

A. Optical Measurements

Figure 1 shows the experimental arrangement for SSFD measurements. In all cases, light is delivered via optical fiber to the surface of the sample and collected at some distance ρ away. For the liquid phantom measurements, ρ was 15.5 mm; for the breast, 21.5 (FD) and 24 (SS) mm (the slight difference was due to instrumental limitations; a future instrument will utilize identical distances). In FD mode (upper dashed rectangle), the light arrives sequentially from one of seven amplitude-modulated diode lasers (672, 800, 806, 852, 896, 913, and 978 nm, all with output powers of <20 mW at the sample) and is detected by an avalanche photodiode unit (Hamamatsu C556P-56045-03) that amplifies the ac component of the signal. A network analyzer (Hewlett-Packard 8753C) delivers 251 modulation frequencies from 100 to 700 MHz and measures phase and modulation amplitudes of the photon intensity signal, as described elsewhere.^{7,16} In SS mode (lower dashed rectangle), light comes from a 150-W halogen lamp (Fiber-Lite) and is analyzed by a fiber-coupled spectrograph (Ocean Optics S2000) with a linear CCD detector from 525 to 1155 nm, with the useful range for our experiments being 650–1000 nm. The spectrograph records a total of 2048 points (0.35 nm/pixel), and the spectral resolution is 5 nm (full width at half-maximum). Light is delivered to the sample through a bundle of four fibers (bundle diameter, 600 μm) and collected with a single fiber of 1-mm diameter. We measure the spectrum of the light source separately by inserting the source and detector fibers into different ports of an integrating sphere (Labsphere, IS-040-SF). Relative reflectance is calculated to be the sample spectrum divided by the source spectrum (note that both measurements use the same delivery fiber, collection fiber, and detector apparatus). Total acquisition time per sample for SSFD measurements is of the order of 40 s (30 s for FD and 10 s for SS). We calculated $\mu_a(\lambda)$ according

to the methods of Section 3 with an in-house Matlab (The MathWorks, Inc.) code, making use of the optimization toolbox.

B. Samples

The phantom contained 17 mg of green dye (naphthol) and 50 mL of an aqueous scattering suspension (Intralipid-20%, Pharmacia, Inc.) dissolved in 950 mL of water. Before the addition of Intralipid, the absorbance spectrum of the dye-water solution was measured in a 1-cm plastic cuvette by a spectrophotometer (Beckman Instruments, DU630) with water as a reference. Optical measurements were performed as indicated in Fig. 1, with source and detector fibers placed at the surfaces of the samples.

In vivo measurements were performed on the left breasts of two supine female volunteers, aged 37 and 21 years. Data were gathered from two regions on one volunteer (a region on the areolar border and a region of inner breast, i.e., close to the middle of the chest) and from one region (inner breast only) on the other volunteer, yielding a total of three samples. In this modality, the source light was again delivered by optical fiber but the FD detector was placed directly against the tissue, without a collection fiber. Fiber and detector were bundled into a single hand-held device that was placed gently against the breast. SS reflectance was measured subsequently, at the exact same location, in the two-fiber mode described above. All procedures were approved by the Institutional Review Board of the University of California, Irvine (study 95-563).

3. Background Theory

A. Diffusion Model

The measured reflectance signal R can be predicted theoretically by use of the diffusion approximation to the radiative transfer equation, as many groups of researchers have discussed.^{7,17-21} In this theoretical framework, the reflectance is a function of the optical properties of the medium, defined by absorption coefficient μ_a , reduced scattering coefficient μ'_s , and index of refraction n . The diffusion approximation is valid for large source-detector separation r [$r > 10(\mu_a + \mu'_s)^{-1}$] and high (reduced) albedo [$\mu'_s/(\mu_a + \mu'_s) > 0.95$]. The SS and FD cases can be described by a single formalism in which the solution for the reflectance is built from the Green's function for the diffusion equation, i.e., the fluence [W/cm²] that is due to an isotropic point source in an infinite, homogeneous medium. This function takes the form $\exp(-kr)/(Dr)$, where $D \equiv [3(\mu_a + \mu'_s)]^{-1}$, the complex wave number is $k = k_{\text{real}} + ik_{\text{imag}}$, and

$$k_{\text{real}} = \left[\frac{3}{2} \mu_a (\mu_a + \mu'_s) \right]^{1/2} \left\{ \left[1 + \left(\frac{\omega}{\mu_a c} \right)^2 \right]^{1/2} + 1 \right\}^{1/2},$$

$$k_{\text{imag}} = \left[\frac{3}{2} \mu_a (\mu_a + \mu'_s) \right]^{1/2} \left\{ \left[1 + \left(\frac{\omega}{\mu_a c} \right)^2 \right]^{1/2} - 1 \right\}^{1/2},$$

where ω is the modulation frequency in radians per second. The steady-state solution is simply the limit when $\omega = 0$. In this case the solution for R is a real number [$k_{\text{real}} = [3\mu_a(\mu_a + \mu'_s)]^{1/2}$ and $k_{\text{imag}} = 0$]. When $\omega > 0$, R becomes a complex number $A \exp(-i\phi)$, where A is the modulation amplitude and ϕ is the phase shift relative to the source. As we explain in Subsection 3.B, these quantities can be obtained from the FD measurement.

In treating reflectance problems, we model the sample-air interface, using an extrapolated boundary condition²¹ in which the fluence is set to zero at a distance $z_b = 2D(1 + R_{\text{eff}})/(1 - R_{\text{eff}})$ above the sample (R_{eff} depends on the refractive mismatch and equals 0.493 for tissue of $n = 1.4$ and air of $n = 1.0$). The method of images is employed, with an isotropic point source at a depth $z_o = (\mu_a + \mu'_s)^{-1}$ contributing a signal S_r and a negative image point at a height $z_o + z_b$ above the extrapolated boundary contributing S_i . The result is the fluence Φ at any point in the sample. The detected signal along the boundary is then written as a combination of terms proportional to the fluence and to its flux normal to the surface:

$$R = c_1 \Phi - c_2 D \nabla \Phi \cdot (-\hat{z}), \quad (1)$$

where values for the constants c_1 and c_2 are determined by the refractive-index mismatch between the two media²¹ (for tissue of $n = 1.40$ and air of $n = 1$, for these constants the values 0.118 and 0.306, respectively, are assumed), $-\hat{z}$ is a unit vector pointing normally upward out of the sample, and

$$\Phi = \frac{P}{4\pi D} \left[\frac{\exp(-kr_s)}{r_s} - \frac{\exp(-kr_i)}{r_i} \right],$$

$$D \nabla \Phi \cdot \hat{z} = \frac{P}{4\pi} \left[z_o \left(k + \frac{1}{r_s} \right) \frac{\exp(-kr_s)}{r_s^2} + (z_o + 2z_b) \right. \\ \left. \times \left(k + \frac{1}{r_i} \right) \frac{\exp(-kr_i)}{r_i^2} \right], \quad (2)$$

where P is the incident power and r_s (r_i) is the distance from the source (image) to the detector.

B. Frequency-Domain Fitting

Like the theory of Subsection 3.A, our FD fitting process, which provides μ_a and μ'_s values at a few wavelengths, has been described at length elsewhere,^{7,16} and a brief description is provided here as background.

Each FD measurement contains instrumental artifacts; i.e., the measured reflectance is actually

$$R = C_o A \exp[-i(\phi + \phi_o)], \quad (3)$$

where C_o and ϕ_o are sample-independent instrumental constants. A and ϕ are, respectively, the modulation amplitude and phase of the FD reflectance, as defined in Subsection 3.A.

For calibration, we gather FD data from a prepared sample whose μ_a and μ'_s values are known *a priori* from a set of two-distance FD measurements.⁷

Frequency-dependent values of ϕ_0 and C_0 are calculated from the discrepancies between measured [Eq. (3)] and predicted [Eq. (1)] phase and modulation amplitude, thus calibrating our future measurements.

With the instrumental constants thus determined, the 502 data points per sample (251 for both phase and amplitude as a function of the FD modulation frequency ω) depend on two unknowns, μ_a and μ'_s . We select the best μ_a and μ'_s values to fit the predictions of Eq. (1) to the data, using the iterative, nonlinear, least-squares method of Levenberg and Marquardt,²² simultaneously fitting the phase and the amplitude until overall convergence is achieved.⁷ As was noted by various authors,^{2,21} the reflectance in Eq. (1) is nearly proportional to either the flux or the fluence term alone (i.e., the ratio of the two is independent of μ_a and μ'_s) for the large source-detector separations that we employ [$>10(\mu_a + \mu'_s)^{-1}$]. We therefore use only the fluence term Φ from Eq. (1), absorbing the additional proportionality factor into the instrumental constant C_0 .

4. Determination of Broadband μ_a Spectrum

Section 3 provided background information regarding diffusion theory models and a method for extracting μ_a and μ'_s values from FD measurements at specific wavelengths. We now describe how FD and SS measurements can be combined to yield quantitative, broadband μ_a spectra.

Our goal is to compute μ_a at each wavelength, given the measured SS reflectance. However, single-distance SS reflectance cannot itself provide μ_a : R depends on μ'_s as well as on μ_a , so one measurement cannot provide a unique determination of either parameter. In addition, the instrumental constant C_0 is not known. The single SS measurement at each wavelength therefore needs to be supplemented with both a means of establishing the absolute reflectance intensity and an additional piece of information about μ_a or μ'_s (or a combination of the two).

A. Use of Frequency-Domain Data to Provide Additional Information

The FD system can provide both pieces of necessary information at each SS wavelength. At first glance this is surprising, as the FD system operates at only seven wavelengths, whereas the SS system covers 450 nm with continuous 5-nm resolution. It would seem then that the needed values of μ'_s and C_0 could be determined only at these seven wavelengths, and strictly speaking such is indeed the case. Significantly, however, the wavelength dependence of both μ'_s and C_0 is smooth and predictable in shape, as is discussed below. It is this fact that enables us to use the discrete FD information to supplement our broadband SS measurements at all desired wavelengths.

B. Amplitude Calibration of the Reflectance Spectrum

The FD measurements permit calculation of the instrumental factor C_0 at all wavelengths because we

expect no wavelength dependence at all: The sample and source spectra are measured with the same delivery and collection system and only a few seconds apart, so there should be negligible wavelength-dependent artifacts in the ratio of the two. Therefore the task reduces to that of calculating C_0 at a single wavelength. This is readily done at any of the FD wavelengths, as μ_a and μ'_s are both known and absolute reflectance is a function only of these variables [cf. Eqs. (1) and (2) in the $\omega = 0$ limit]. Using all the FD data to increase robustness, we can calculate the value of C_0 that scales the measured SS reflectances to match the predicted reflectances as closely as possible (in the least-squares sense). Once this is done, the scale factor C_0 is known for the entire spectrum. Examples of this scaling are given below.

C. Determination of $\mu'_s(\lambda)$

The FD values of μ'_s also allow us to obtain information about μ'_s across the entire wavelength range. As numerous groups of researchers have observed,²³⁻²⁵ the particle size distribution of scatterers (0.1–10 μm) in many biological media and phantoms tends to have smooth wavelength dependence over the range 650–1000 nm, which is well described by a power function of the form

$$\mu'_s(\lambda) = A\lambda^{-B} \quad (4)$$

(the parameter A here has no relation to the modulation amplitude). As a result, measuring several μ'_s values allows us to fit those values to a simple function of wavelength and to obtain good estimates of μ'_s at all other wavelengths needed.

D. Iterative Solving for the $\mu_a(\lambda)$ Spectrum

With $\mu'_s(\lambda)$ calculated and the reflectance correctly scaled, the equation for steady-state reflectance ([Eq. (1)] contains only one unknown, μ_a . Because it is difficult to obtain an analytical solution for μ_a from this equation, numerical solving methods were employed. Proceeding one wavelength at a time, we used the Matlab nonlinear zero-finding function `fzero` to choose μ_a such that $R_{\text{meas}} - R_{\text{thy}}(\mu_a) = 0$, where R_{meas} is the calibrated SS reflectance measurement and $R_{\text{thy}}(\mu_a)$ is the theoretical reflectance predicted by Eqs. (1) and (2) for a given trial value of μ_a . Solving for the entire μ_a spectrum required ~ 10 s on a personal computer.

5. Results

Figure 2 displays the SS reflectance measured from the phantom and the predicted absolute reflectance calculated from diffusion theory based on the FD measurements of μ_a and μ'_s . Because of strong absorption at wavelengths above 950 nm, the FD measurement at 978 nm was noisy, which in turn made the calculation of SS data at wavelengths above 950 nm unstable. Data are therefore presented for 650–950 nm for the phantom only. As anticipated, all the measurements differ from the predictions by essen-

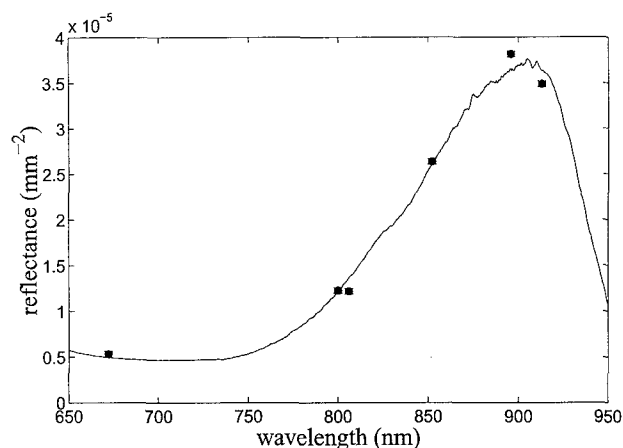


Fig. 2. SS reflectance spectrum acquired from a dye-Intralipid phantom, scaled to fit the discrete reflectance values (filled circles) predicted by Eqs. (1) and (2) with FD-derived values of μ'_s and μ_a . This scaling causes the entire spectrum to be converted into absolute reflectance units; see text for a discussion. The error in FD reflectance is estimated to be $\pm 3 \times 10^{-7}/\text{mm}^{-2}$; in SS reflectance, $\pm 1 \times 10^{-7}/\text{mm}^{-2}$.

tially the same scale factor. The entire SS spectrum is thus converted into absolute reflectance units. Similar results were observed for the three breast samples, as shown in Fig. 3. From top to bottom, sample 1 is the inner breast region of the 37-year-old volunteer and samples 2 and 3 are from the areolar border and the inner breast, respectively, of the 21-year-old volunteer.

Figure 4 shows the least-squares power-law fit to the μ'_s values measured by the FD on the phantom. As expected, the wavelength dependence is fairly smooth and is easily described by the fit. Corresponding fits for the three breast samples appear in Fig. 5. Note that the values change by only a factor

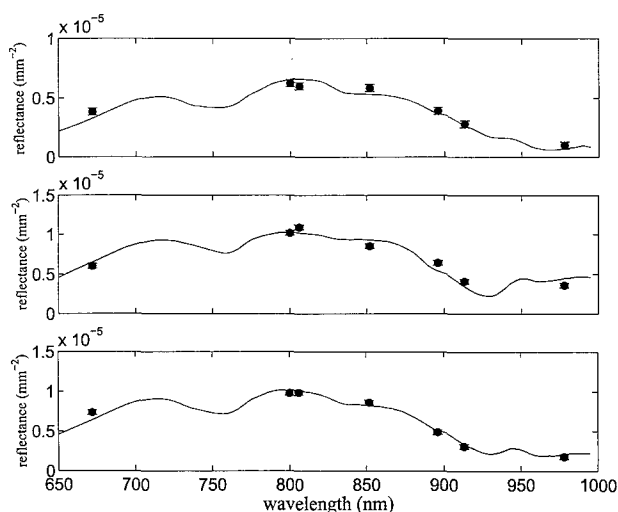


Fig. 3. SS reflectance spectra acquired from three locations in breast tissue of female volunteers. The spectra have been scaled to fit reflectance values (filled circles) calculated from FD data in the same manner as for Fig. 2. Errors are the same as for Fig. 2.

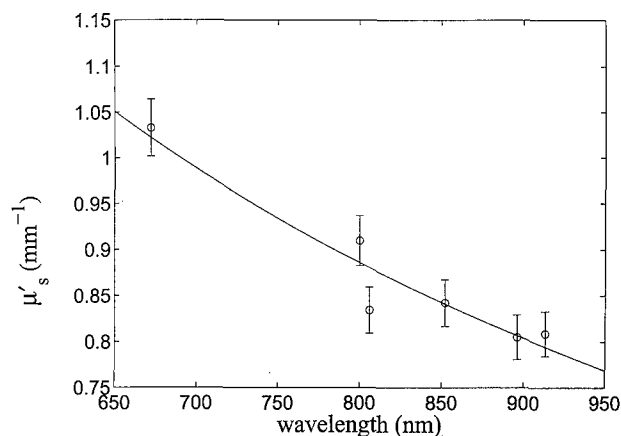


Fig. 4. Determination of the broadband μ'_s spectrum for the dye-Intralipid phantom. Open circles, discrete μ'_s values measured by the FD technique; solid curve, best power-law fit to Eq. (4). Fitting parameters are $A = 2200$ and $B = -0.82$. Error bars on μ'_s are 3%.⁷

of 2 over the entire range, so the wavelength dependence is weak in addition to being predictable.

Figure 6 summarizes the absorption values calculated for the dye-Intralipid phantom. The thicker curve shows the μ_a values that we found make Eq. (1) reproduce the measured reflectance data as closely as possible, using the *fzero* algorithm as described above. The thinner curve represents a linear least-squares fit to the thicker curve based on reference spectra of pure water (from Kou *et al.*²⁶) and pure dye (measured by a spectrophotometer as described above). As the figure shows, the two-component fit accurately models the measured spectrum across the entire spectral range. The least-squares fitting coefficient for the dye spectrum is 1.00. Also shown are the values of μ_a derived by FD analysis alone, demonstrating an agreement between the FD and

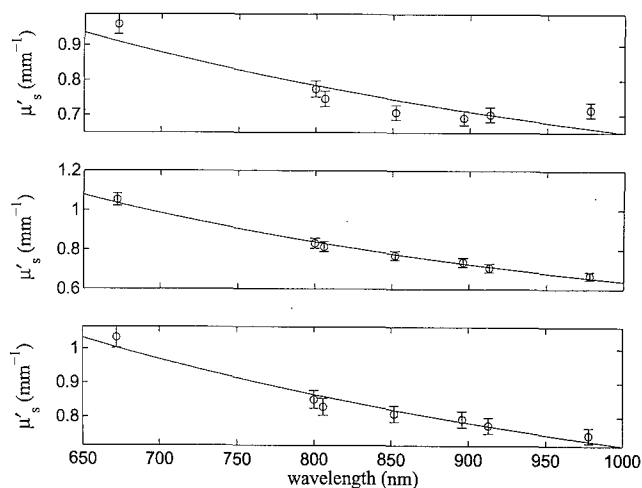


Fig. 5. Determination of broadband μ'_s spectra for the three breast samples. Circles, the discrete μ'_s values measured by the FD technique; solid curves, best power-law fits to Eq. (4). Fitting parameters (A, B) from top to bottom are (240, -0.86), (2700, -12), and (250, -0.85). Error bars on μ'_s are 3%.⁷

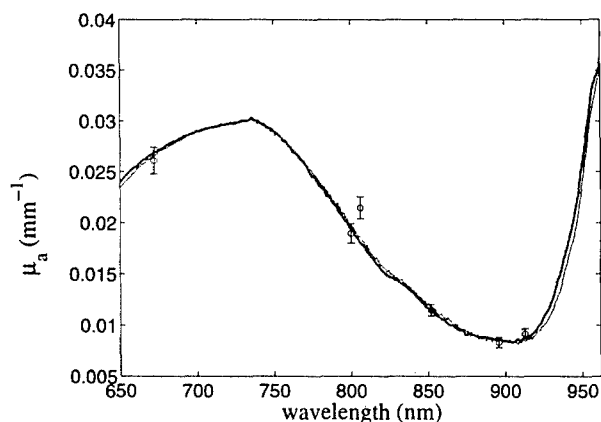


Fig. 6. Comparison of μ_a values generated by FD (open circles) and by SSFD (thicker curve) for the dye-Intralipid phantom. Also shown is the best fit (thinner curve) to the SSFD data by use of the spectra of naphthol (measured with a spectrophotometer) and of water (from Kou *et al.*²⁶). Open circles, discrete μ_a values from FD alone. Error bars, $\pm 0.0005 \text{ mm}^{-1}$ or 5%, whichever is larger.

SSFD methods at these wavelengths, as would be expected because the FD data have been used to calibrate the SS data.

Corresponding plots that show absorption spectra of the three breast samples appear in Figs. 7–9. As before, the thicker curve is the experimental data, the thinner curve is a full-spectrum fit, and the circles are FD values. In these cases, however, the fit is built from published spectra (see Fig. 10) of oxyhemoglobin, deoxyhemoglobin,²⁷ water,²⁶ and fat,²⁸ which are commonly regarded as the four major absorbers in breast tissue in the 650–1000-nm range. Coefficients from the fit thus provide estimates of these

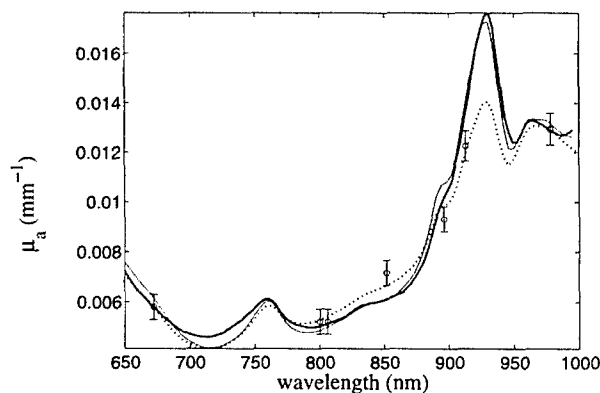


Fig. 7. μ_a predictions for the first breast measurement (inner breast; 37-year-old volunteer). Thicker curve, the SSFD data; thinner curve, least-squares fit for a superposition of Hb, HbO₂, water, and fat spectra; filled circles, the FD values (error bars, $\pm 0.0005 \text{ mm}^{-1}$ or 5%, whichever is larger); dotted curve the least-squares fit when only the FD values are weighted. Physiological parameters from the SSFD spectral fit: total hemoglobin concentration, 22 μM ; oxygen saturation, 73%; water, 15 g/cm^3 ; fat, 0.75 g/cm^3 . See Table 1 for more details. Note that the fat peak between 900 and 950 nm is significantly underfitted by the FD calculation.

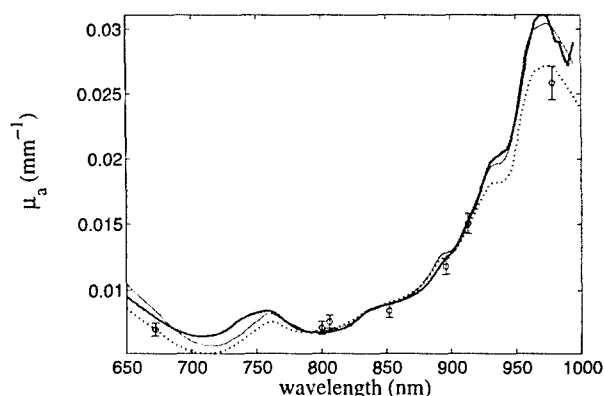


Fig. 8. μ_a predictions for the second breast measurement (areolar border; 21-year-old volunteer). Curves and circles have the same assignments as for Fig. 7. Physiological parameters: total hemoglobin concentration, 30 μM ; oxygen saturation, 70%; water, 0.51 g/cm^3 ; fat, 0.42 g/cm^3 . See Table 1 for more details.

components' concentrations. The estimates are useful for comparing one sample with another; no independent attempt to validate concentrations has been made (however, the concentrations are approximately correct in magnitude and, as we note in Section 6 below, the values are consistent with others from the recent literature^{3,15}). For comparison purposes, the dotted curves in Figs. 7–9 show the spectral fit obtained when only the FD wavelengths are weighted, as in a customary FD-only experiment. The two spectral reconstructions are clearly different, and these different reconstructions lead to different concentration estimates. All the concentration predictions, both SSFD and FD, are listed in Table 1, along with the percent deviation of the FD value from the SSFD value. The hemoglobin results are reported in terms of total hemoglobin (oxyhemoglobin plus deoxyhemoglobin) and oxygen saturation (oxyhemoglobin divided by the total).

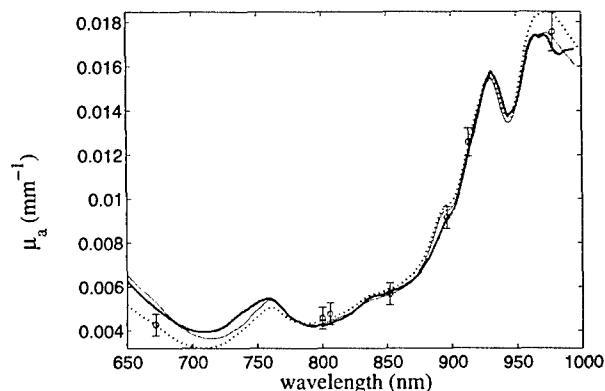


Fig. 9. μ_a predictions for the third breast measurement (inner breast; 21-year-old volunteer). Curves and circles have the same assignments as for Fig. 7. Physiological parameters: total hemoglobin concentration, 19 μM ; oxygen saturation, 72%; water, 28 g/cm^3 ; fat, 0.56 g/cm^3 . See Table 1 for more details.

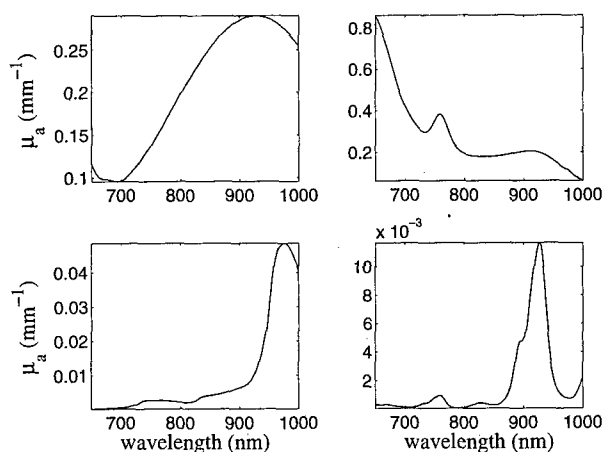


Fig. 10. Absorption spectra of major absorbers in breast tissue. Upper left, oxyhemoglobin, 1 μM ; upper right, deoxyhemoglobin, 1 μM ; lower left, water, 1 g/cm^3 ; lower right, fat (soybean oil), 0.9 g/cm^3 . The hemoglobin spectra are from Wray *et al.*,²⁷ the water is from Kou *et al.*,²⁶ and the fat is from the doctoral dissertation of Eker.²⁸

6. Discussion

To extract μ_a from a single SS reflectance spectrum, one has to convert the data into absolute units (i.e., the instrumental factor C_o must be removed) and determine μ'_s values at all wavelengths. We have demonstrated that FD measurements at a few wavelengths can accomplish these goals across the entire 650–1000-nm spectrum. This somewhat surprising result arises because $\mu'_s(\lambda)$ follows a power law, whereas C_o has no wavelength dependence at all. Two innovations that combine FD and SS methods are thus available. First, when the SS reflectance is scaled to match FD predictions of absolute reflectance, the entire reflectance spectrum is automatically calibrated. Second, fitting the FD μ'_s values to a wavelength-dependent function yields the extra information that one needs to extract μ_a from diffusion theory [Eqs. (1) and (2)]. We note that the FD-derived μ_a and μ'_s values could just as readily be

supplied by time-domain measurements at a single source–detector separation.

The interpolation of the reduced scattering spectra by use of a fit is an important component of this technique. The lower two parts of Fig. 5 show excellent agreement with the power law. The top part of the figure shows reasonably good agreement, but small discrepancies (of the order of 5–8%) can nevertheless be observed. This behavior is likely not to be an actual divergence from the power law but is probably due to a coupling effect between the scattering and absorption quantification in the FD fit. Such coupling appears when the diffusion model's assumptions are not sufficiently fulfilled. The tissue heterogeneity, i.e., the layered superficial structure and the mix of deeper fat globules and fibrous tissue, could be a possible source of deviation from the model. Interestingly, the highest fat concentration was measured for this breast location (see Table 1). As described recently by Doornbos *et al.*,¹⁵ using a power-law fit to calculate the μ'_s spectrum can in fact provide an advantage in computing μ_a . Indeed, by smoothing the spectrum, the power-law fit reduces the spurious coupling between scattering and absorption caused by inaccurate modeling.

Compared with discrete-wavelength FD measurements, access to a continuous absorption spectrum offers two important advantages: better chromophore identification and improved concentration quantification. The ability of the method to recover the continuous shape of the true absorption spectrum is evidenced by the phantom measurement. Figure 6 shows that the experimental spectrum is accurately fitted by use of known spectra of dye and water. The fitting coefficient of 1.00 for the dye additionally demonstrates the accurate recovery of chromophore concentrations.

The breast spectra (Figs. 7–9) further illustrate the usefulness of the SSFD technique for clinical investigations. As expected, the fit that uses oxyhemoglobin, deoxyhemoglobin, fat, and water accounts for most of the absorption in the 650–

Table 1. Results of Physiological Predictions for Breast Samples 1–3^a

Breast Sample Number	Component	SSFD Method	FD Method Only	Percent Difference
1	Total Hb (μM)	22	25	13
	O ₂ saturation (%)	73	78	7
	Water (g/cm^3)	0.15	0.14	–7
	Fat (g/cm^3)	0.75	0.44	–41
2	Total Hb (μM)	30	30	0
	O ₂ saturation (%)	70	79	13
	Water (g/cm^3)	0.51	0.40	–22
	Fat (g/cm^3)	0.42	0.39	–7
3	Total Hb (μM)	19	19	0
	O ₂ saturation (%)	72	81	13
	Water (g/cm^3)	0.28	0.27	–4
	Fat (g/cm^3)	0.56	0.54	–4

^aColumn 5 gives the percent difference between the FD and the SSFD values, defined as $100 \times (\text{FD} - \text{SSFD})/\text{SSFD}$.

1000-nm range in breast tissue. The quality of the fit is especially striking for wavelengths longer than 800 nm. In particular, the fat spectrum used in the fit seems accurate, matching the main peak at 928 nm and the shoulder at 895 nm. These results are surprisingly good considering that the pure-fat spectrum was measured in soybean oil.²⁸ These measurements stress the important contribution of fat to tissue absorption, as this chromophore sometimes was neglected in previous research.^{6,15} The water peak at 976 nm is also well reproduced in the measurements. We observe that the highest water content was measured for the areolar border sample (sample 2). Interestingly, we note that for both dye and breast tissue, data fits to the water spectrum of Kou *et al.* were superior to those of Hale and Querry,²⁹ particularly in the 920–960-nm regime where the water absorption spectrum increases sharply.

In the 650–800-nm region, the major features of tissue absorption are clearly due to oxyhemoglobin and deoxyhemoglobin. The deoxyhemoglobin peak at 760 nm is distinctly visible in the experimental data. Nevertheless, we observe small but consistent spectral differences, of the order of 0.001 mm^{-1} , between fit and measurement in this regime (see Figs. 7–9). These discrepancies, revealed in the full SSFD spectrum, are not evident when the FD data alone are fitted. Two reasons for the imperfect fits can be suggested. First, the oxyhemoglobin and deoxyhemoglobin absorption spectra that we used could be slightly incorrect. Indeed, small variations are found among various published spectra, and changes could be also expected between *in vitro* and *in vivo* values. Second, other, background, chromophores should probably be taken into account. For example, the tails of several protein absorption bands that were not included in the modeling might contribute to absorption in this wavelength region. A more extensive spectral library is therefore desirable for future studies. Alternatively, one could model the background empirically, either with predetermined mathematical functions of wavelength (see, e.g., Hull *et al.*¹⁴) or with a principal-component analysis of several background residuals once many samples have been studied.³⁰

For the sake of comparison, we used the same least-squares fitting algorithm to calculate the spectral fits and concentrations twice, once with the full spectrum and once with only the FD wavelengths, even though the second procedure does not fully exploit the potential of the SSFD method. Interesting differences are found between the FD and SSFD calculations. Figure 7 and Table 1 show that FD significantly underestimates the fat concentration in the first breast sample: 0.75 g/cm^3 with the SSFD as opposed to 0.44 g/cm^3 with the FD. The reason for this discrepancy lies in the fact that no laser wavelength is close enough to the fat peak (at present, commercial laser diodes at this particular wavelength are uncommon). Thus, with no weighting in this region, the FD fit tolerates large fitting errors

near the absorption maximum of fat (as illustrated in Fig. 7), leading to large errors in the fat concentration. Such a discrepancy is naturally enhanced for this sample, for which the fat concentration is highest. This example illustrates the shortcomings of using a limited number of sources (i.e., wavelengths), especially when a significant chromophore lies in an undersampled spectral region. A similar error is seen in the fitting of the areolar breast location (Fig. 8); this time it is the water peak that is poorly addressed by the FD analysis.

The total hemoglobin determination is more consistent between the FD and SSFD calculations, owing to the smoother spectral features of these chromophores and better diode coverage of the 650–850-nm regime. However, the oxygenation determination by FD is systematically higher. As discussed above, consistent small differences occur between the fit and the experiments in the 650–800-nm region because of some incompleteness in our library of fitting line shapes. Fitting the curve with a limited number of wavelengths naturally exacerbates the incompleteness and produces a bias in the results.

As mentioned above, Cubeddu *et al.*,³ working in the time domain, obtained similar optical properties and physiological parameters for premenopausal breast. Conceptually, the two experiments exploit the same optical phenomena and are essentially complementary techniques in different domains. A technical advantage of the SSFD measurement is the use of a white-light source rather than a tunable laser. Thus the SS measurement covers all wavelengths simultaneously, whereas the laser(s) must be tuned separately to each wavelength.³ Additionally, the heart of the SSFD system (a few laser diodes, a frequency generator, an avalanche photodiode, a network analyzer or lock-in amplifier, and a SS reflectance system) is inexpensive and easy to maintain compared with a tunable laser system and a single-photon-counting detection apparatus.

As was already stated, the method presented here has the advantage of being compatible with a single, large source–detector separation ($\gg 10$ transport mean free paths). In contrast to spatially resolved methods, it is well suited for interrogating deep structures in relatively heterogeneous samples. As numerous authors have shown,^{15,31,32} the layered structure of tissue affects reflectance differently at different source–detector separations, raising doubts about the applicability of spatially resolved techniques that assume sample homogeneity over a large range. Whereas variations in the FD modulation frequency ω do change the optically explored tissue volume, these effects are modest in comparison with changes in ρ , particularly at high absorption.²¹ Consequently, the assumption of homogeneity is less extreme for the single-distance measurements proposed here: Its essence is that all measurements at one wavelength explore a more consistent volume; this does not

mean that different wavelengths will explore the same volume. Indeed, less-absorbed wavelengths will explore larger regions than wavelengths that attenuate more rapidly.

7. Conclusion

A combination of SS and FD reflectance measurements has been described for absorption spectroscopy of turbid media; beneficial aspects of both techniques have been described. As with SS, the wavelength coverage is continuous, detecting absorption features that may not be discernable in the discrete wavelengths chosen for FD. The prediction of constituent concentrations, for instance, in breast tissue, is substantially improved when full-spectrum absorption data rather than a handful of wavelengths are used. As with FD, however, only a single source-detector separation is required, making the technique more amenable to reporting volume-averaged values for heterogeneous samples. In addition, the source-detector separation can be large, allowing for centimeter-scale mean probing depths that cannot be achieved with spatially resolved SS techniques. This advantage for deeply probing studies is significant for many clinical purposes. An application to breast analysis has been demonstrated, with quantitative *in vivo* spectra of human breast obtained rapidly (<1 min). The total hemoglobin content, oxygen saturation, and water and fat content of the breast samples have been calculated from the spectra, and failures of FD-only fitting have been highlighted. The technique is relatively inexpensive and could prove valuable for improving accuracy in the development of quantitative photon migration for clinical instruments.

This study was supported by the National Institutes of Health under grants GM50958 and RR01192 (Laser Microbeam and Medical Program), the U.S. Department of Energy (grant DE-FG03-91ER61227), and the U.S. Office of Naval Research (grant N00014-91-C-0134). The authors gratefully acknowledge postdoctoral fellowships: A. J. Berger from the George E. Hewitt Foundation for Medical Research; F. Bevilacqua from the Swiss National Science Foundation; and A. E. Cerussi from the U.S. Army (grant DAMD17-98-1-8186). We used the facilities and support of the Avon Breast Center of the Chao Family Comprehensive Cancer Center at the University of California, Irvine, to complete clinical portions of this study.

References

1. M. S. Patterson, B. Chance, and B. C. Wilson, "Time resolved reflectance and transmittance for the noninvasive measurement of tissue optical properties," *Appl. Opt.* **28**, 2331-2336 (1989).
2. A. Kienle and M. S. Patterson, "Improved solutions of the steady-state and the time-resolved diffusion equations for reflectance from a semi-infinite medium," *J. Opt. Soc. Am.* **14**, 246-254 (1997).
3. R. Cubeddu, A. Pifferi, P. Taroni, A. Torricelli, and G. Valentini, "Noninvasive absorption and scattering spectroscopy of bulk diffusive media: an application to the optical characterization of human breast," *Appl. Phys. Lett.* **74**, 874-876 (1999).
4. B. W. Pogue and M. S. Patterson, "Frequency-domain optical absorption spectroscopy of finite tissue volumes using diffusion theory," *Phys. Med. Biol.* **39**, 1157-1180 (1994).
5. S. Fantini, M. A. Franceschini-Fantini, J. S. Maier, S. A. Walker, B. Barbieri, and E. Gratton, "Frequency-domain multichannel optical detector for noninvasive tissue spectroscopy and oximetry," *Opt. Eng.* **34**, 32-42 (1995).
6. J. B. Fishkin, O. Coquoz, E. R. Anderson, M. Brenner, and B. J. Tromberg, "Frequency-domain photon migration measurements of normal and malignant tissue optical properties in a human subject," *Appl. Opt.* **36**, 10-20 (1997).
7. T. H. Pham, O. Coquoz, J. B. Fishkin, E. Anderson, and B. J. Tromberg, "Broad bandwidth frequency domain instrument for quantitative tissue optical spectroscopy," *Rev. Sci. Instrum.* **71**, 2500-2513 (2000).
8. L. Reynolds, C. Johnson, and A. Ishimaru, "Diffuse reflectance from a finite blood medium: applications to the modeling of fiber optic catheters," *Appl. Opt.* **15**, 2059-2067 (1976).
9. T. J. Farrell, M. S. Patterson, and B. C. Wilson, "A diffusion theory model of spatially resolved, steady-state diffuse reflectance for the noninvasive determination of tissue optical properties *in vivo*," *Med. Phys.* **19**, 879-888 (1992).
10. A. Kienle, L. Lilge, M. S. Patterson, R. Hibst, R. Steiner, and B. C. Wilson, "Spatially resolved absolute diffuse reflectance measurements for noninvasive determination of the optical scattering and absorption coefficients of biological tissue," *Appl. Opt.* **35**, 2304-2314 (1996).
11. R. Bays, G. Wagnières, D. Robert, D. Braichotte, J.-F. Savary, P. Monnier, and H. van den Bergh, "Clinical determination of tissue optical properties by endoscopic spatially resolved reflectometry," *Appl. Opt.* **35**, 1756-1766 (1996).
12. R. A. Weersink, J. Hayward, K. Diamond, and M. Patterson, "Accuracy of noninvasive *in vivo* measurements of photosensitizer uptake based on a diffusion model of reflectance spectroscopy," *Photochem. Photobiol.* **66**, 326-335 (1997).
13. F. Bevilacqua, D. Piguet, P. Marquet, J. Gross, B. Tromberg, and C. Depeursinge, "In vivo local determination of tissue optical properties: applications to human brain," *Appl. Opt.* **38**, 4939-4950 (1999).
14. E. L. Hull, M. G. Nichols, and T. H. Foster, "Quantitative broadband near-infrared spectroscopy of tissue-stimulating phantoms containing erythrocytes," *Phys. Med. Biol.* **43**, 3381-3404 (1998).
15. R. M. P. Doornbos, R. Lang, M. C. Aalders, F. W. Cross, and H. J. C. M. Sterenberg, "The determination of *in vivo* human tissue optical properties and absolute chromophore concentrations using spatially resolved steady-state diffuse reflectance spectroscopy," *Phys. Med. Biol.* **44**, 967-981 (1999).
16. B. J. Tromberg, O. Coquoz, J. B. Fishkin, T. Pham, E. R. Anderson, J. Butler, M. Cahn, J. D. Gross, V. Venugopalan, and D. Pham, "Non-invasive measurements of breast tissue optical properties using frequency-domain photon migration," *Phil. Trans. R. Soc. London* **352**, 661-668 (1997).
17. A. Ishimaru, *Wave Propagation and Scattering in Random Media* (Academic, Orlando, Fla., 1978).
18. J. B. Fishkin and E. Gratton, "Propagation of photon-density waves in strongly scattering media containing an absorbing semi-infinite plane bounded by a straight edge," *J. Opt. Soc. Am.* **10**, 127-140 (1993).
19. B. J. Tromberg, L. O. Svaasand, T.-T. Tsay, and R. C. Haskell, "Properties of photon density waves in multiple-scattering media," *Appl. Opt.* **32**, 607-616 (1993).
20. S. Fantini, M. A. Franceschini, J. B. Fishkin, B. Barbieri, and E. Gratton, "Quantitative determination of the absorption

- spectra of chromophores in strongly scattering media: a light-emitting-diode based technique," *Appl. Opt.* **33**, 5204–5213 (1994).
21. R. C. Haskell, L. O. Svaasand, T.-T. Tsay, T.-C. Feng, M. S. McAdams, and B. J. Tromberg, "Boundary conditions for the diffusion equation in radiative transfer," *J. Opt. Soc. Am.* **11**, 2727–2741 (1994).
 22. W. H. Press, S. A. Teukolsky, W. T. Vetterling, and B. P. Flannery, in *Numerical Recipes in C: The Art of Scientific Computing*, 2nd ed. (Cambridge U. Press, Cambridge, 1993), Chap. 15, pp. 683–688.
 23. R. Graaff, J. G. Aarnoose, J. R. Zijp, P. M. A. Sloot, F. F. M. de Mul, J. Greve, and M. H. Koelink, "Reduced light-scattering properties for mixtures of spherical particles: a simple approximation derived from Mie calculations," *Appl. Opt.* **31**, 1370–1376 (1992).
 24. J. R. Mourant, T. Fuselier, J. Boyer, T. Johnson, and I. J. Bigio, "Predictions and measurements of scattering and absorption over broad wavelength ranges in tissue phantoms," *Appl. Opt.* **36**, 949–957 (1997).
 25. J. M. Schmitt and G. Kumar, "Optical scattering properties of soft tissue: a discrete particle model," *Appl. Opt.* **37**, 2788–2797 (1998).
 26. L. H. Kou, D. Labrie, and P. Chylek, "Refractive indices of water and ice in the 0.65- to 2.5- μm spectral range," *Appl. Opt.* **32**, 3531–3540 (1993).
 27. S. Wray, M. Cope, D. T. Delpy, J. S. Wyatt, and E. O. R. Reynolds, "Characterization of the near-infrared absorption spectra of cytochrome-AA3 and hemoglobin for the non-invasive monitoring of cerebral oxygenation," *Biochim. Biophys. Acta* **933**, 184–192 (1988).
 28. C. Eker, *Optical Characterization of Tissue for Medical Diagnostics*, Ph.D. dissertation (Lund University, Lund, Sweden, 1999).
 29. G. M. Hale and M. R. Querry, "Optical constants of water in the 200-nm to 200- μm wavelength region," *Appl. Opt.* **12**, 555–563 (1973).
 30. A. J. Berger, T.-W. Koo, I. Itzkan, and M. S. Feld, "An enhanced algorithm for linear multivariate calibration," *Anal. Chem.* **70**, 623–628 (1998).
 31. G. Alexandrakis, T. J. Farrell, and M. S. Patterson, "Accuracy of the diffusion approximation in determining the optical properties of a two-layer turbid medium," *Appl. Opt.* **37**, 7401–7409 (1998).
 32. M. A. Franceschini, S. Fantini, L. A. Paunescu, J. S. Maier, and E. Gratton, "Influence of a superficial layer in the quantitative spectroscopic study of strongly scattering media," *Appl. Opt.* **37**, 7447–7458 (1998).

Spectroscopy enhances the information content

of optical mammography

A. E. Cerussi¹, D. Jakubowski¹, N. Shah¹, F. Bevilacqua¹, R. Lanning¹, A. J. Berger⁴,
D. Hsiang², J. Butler², R. F. Holcombe³, and B. J. Tromberg¹

¹ Beckman Laser Institute and Medical Clinic
University of California, Irvine
1002 Health Sciences Rd.
Irvine, CA 92612

² Department of Oncological Surgery
University of California, Irvine Medical Center
101 The City Dr.
Orange, CA 92868

phone: (949) 824-4713 / fax: (949) 824-8413

phone: (714) 456-8030 / fax: (714) 456-7244

³ Division of Hematology/Oncology
University of California, Irvine Medical Center
101 The City Dr.
Orange, CA 92868

⁴ Present address: Institute of Optics
University of Rochester
Wilmot 418
Rochester, NY 14627

phone: (714) 456-5153 / fax: (714) 456-2242

phone: (716) 273-4724 / fax: (716) 244-4936

*corresponding author: tromberg@bli.uci.edu

ABSTRACT

Near infrared (NIR) diffuse optical spectroscopy and imaging may enhance existing technologies for breast cancer screening, diagnosis, and treatment. NIR techniques are based on quantitative measurements of functional contrast between healthy and diseased tissue. In this study we measured the spectral dependence of tissue absorption (μ_a) and reduced scattering (μ_s') in the breasts of 30 healthy women and one woman with a fibroadenoma using a seven-wavelength frequency-domain photon migration probe. Subjects included pre- and post-menopausal women between the ages of 18 and 64.

Multi-spectral measurements were used along with a four-component fit to determine the concentrations of de-oxy and oxy-hemoglobin, water and lipids in breast. The scattering spectral shape was also quantified. Our measurements demonstrate that the measured concentrations of NIR analytes correlate well with known breast physiology. Although the tissue scattering at a single wavelength was found to have little value as a functional parameter, the dependence of the scattering on wavelength provided key insights into breast composition and physiology. Lipids and scattering spectra in the breast were found to increase and decrease respectively with increasing body mass index. Simple calculations are also provided to demonstrate potential penalties from ignoring the contributions of water and lipids in breast measurements. Finally, water is shown to be a possible indicator for detecting a fibroadenoma whereas the hemoglobin saturation was found to be a poor indicator. Multi-spectral measurements, compared to measurements restricted to one or two wavelengths, provide additional information that may be useful in managing breast disease.

keywords

breast, photon migration, breast optics, quantitative NIR spectroscopy,
non-invasive, diaphanography

I. INTRODUCTION

I.a. The Role of optics

Near-infrared (NIR) photon migration spectroscopy provides quantitative functional information from breast tissue that cannot be obtained by conventional radiologic techniques. NIR techniques are sensitive to several important physiological components in tissue such as hemoglobin and water. In the clinical management of breast disease, such functional information suggests a variety of potential medical applications: therapeutic monitoring (angiogenesis, chemotherapy), supplemental lesion characterization (benign versus malignant), and risk assessment (origins of breast density). A non-invasive optical imaging technique that provides unique, quantitative physiological information can greatly enhance current screening and diagnostic monitoring for the breast. Emerging techniques for the breast such as magnetic resonance imaging and positron emission tomography have shown promise in providing functional images. However, these techniques are costly, cumbersome, and rely upon the use of contrast agents. On the contrary, NIR techniques may be used with either endogenous or exogenous contrast, and can be fashioned into inexpensive and portable systems.

I.b. A History of early breast optics

Although white-light transillumination was introduced into medicine in the early 1800's, it was not until 1929 that the technique was formally applied as a tool to visualize the shadows cast by breast lesions [1]. Carlsen introduced spectral breast imaging in 1980 by restricting the light source of a medical transillumination imager to red and NIR bands [2]. Images consisted of the

ratios between red and NIR light traveling through the breast. Throughout the 1980's there were a variety of clinical trials attempting to compare various transillumination/diaphanography¹ instruments with mammography as a screening tool; a potpourri of conflicting clinical conclusions was the result. Some studies, most notably those of Bartrum *et al.* [3], Wallberg *et al.* [4], and Budred *et al.* [5], have shown very favorable results comparing optical and radiographic devices as screening tools. Other studies, most notably by Drexler *et al.* [6], Monsees *et al.* [7], and Alveryd *et al.* [8] have shown quite the opposite. Such studies, and in particular the one by Alveryd *et al.* dissuaded further development of the technique, as evidenced by the refusal of insurance companies to offer coverage for optical breast exams.

Many reasons have been cited to explain the failures of these early optical methods to detect and to classify breast lesions. Some cited study-dependent issues such as poor operator experience and inadequate statistical analysis. More seriously, there were physical limitations such as inadequate light penetration, poor dynamic range, inadequate spatial resolution, uncorrected geometrical and boundary effects, and tissue scattering. Clinically, the physical limitations of diaphanography manifested as very high false positive rates as well as low true positive rates. Although the highly scattering nature of tissues could never allow resolution comparable to radiography, the early stages of optical breast exams relied upon direct visualization of the lesion [9]. Although direct visualization of lesion anatomy is difficult, if not impossible with visible/NIR optics, *spectroscopic* visualization of tissue function is an entirely different matter.

¹ The literature is often vague in distinguishing transillumination/lightscanning from diaphanography. Typically, transillumination refers to white-light illumination, whereas diaphanography refers to red & NIR illumination.

1.c. The Importance of spectroscopy

Recent developments in functional methods such as diffuse optical spectroscopy (DOS) and diffuse optical tomography (DOT) offer distinct advantages over traditional diaphanography. DOS may be used to quantify tissue biochemical composition. For example, dual-wavelength spectroscopy has been widely used to determine the absorption coefficient (μ_a) and hence the concentrations of reduced hemoglobin (Hb-R) and oxygenated hemoglobin (Hb-O₂) in tissue [10]. However, NIR light absorption in breast is due to more than just hemoglobin [11]. Although water and lipid are weak NIR absorbers, their high abundance in breast tissue relative to hemoglobin translates into significant absorption, particularly in the 900-1000 nm range [11],[12],[13]. Moreover, the balance of water and lipid in the breast depend on factors such as age and hormonal status. A complete physiological picture of breast requires knowledge of this balance [14],[15]. Restricting measurements to only two wavelengths to measure Hb-R and Hb-O₂, compromise both the accuracy and completeness of tissue characterization.

The spectral dependence of tissue scattering in its own right may also contain important functional information. Tissues scatter NIR light very strongly, such that the separation of reduced scattering (μ_s') from absorption is critical for extracting the true absorption spectrum of the tissue. Although the distribution of NIR scattering centers in tissue is not well understood, multi-spectral NIR measurements of μ_s' have shown a relationship between scattering and wavelength [16],[17]. Spectral measurements of tissue scattering may provide information about the types of scattering centers found in a given region of tissue, and in turn provide information about tissue cellularity [18], composition [19], and disease state [20].

thus demonstrating the feasibility of NIR methods for breast cancer screening and detection [29][30][31][32]. Simultaneous acquisition of multi-spectral information is also being considered [33].

In recent years NIR tissue spectroscopy has been used to study healthy breast tissue and changes that occur with age, hormone use, and other factors. Kang *et al.* apparently supplied one of the first *in vivo* optical measurements of breast tissue [34]. Suzuki *et al.* performed time-resolved spectroscopy at a single wavelength to detect changes in optical properties as a factor of age [35], menopause and body mass index (BMI) [36]. Heusmann *et al.* measured the effects of water in normal breast tissues using incomplete published scattering curves [37]. Quaresima *et al.* measured the intra- and inter-subject variability of the optical properties of healthy women using second-derivative spectroscopy, again using published scattering data [12]. Cubbedu *et al.* studied physiological changes in breast optical properties during the five phases of the menstrual cycle using a time-resolved, multi-spectral approach [13].

I.e. The Scope of this work

We believe that the key to the success of optical methods in breast lies in the spectroscopic content of the optical signals. Common procedure has been to compare the optical properties of diseased tissue to "normal" breast tissue. "Normal" breast tissue is a vague concept, given the frequency and magnitude of changes that occur over a variety of time scales. Despite this fact, there is a scarce amount of information available on the optical signature of non-diseased breast tissue. The physiology of healthy breast tissue is complex, influenced by multiple internal and external factors such as menstrual cycle, menopause, exogenous hormones, lactation and

Early studies have shown that red and NIR light absorption in breast is highly sensitive to hemoglobin [21][22]. However, the presence of blood alone is not sufficient criteria for the diagnosis of cancer, a weakness that probably contributed to the high false positive rate of diaphanography. Neglecting scattering diminishes contrast even further. Additional information about metabolism and water content may be the key to avoiding poor sensitivity and specificity. Limiting measurements to a few wavelengths greatly limits sensitivity, and does not take advantage of the full capabilities of optical spectroscopy.

I.d. Modern breast optics

Continuous wave, fixed distance methods (i.e., source detector separation) measure light attenuation. Recent advances in the understanding of the propagation of pulsed light in multiply-scattering media such as tissues have provided methods to separate μ_s and μ_a in both the time [23] and frequency domains [24]. Scattering values for breast lesions have been measured *in vivo* to be both lower [25][19] and higher [19] than normal tissue. The nature of these differences is not clear.

Prototype commercial instruments have implemented raw intensity [26], [27] because it is simple and inexpensive. One commercial device used a frequency-domain correction for breast thickness, which dramatically improved their results [28]. Modern time-resolved and frequency-domain NIR spectroscopy can monitor tissue physiological activity such as hemoglobin saturation and thereby distinguish between diseased and healthy tissue upon a functional basis. Such techniques have quantified the metabolism of small palpable lesions *in vivo* in humans,

pregnancy. Some of these changes have been monitored qualitatively by mammography and magnetic resonance imaging [38], [39], [40].

This paper represents a continuing effort to quantify the composition and function of breast tissue using NIR spectroscopy. All of the 30 healthy subjects we studied had not manifested any forms of breast disease at the time of the measurement. We have shown that both absorption and scattering spectral signatures provide important clues about the functional state of breast tissue. Such information may prove critical to the advancement of modern biomedical optics in the breast, and improve upon measurements of intensity alone [26]. In addition, we provide broadband spectroscopic measurement of a fibroadenoma *in vivo*, demonstrating the enormous contrast available to multi-spectral optical measurements.

II. MATERIALS AND METHODS

II.a General Approach

The dependence of the chromophore concentration on the absorbance of light is $AB = \epsilon [c] l$, where ϵ is the molar extinction coefficient ($M^{-1} cm^{-1}$), $[c]$ is the concentration of chromophore c ($M L^{-1}$), and l is the photon path length (cm). l is increased by scattering and is not known *a priori*. Time-resolved and phase-sensitive methods that measure the time-course of photons (or equivalently, l) have been used to separate the effects of absorption and scattering on the attenuation of light [23], [24]. The absorption coefficients translate into tissue chromophore concentrations using the equation:

$$\mu_a = 2.303\epsilon[c] \quad (1)$$

The factor of 2.303 originates from the base conversion between the logarithm for absorbance and the natural logarithm for μ_a .

II.b Measurement of Absorption and Scattering

The theory of frequency-domain photon migration (FDPM) is based upon the formation, the propagation, and the characterization of density waves of individual photons inside a multiply scattering medium. The technical aspects of this theory have been discussed in the literature [41], [42]. The behavior of these photon density waves (PDW) is mediated by two wave characteristics, (frequency, f (MHz) and distance traveled, r (mm)), and two media characteristics (μ_a and μ_s). The modulation frequency is the rate at which a light source is turned on and off and has nothing to do with the energy or color of the light.

Our typical experimental configuration is to measure the real and imaginary parts of this wave at a fixed distance between light source and optical detector over a range of source modulation frequencies, ranging from 50 to 1000 MHz. For the purposes of physical intuition, we may translate these real and imaginary parts of the photon density, U (photons per cubic mm), into the amplitude (ψ) and phase (ϕ) of the photon density wave:

$$\psi = \sqrt{\text{Re}(U)^2 + \text{Im}(U)^2} \quad (2)$$

$$\phi = \arctan\left(\frac{\text{Im}(U)}{\text{Re}(U)}\right) \quad (3)$$

The frequency-domain expression for U is given by the P_I approximation to the Boltzmann Transport equation [43], [44]. We selected the P_I model over the standard diffusion model because the P_I approximation has a more accurate frequency response at higher modulation frequencies and introduces little additional complexity. The model geometry used in this paper was a semi-infinite medium, where the solution was obtained by using the method of images for the infinite medium solution along with an extrapolated boundary [23]. The index of refraction mismatch was taken into account using the empirical polynomial fit of Groenhuis *et al.* [45] and assuming a tissue index of refraction of 1.4 [46]. We assume that both μ_r and μ_s' represent a macroscopically homogeneous average value of the tissue that is sampled by the light.

IIc Fitting Considerations

By fitting instrument-corrected data to the appropriate physical model, we can recover μ_r independently from μ_s' for the tissue. We typically fit data from 100 to 700 MHz while keeping r fixed at 22 mm in order to recover μ_r and μ_s' . A Levenberg-Marquardt minimization algorithm was adapted to fit simultaneously both the real and imaginary (i.e., phase and amplitude analogs) parts of the signal by minimizing a χ^2 merit function. Several initial guesses were used in order to verify that the minimum χ^2 was not strictly a local minimum. Figure 1 presents an example of the fitting procedure. The frequency-domain P_I model of light transport was fit from 100 to 700 MHz to the imaginary and real parts of the measured PDW in panel (a). Application of Eqs. (2) and (3) transform these quantities into the more tangible wave amplitude and phase in panel (b).

Instrumentation artifacts such as cable length and source strength variability introduce additional unwanted phase shifts and amplitude decreases. These artifacts may be removed by calibrating the measured PDW phase and amplitude with the phase and amplitude of light detected in a tissue-simulating phantom with known optical properties. Such a calibration scheme is similar in spirit to the lifetime referencing calibration that is routinely performed in frequency-domain fluorescence-lifetime instruments.

Error bars in our results represent the result of many separate measurements and calibrations. In a typical measurement, we measured the tissue several times, and then measured the phantom several times. This procedure provided precision errors that emerge from coupling variability between the probe to the phantom and from the probe to the tissue. The biggest variation in our measurements was due to the variability in coupling to the phantom.

We also made use of some *a priori* information in order to reduce fitting errors. In the NIR it is well known that scattering follows a simple power-law dependence of the form:

$$\mu_s' = A\lambda^{-SP} \quad (4)$$

where A is a constant and SP , the magnitude of the exponent, is the scatter power. Outlier scattering points, as judged arbitrarily by a robust non-linear fit of μ_s' , were constrained to fit the line described by Eq. (4). [47]. The real and imaginary components were then re-fit, while keeping μ_s' fixed.

II.d Calculation Tissue Physiology: Absorption

Knowledge of the absorption spectrum provides the information needed to solve a weighted least-squares problem to recover the concentrations of the four principal NIR absorbers in tissues: Hb-R, Hb-O₂, H₂O, and lipids. We assume that other NIR chromophores such as myoglobin are negligible in breast tissue. The term 'weighted' refers to weighting the value of μ_a with its measured error. The least-squares problem expressed as a matrix takes the general form:

$$\bar{\mu} = \mathbf{E} \bar{c} \quad (5)$$

where $\bar{\mu}$ is a vector of length N containing the measured μ_a values and \bar{c} is a vector of length M containing the chromophore concentrations. The matrix \mathbf{E} has dimensions $N \times M$ and contains the extinction coefficients ($\text{cm}^2 \text{M}^{-1}$) for the M chromophores at each of the N wavelengths. To convert traditional literature molar extinction coefficients ($\text{cm}^{-1} \text{M}^{-1}$) into extinction coefficients for use in Eq. (5), multiply ϵ by 23030. Since it is difficult to quantify lipids in terms of a concentration, the molar extinction coefficients were used as $\text{cm}^2 \text{Kg}^{-1}$.

The general solution to the matrix problem expressed in Eq. (5) is

$$\bar{c} = (\mathbf{E}^T \mathbf{E})^{-1} \mathbf{E}^T \bar{\mu} \quad (6)$$

The extinction values for both Hb-R and Hb-O₂ were acquired from the work of S. Wray *et al.*, who used lysed cells in a non-scattering medium [48]. The extinction values for water were interpolated from the work of Hale and Querry [49]. Finally, values for lipids were obtained from Eker, who measured the absorption of soybean oil [50]. We have found using CW spectroscopy that the water spectrum provided by Kou *et al.* provides an overall better spectrum

for use in tissue optics studies, although it did not change the essence of our results for the FDPAM wavelengths used in this work [51].

For each measurement we report four hemoglobin parameters: [Hb-R], [Hb-O₂], total hemoglobin concentration (THC), and the hemoglobin saturation (SO_2), where:

$$THC = [\text{Hb-R}] + [\text{Hb-O}_2] \quad (7)$$

$$SO_2 = \frac{[\text{Hb-O}_2]}{[\text{Hb-R}] + [\text{Hb-O}_2]} \quad (8)$$

Values for water and lipid content are reported as percentages. The water fraction is the concentration of measured tissue water divided by the concentration of pure water (55.6 M). The lipid percentage absorption of lipid measured relative to an assumed 'pure' lipid density of 0.9 g mL^{-1} . Thus, the reported water and lipid percentages are relative figures of merit compared to pure solutions of the substance, and neither are strict volume or mass fractions, nor add to 100%.

II.e Measured Tissue Physiology: Scattering

The scattering properties of the tissue also may yield important physiological information. As an example, when the particle size is much smaller than the optical wavelength, SP approaches the Rayleigh limit of -4 . In this work, the magnitude of the slope is referred to as the "scatter power." Intralipid, which is a intravenous fat emulsion that is commonly used as a tissue phantom, has globules of soybean oil that are on average about 97 nm, and yield a value of scatter power of 2.4 [52]. Nilson *et al.* provided an empirical link between scatter power and the

average particle size [53]. This value is not rigorous, but may provide meaningful insight into the origin of the tissue scattering, and ultimately the composition and structure of the breast.

II.f Instrumentation

The specific details of this FDPM instrument has been described in detail elsewhere [54], but the relevant technical information is mentioned here. The instrument employs seven diode lasers that provided visible and NIR light (672, 800, 806, 852, 896, 913, and 978 nm). A hand-held probe housed an avalanche photodiode (APD) that recorded the modulated diffuse light signals after propagating through the tissue. This probe has a plastic attachment on the casing to position a source optical fiber 22 mm away from the APD. The optical power launched into the tissue ranged from 5–25 mW. A sweep over all seven wavelengths ranged from approximately 35 to 60 s. The system acquired data in less than 3 s per wavelength, with a 2 s delay between each laser diode in the system because of switching considerations. The system was wheeled into a medical clinic for the each measurement.

One additional measurement was performed using a steady-state (SS) spectrometer system in conjunction with the FDPM instrument. The technique, known as steady-state FDPM (SSFDPM), has been described in detail elsewhere [55]. In short, the SS system interpolates values of μ_s between the discrete FDPM measurements.² The SS system utilizes a separate

² The NIR scattering spectrum power law dependence (i.e., Eq. (4)), renders μ_s' known at all wavelengths of interest. Removing μ_s' from the problem facilitates the calculation of μ_s from the steady-state spectrum. See reference #55 for details.

plastic handheld probe in which were embedded a source fiber and a detector fiber. The probe fixed the distance between these fibers at 22 mm. Spectra were recorded from 650 to 1000 nm in 2 nm increments, using a 1 s integration time. The system was calibrated using an integrating sphere.

II.g Measurement Procedure

All of the subjects we measured in this study provided informed consent to participate in one of two trials (#95-563 and #99-2183) that were approved by the Internal Review Board of the University of California at Irvine. All 31 subject ages ranged between 18 and 64. Each subject was in a supine position during the measurement. As outlined above, the instrument probe was the only item placed in contact with the subject. All measurements were performed in a reflection geometry, where we estimate the average depth of penetration was approximately 1 cm below the skin. The probe was placed onto the breast by using the force of gravity as pressure. No compression was used during the measurement. We performed measurements on normal subjects in the center of each of the four quadrants of each breast. Data from the left upper outer quadrant is presented here, although the data presented here is representative of other sites.

One SSFDPM measurement was also performed upon a 37-year-old woman with a lesion located in the upper inner quadrant of her left breast (Figure 2a). The subject was post-menopausal surgically since age 28. Prior fine-needle aspiration confirmed the lesion to be a fibroadenoma. The lesion dimensions were determined by conventional clinical ultrasound at the time of the SSFDPM measurement to be approximately 19 by 19 by 10 mm at a depth of 11 mm below the skin. SSFDPM measurements were performed at seven discrete positions in a line on the skin

Figure 2b. FDPMP measurements were first performed along the 7 points, and then followed by SS measurements at the same locations. This process was repeated for the same location on the healthy breast. Only the line scan from medial to lateral is presented here.

III. RESULTS

III.a. Measurement of water and lipids in vivo

Age-dependent changes in water and lipid fractions are presented in Figure 3 and Figure 4, respectively. Premenopausal subjects (i.e., age <50) display a variety of values. Inter-subject variations include, but are not limited to, menstrual cycle differences and gynecological age. The same general trend occurs in the THC [15]. The water seems to increase in pre-menopausal subjects (ages 18 to 39), perhaps reaching a peak value near the age of 30. Between the ages of 40 to 49, water seems to decline. After age 50 (predominantly post-menopausal) there is a general decrease with age in water, and an increase in lipids. Error bars represent the results of repeated measurements. The late decrease in THC and water correlates well the atrophy of well-vascularized lobular tissue and the increase of the fat-to-collagen ratio after menopause [14]. Compositional analysis data show lower blood and water content for fat versus glandular tissue [56].

Measured lipid and scatter power are presented as functions of body-mass index (BMI) in Figure 5 and Figure 6, respectively. The BMI scale is determined by dividing body mass (Kg) by height squared (m^2), and numbers between 20-25 are considered normal [57]. The histograms

represent an average over all BMI values within a single BMI unit. The error bars represent the subject variation within a given BMI bin. There is a general correlation between lipid mass density with BMI. Overall body mass and breast mass are not perfectly correlated, so that this correlation is not expected to be perfect. Collagen-rich glandular tissue scatters light with a higher scatter power than adipose tissue [58]. Thus, smaller scatter powers are expected in fatty tissue. In the post-menopausal breast the ratio of adipose to glandular tissue generally decreases, which should result in a lower scatter power. Such an interpretation may not be valid given that the amount of collagen in each breast is not known. However, it should be emphasized that the scattering and the absorption information together provide a consistent picture of the components in the breast.

III.b. Spectral content in scattering

Figure 7 and Figure 8 further support the idea that tissue scattering spectra provides important physiological content. In Figure 7, the measured scattering at 800 nm does display a clear pattern that may provide any significant information content. The scattering spectral dependence, however, tells a different story. Figure 8 clearly demonstrates that the scattering spectrum (i.e, scatter power), shows a marked decrease as a function of age. Again, we expect that breasts full of highly scattering, collagen-rich tissue would display a higher scatter power than breasts with more adipose.

III.c. Effect of water and lipids in breast

All of the previous figures demonstrate the highly variable, but physiologically intuitive, amounts of water, lipids, and scatter power found in normal breast tissue. The next two Figures demonstrate how neglecting an individual's water and lipid content affects measurements of breast THC and S_tO_2 . The following calculations represent the percent deviation between the "true" values and the values one would measure using only μ_a at 672, 806, and 849 nm, three abovementioned wavelengths; note that the "abs %" refers to an absolute change in S_tO_2 , i.e., 80 to 85%. Panels (a) and (b) present the THC and S_tO_2 respectively of a pre-menopausal breast, assuming that $THC = 27.4 \mu M$ and $S_tO_2 = 76.6\%$. Panels (c) and (d) provide the same information, but for a post-menopausal breast using $THC = 14.6 \mu M$ and $S_tO_2 = 82.2\%$.³ Figure 9 ignores entirely the contribution of water and lipids, whereas Figure 10 assumes a background value of water and lipids, using 33% and 44% for the pre-menopausal breast in (a) and (b), and 19% and 61% for the post-menopausal breast in (c) and (d), respectively.³

Figure 9 readily displays that serious errors may result by ignoring contributions from water and lipids. Values of water are provided over a wide range for three different lipid fractions; the three lines represent lipid fractions of 20, 45, and 70%, in ascending order. Water is highly variable in breast, leading from anywhere between 10-30% overestimation of THC (panel (a)) and 2-6% rise in S_tO_2 (panel(b)). The effect is even more pronounced in the post-menopausal case (panels (c) and (d)), where the error in THC and S_tO_2 jump to higher errors.

³ These average values are based upon averages measured in our trial.

Figure 10, which assumes reasonable background water and lipid values reflective of our measurements in both pre- and post-menopausal cases, has some definite improvements. Of course, if the true water and lipid content is close to the assumed background value, the error is small. The effect of the background is to shift the error curves from always positive, to both positive and negative estimations of THC and S_tO_2 . The errors may be significant if the assumed value differs significantly from the true value.

III.d Fibroadenoma as an example

Figure 11 and Figure 12 display the results of SSFDPM measurements performed over regions of normal and diseased tissue. In both figures, triangles represent measurements performed on or near the site of the fibroadenoma, whereas the squares represent measurements performed on the healthy breast in the same anatomical site as the fibroadenoma. The THC in Figure 11 is higher over the fibroadenoma, and slightly decreased relative to normal outside the lateral extent of the lesion. Figure 12 provides a more convincing case, but this time in water fraction. Although not shown, the lipid fraction takes a similar course, though to a lesser extent; the lipid fraction on the fibroadenoma was about 5% lower than over normal tissue. Equally important is the fact that S_tO_2 (i.e., Figure 13) decreases only slightly over the fibroadenoma site, and may not provide enough contrast by itself for detection. Interestingly, the largest decreases in S_tO_2 occur near the fibroadenoma boundaries.

IV. DISCUSSION

IV.a Spectroscopy is the key

The results presented in this work strongly suggest that the spectral signature of diffuse optical signals provide distinctive functional information in the breast. It is not surprising that the pre- and post-menopausal breast display the physiological trends that we have observed. Regardless, it should be stressed that we have been able to quantify these functional changes non-invasively.

A single wavelength of light may be used to detect some breast lesions, but it will not compete with the spatial resolution offered by conventional techniques. However, by providing spectroscopic information about a suspicious region of tissue, optics may prove useful in the management of breast disease. Note that the advantages of spectroscopy are not solely restricted to measurements of μ_a ; the spectral dependence of μ_s' also contains important information. Tissue absorption and scattering information together appear to paint a more complete picture of the tissue composition than direct measurements of optical attenuation.

We have demonstrated that our measurements at seven discrete wavelengths are enough to account for the blood, water and lipid content of breast. Instruments restricted to two or three wavelengths sacrifice important spectroscopic information. It is fortunate that two of the diodes, namely at 913 and 978 nm lie very close to the absorption peaks of lipids and water, respectively. The SSFDPM technique adds tremendous spectral bandwidth to a discrete wavelength measurement, but it is still reliant upon discrete measurements of μ_s' . The topic of determining the optimal selection of wavelengths is currently under investigation.

IV.b Normal optical properties needed

Ignoring the contributions of water and lipids in the breast leads to errors in the measurement of THC and S_tO_2 . Earlier work has also suggested that ignoring water in NIR measurements will lead to significant errors in some conditions. Franceschini *et al.* asserted that knowledge of the water concentration was required in order to determine accurately the S_tO_2 of 23 μM of blood suspended in a scattering medium using a two wavelength technique (715 and 825 nm) [59]. Hemoglobin concentrations in adult muscle can easily be on the order of 100 μM as determined by deep-tissue measurements in a reflection geometry. Neglecting water in high Hb concentration environments translate into errors less than 5 % in S_tO_2 for values above 50 % [59]. However, the breast is a totally different matter. The overall concentrations of Hb are much lower in breast than in muscle. Hull *et al* point out clearly that two or three wavelength systems can produce significant errors as well, although their three wavelength system did not include a water peak [60]. Thus, it is not just the number of wavelengths, but also the sensitivity of those wavelengths to selected chromophores that are important in discrete wavelength measurements. Adding wavelengths more sensitive to water (such as 980 nm) can help quantify the water concentration. The SSFDPM technique adds even more bandwidth.

IV.c The Necessity of control values

In general, pre-menopausal breast is more optically attenuating than post-menopausal breast, both in absorption and scattering. It is important to note that this trend, particularly in scatter power, is also true for mammographic density. The balance between fat, collagen, epithelium, and water is responsible for changes in mammographic density [61]. Our measurements suggest that the collagen to lipid ratio strongly influences NIR optical scattering. NIR spectroscopy has

unique potential for quantifying the specific elements of breast tissue that contribute to mammographic density. This observation may be of importance in risk assessment, since mammographic density has been cited as a risk for breast cancer [61]. Thus, optical methods may identify breast tissue at physiological risk for malignant transformation and can be performed easily in all women at any age.

Knowledge of the "normal" values of NIR chromophores will play an important role in evaluating the usefulness of optical methods in detecting and characterizing lesions in the breast. Several investigators have reported a 2-4 fold THC contrast between normal and tumor structures; *in vivo* tumor S_{O_2} values are also typically lower than normal tissue [29][30][31]. Neglecting the effects of water and lipids further complicates efforts for accurate quantitative diagnosis. The effect of falsely ascribing lipid and water absorption to hemoglobin will inflate measured values of $Hb-O_2$, and thus inflate measurements of THC and S_{O_2} . This change in contrast will decrease the probability for success of non-invasive optical lesion characterization. For every woman, the effect of water and lipids will vary so that the error in measured hemoglobin levels will be different, and potentially unpredictable. The effect will be more severe for patients with lower THC levels, i.e., older women. There is also no reason to assume that the distribution of water and lipids will be uniform across the whole breast.

Detailed studies of normal tissue are essential for determining the sensitivity required of optical instrumentation for detecting lesions in women of varying age and hormonal status. As baseline levels are characterized, data on an individual's absorption and scattering variations could provide important insight into disease appearance and progression. When applied to patients

receiving chemotherapy and/or hormone replacement therapies, this information could also be used to generate feedback that would permit customized treatment planning based upon individual physiologic response. Experiments such as these are currently underway.

IV.d Additional Comments

For the case of fibroadenoma versus normal the water content differences were substantial. This is in part due to the low post-menopausal water concentrations; such contrast may not be present in the case of a pre-menopausal subject. THC and S_{O_2} alone may not provide enough unique information to adequately distinguish benign lesions such as fibroadenoma from malignant ones. A combination of hemodynamic information with the water and lipid content may be necessary for the successful NIR classification of breast lesions. More subjects will be needed to establish this conjecture.

One potential problem with our analysis of the 30 normal subjects is the absorption overlap between lipids and water. Seven wavelengths may not provide enough spectral resolution to quantify these two chromophores independently. We have shown in another work that the water and lipid absorption information parallels information obtained from the scatter power [15]. Thus, we do not expect this crosstalk to affect the general trends we have observed in our normal subjects. The SSFDPM technique has a much wider spectral bandwidth, which minimizes these crosstalk problems. We now use the SSFDPM in all our measurements.

V. CONCLUSIONS

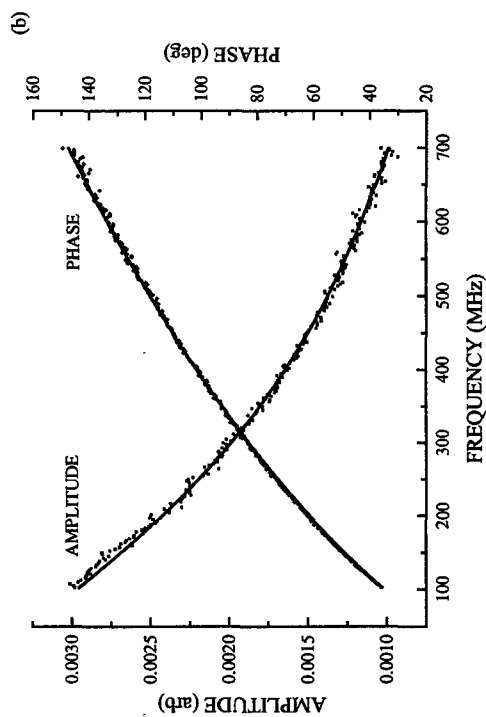
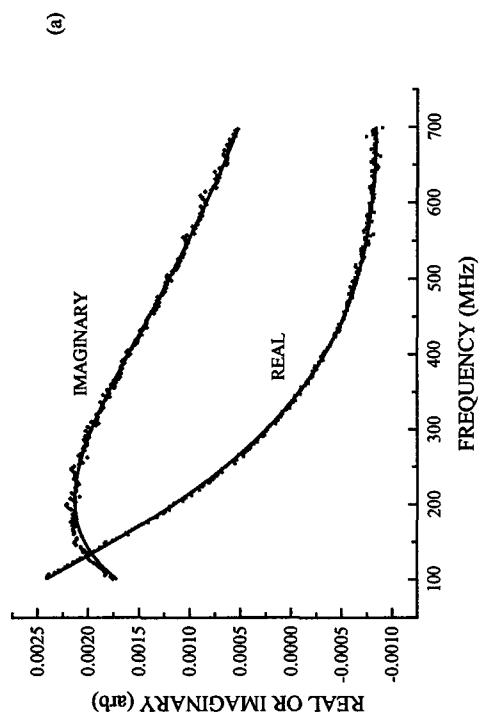
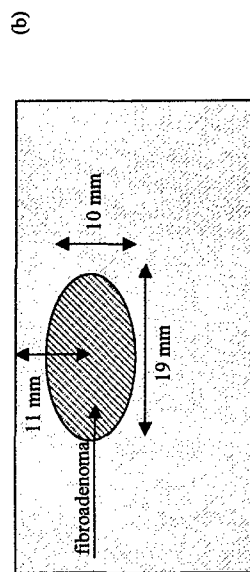
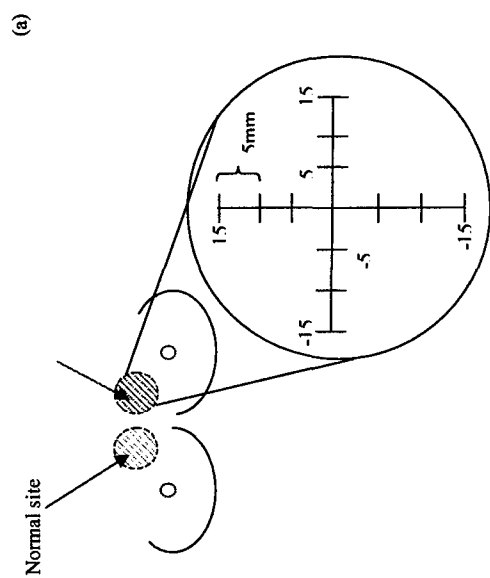
Multi-spectral measurements provide distinct advantages over two or three wavelength measurements. Although a large *number* of wavelengths may enhance sensitivity to hemoglobin, a large spectral *range* is also important. In addition, the reliability of water and lipid measurements improves substantially when spectral information beyond approximately 830 nm is included.

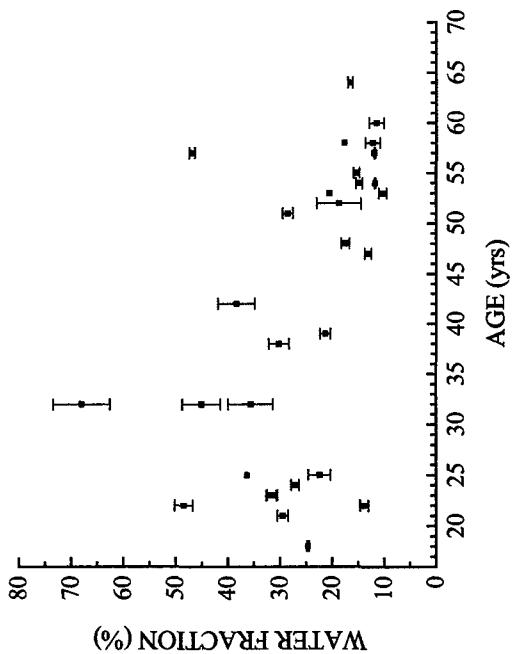
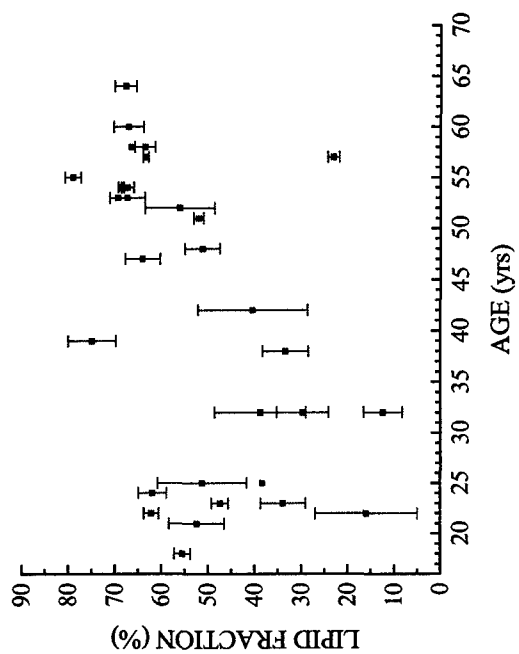
The water and lipid levels in normal breast vary significantly with age and hormonal status, particularly between pre- and post-menopausal subjects. Ignoring water and lipid absorption can produce artificially high THC and SiO_2 values of perhaps 20-30% and 5%, respectively. These errors will be different for each individual patient. Tissue scattering may also prove to be a useful diagnostic parameter. Our results show that the spectral dependence of scattering can provide key insights into breast composition and physiology whereas scattering at a single wavelength may not. Overall, the wealth of additional information provided by broadband, multi-spectral measurements appears to be a key step towards improving accuracy in breast diagnostics.

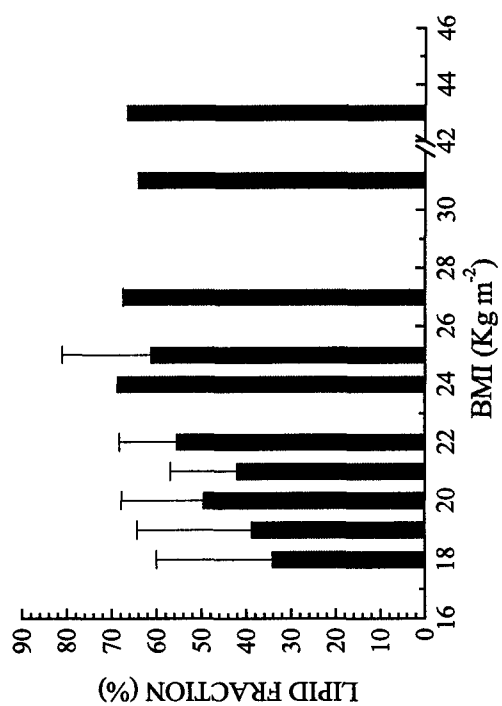
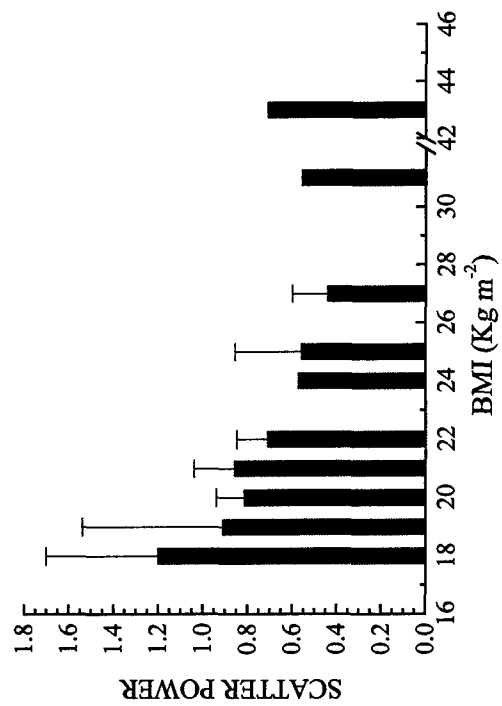
VI. ACKNOWLEDGEMENTS

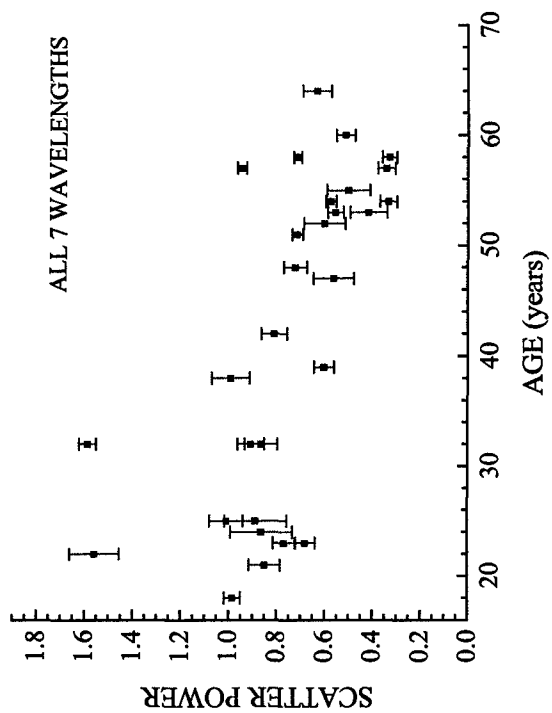
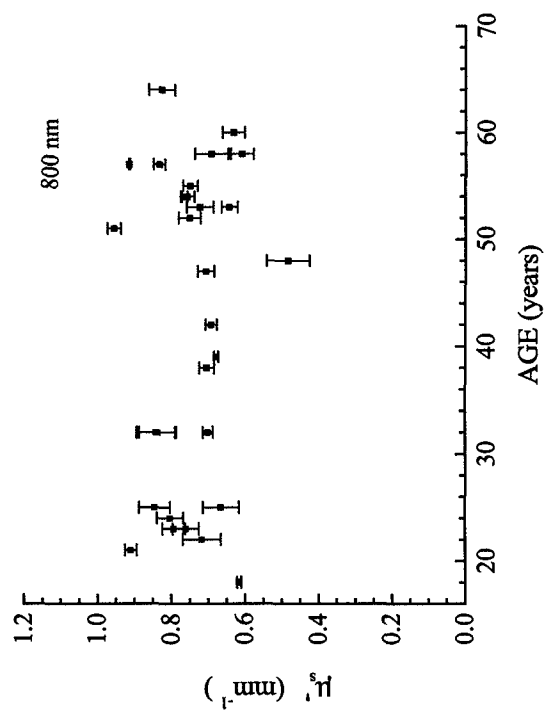
This work was made possible, in part, through two National Institutes of Health funded facilities at the University of California at Irvine: the Laser Microbeam and Medical Program (#RR-01192) and the Chao Family Comprehensive Cancer Center (CA-62203). Support was also

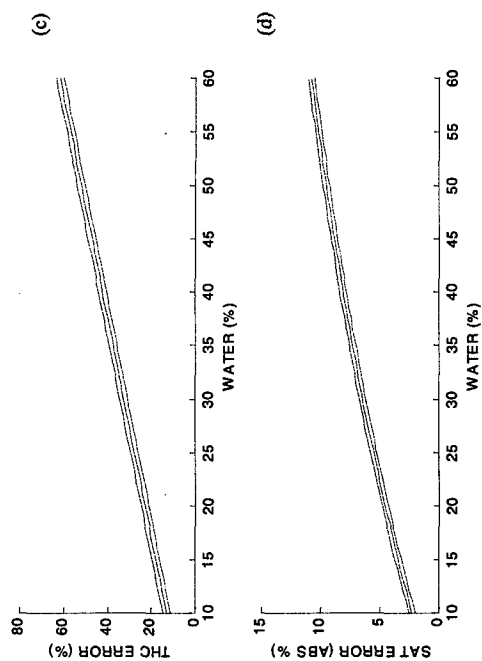
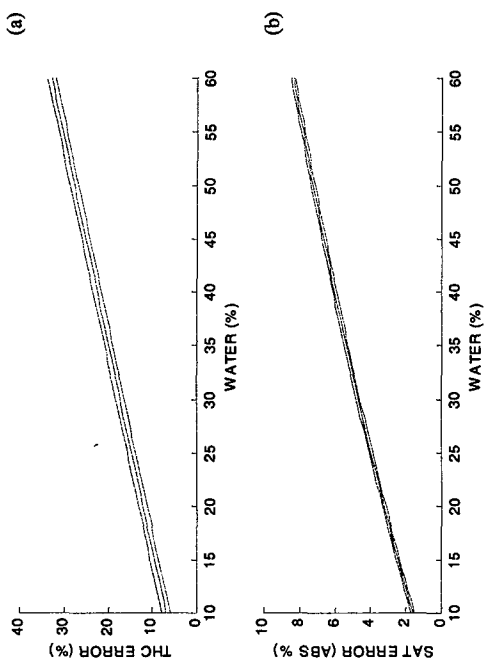
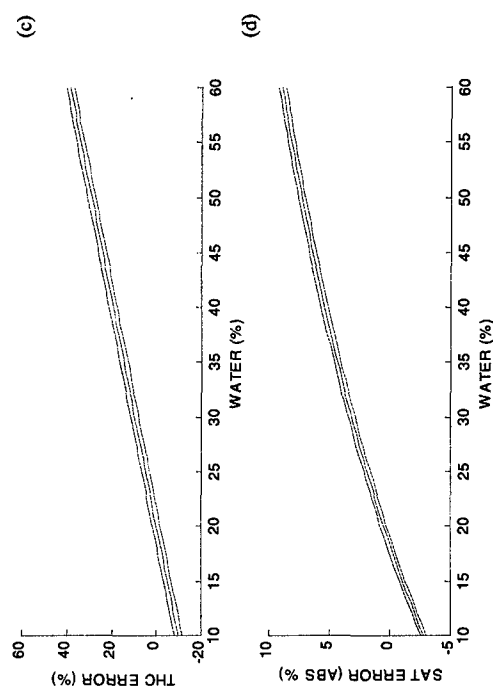
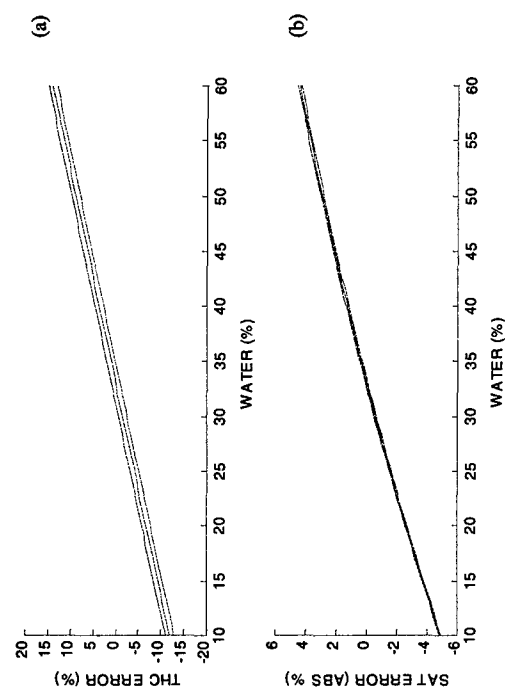
obtained from: Department of Energy (DOE #DE-FG03-91ER61227), Office of Naval Research (ONR #N00014-91-C-0134), California Breast Cancer Research Program, and Avon. A.E.C. cheerfully acknowledges support from the U. S. Army Medical Research and Material Command (DAMD17-98-1-8186). The authors also acknowledge additional support from the George E. Hewitt Foundation (AJB) and the Swiss National Science Foundation (FB).











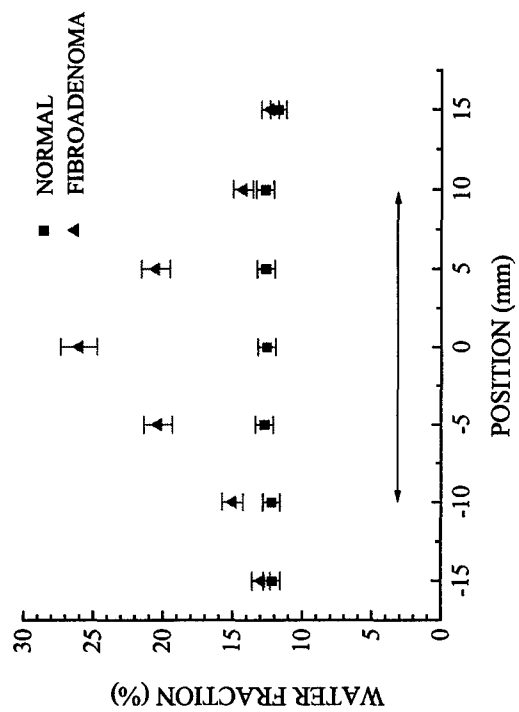
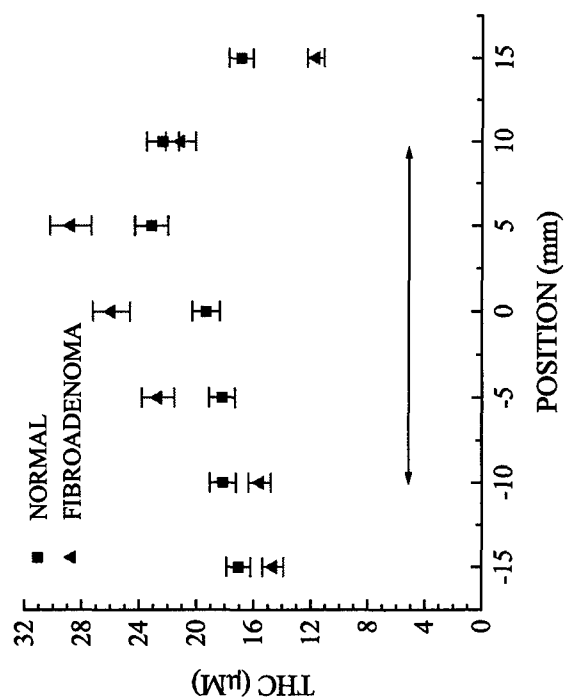


Figure 1 – Photon Density Waves. (a) Points represent measured real and imaginary parts of the wave, and lines represent a fit of the frequency-domain P_I equation. The result of this fit provides both μ_a and μ'_s . Note that the real and imaginary parts of this wave are an analog to the amplitude and phase, as described by Eqs. (2) and (3). The direct transformation is provided in panel (b).

Figure 2 – SSFDPM measurement locations. Panel (a) displays the measurement grid for placement of the probes. The site of the fibroadenoma was determined via standard clinical ultrasound. Panel (b) indicates the dimensions of the fibroadenoma. The axis of the lesion into the page was also 19 mm.

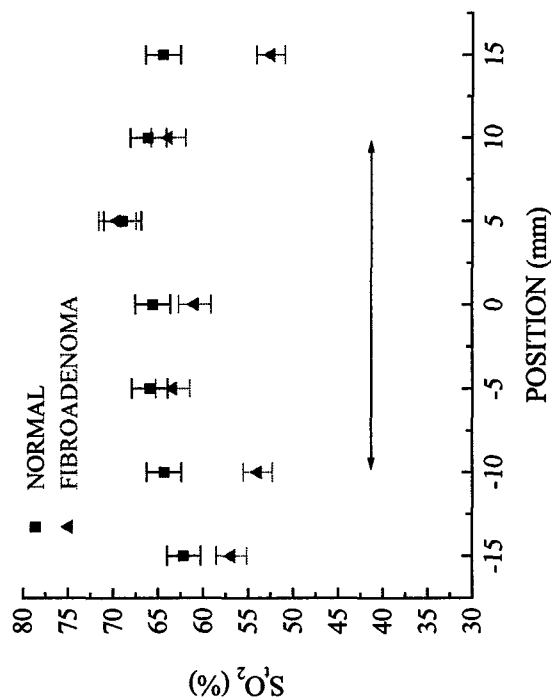


Figure 3 – Water versus age. The water fraction is the water concentration in tissue relative to the concentration of pure water (55.6 M). Pre-menopausal volunteers (< age 50) show considerable variation over age because of intra-subject variations such as menstrual cycle variations and overall hormone production differences. Post-menopausal and peri-menopausal (> age 50) volunteers appear to show a decrease in water content.

Figure 4 – Lipids versus Age. The lipid fraction is the lipid mass density (g mL^{-1}) in tissue relative to a lipid mass density of 0.9 g mL^{-1} . Again, variations exist, although there is a general increasing trend with age.

Figure 5 – Lipid Fraction and BMI. A general check of our ability to measure lipids in breast tissue is to scale them against BMI. Women within a single BMI unit were averaged together to form the histogram. This is a general (not absolute) trend that we would expect to find in breast.

Figure 6 – Scatter Power and BMI. Complimentary information is provided by the scattering properties of the tissue. Women within a single BMI unit were averaged together to form the histogram. Note that we would expect in general a lower scatter power in fattier tissue.

Figure 7 – Scattering in Breast at 800 nm. These points represent the average measured μ_s' values in 29 healthy volunteers as a function of age. No obvious distinctive pattern emerges.

Figure 8 – Scatter Power in Breast. The effect of the spectrum of the tissue scattering is more clearly demonstrated. Scatter power is the exponent of the scattering versus wavelength dependence, as shown in Eq. (4). This time, there is a distinctive general decrease with age, which is not obvious at any single wavelength. This general pattern is also true of mammographic density.

Figure 9 – Effects of Ignoring Water and Lipids. Panels (a) and (b) represent a pre-menopausal woman with $THC = 27.4 \mu M$ and $S_tO_2 = 76.6\%$. Panels (c) and (d) provide the same information, but for a post-menopausal breast using $THC = 14.6 \mu M$ and $S_tO_2 = 82.2\%$. The percent errors are determined by calculating the THC and S_tO_2 perceived by using only

absorption values at 672, 806, and 849 nm and comparing them to the true values listed above. The three lines represent values of 20, 45, and 70% lipids in the calculation, in ascending order.

Figure 10 – Effects of Assuming Water and Lipid Values. Same description as Figure 9, but this time assuming water and lipid fractions of 33% and 44% for the pre-menopausal breast (panels (a) and (b)), and 19% and 61% for the post-menopausal breast (panels (c) and (d)), respectively.

Figure 11 – THC in a Fibroadenoma. SSFDPM measurements of a fibroadenoma (triangles) versus same-site normal tissue on the opposite breast (squares) in a 37-year-old post-menopausal woman. Measurements spanned the region from 650 to 1000 nm, using a four-component fit as described above. The fibroadenoma covers the region between approximately -10 to $+10$ mm (as indicated by the bar), where there is a general increase in THC . Although the fibroadenoma is “visible,” would this be enough information to distinguish it from other lesions or breast components?

Figure 12 – Water Concentration in a Fibroadenoma. The details of this figure are the same as for Figure 11, except water is plotted instead of THC . Notice the high contrast available from water.

Figure 13 – S_tO_2 in a Fibroadenoma. The details of this figure are the same as for the previous two figures. A minor decrease in S_tO_2 over the fibroadenoma is noticeable.

1. M. Cutler, "Transillumination as an aid in the diagnosis of breast lesions," *Surg Gynecol Obstet* **48**, 721-728 (1929).
2. E. Carlson, *Diagnostic Imaging* (Spectrascan, S. Windsor, CT, 1982).
3. R. J. Bartrum, Jr. and H. C. Crow, "Transillumination lightscanning to diagnose breast cancer: a feasibility study," *Ajr. American Journal of Roentgenology* **142** (2), 409-414 (1984).
4. H. Wallberg, A. Alveryd, U. Bergvall, K. Nasiehl, P. Sundelin and S. Tröell, "Diaphanography in breast carcinoma. Correlation with clinical examination, mammography, cytology and histology," *Acta Radiologica: Diagnosis* **26** (1), 33-44 (1985).
5. N. Bundred, P. Leveck, D. J. Watmough and J. A. Watmough, "Preliminary results using computerized tele-diaphanography for investigating breast disease," *British Journal of Hospital Medicine* **37** (1), 70-71 (1987).
6. B. Drexler, J. L. Davis and G. Schofield, "Diaphanography in the diagnosis of breast cancer," *Radiology* **157** (1), 41-44 (1985).
7. B. Monsees, J. M. Destouet and D. Gersell, "Light scanning of nonpalpable breast lesions: reevaluation," *Radiology* **167** (2), 352 (1988).
8. A. Alveryd, I. Andersson, K. Aspegren, G. Balldin, N. Bjurstam, G. Edström, G. Fagerberg, U. Glas, O. Jarlman, S. A. Larsson and et al., "Lightscanning versus mammography for the detection of breast cancer in screening and clinical practice. A Swedish multicenter study," *Cancer* **65** (8), 1671-1677 (1990).
9. A. H. Gandjbakiche, R. Nossal and R. F. Bonner, "Resolution limits for optical transillumination of abnormalities deeply embedded in tissues," *Medical Physics* **21** (2), 185-191 (1994).
10. E. M. Sevrick, B. Change, J. Leigh, S. Nioka and M. Maris, "Quantitation of time-resolved and frequency-resolved optical spectra for the determination of tissue oxygenation," *Analytical Biochemistry* **195** (2), 330-351 (1991).
11. S. Enefei and A. E. Proffo, "Spectral transmittance and contrast in breast diaphanography," *Medical Physics* **12** (4), 393-400 (1985).
12. V. Quaresima, S. J. Matcher and M. Ferrari, "Identification and quantification of intrinsic optical contrast for near-infrared mammography," *Photochemistry and Photobiology* **67** (1), 4-14 (1998).
13. R. Cubeddu, C. D. Andrea, A. Pifferi, P. Taroni, A. Torricelli and G. Valentini, "Effects of the menstrual cycle on the red and near-infrared optical properties of the human breast," *Photochem. Photobiol.* **72** (3), 383-391 (2000).
14. S. Thomsen and D. Taiman, "Physiological and pathological factors of human breast disease that can influence optical diagnosis," *Ann. N. Y. Acad. Sci.* **838**, 171-193 (1998).
15. A. E. Cerussi, A. J. Berger, F. Bevilacqua, N. Shah, D. Jakubowski, J. Butler, R. F. Holcombe and Tromberg, B. J., "Sources of absorption and scattering contrast for non-invasive optical mammography," *Academic Radiology* **8**, 211-218 (2001).
16. S. L. Jacques, "Origins of tissue optical properties in the UVA, visible, and NIR regions," , 1996 (unpublished).
17. S. J. Matcher, M. Cope and D. T. Delpy, "In vivo measurements of the wavelength dependence of tissue-scattering coefficients between 760 and 900 nm measured with time-resolved spectroscopy," *Applied Optics* **36** (1), 386-396 (1997).
18. J. R. Mourant, I. J. Bigio, D. A. Jack, T. M. Johnson and H. D. Miller, "Measurement of absorption coefficients in small volumes of highly scattering media," , 1997 (unpublished).
19. B. J. Tromberg, N. Shah, R. Lanning, A. Cerussi, J. Espinoza, T. Pham, L. Szaasand and J. Butler, "Non-invasive in vivo characterization of breast tumors using photon migration spectroscopy," *Neoplasia* **2** (1), 1-15 (2000).
20. R. Hornung, T. H. Pham, K. A. Keefe, M. W. Berns, Y. Tadir and B. J. Tromberg, "Quantitative near-infrared spectroscopy of cervical dysplasia in vivo," *Human Reproduction* **14** (11), 2908-2916 (1999).
21. D. J. Watmough, "Diaphanography. Mechanism responsible for the images," *Acta Radiologica, Oncology, Radiation Therapy, Physics and Biology* **21** (1), 11-15 (1982).

22. A. E. Profio, G. A. Navarro and O. W. Sartorius, "Scientific basis of breast diaphanography," *Medical Physics* **16** (1), 60-65 (1989).
23. M. S. Patterson, B. Chance and B. C. Wilson, "Time resolved reflectance and transmittance for the non-invasive measurement of tissue optical properties," *Appl. Opt.* **28** (12), 2331-2336 (1989).
24. J. B. Fishkin and E. Gratton, "Propagation of photon-density waves in strongly scattering media containing an absorbing semi-infinite plane bounded by a straight edge," *J. Opt. Soc. Amer. A* **10** (1), 127-140 (1993).
25. S. Andersson-Engels, R. Berg and S. Svanberg, "Effects of optical constants on time-gated transillumination of tissue and tissue-like media," *Journal of Photochemistry and Photobiology B: Biology* **16** (2), 155-167 (1992).
26. S. B. Colak, M. B. van der Mark, G. W. J. Hoof, J. H. Hoogenraad, E. S. van der Linden and F. A. Kuipers, "Clinical optical tomography and NIR spectroscopy for breast cancer detection," *IEEE J. Sel. Top. Quant.* **5** (4), 1143-1158 (1999).
27. R. J. Grable, D. P. Rohler and S. Kla, "Optical tomography breast imaging," 1997 (unpublished).
28. M. A. Franceschini, K. T. Moesta, S. Fantini, G. Gaida, E. Gratton, H. Jess, W. W. Mantulin, M. Setber, P. M. Schlag and M. Kaschke, "Frequency-domain techniques enhance optical mammography: Initial clinical results," *Proc. Natl. Acad. Sci. USA* **94** (12), 6468-6473. (1997).
29. J. B. Fishkin, O. Coquoz, E. R. Anderson, M. Brenner and B. J. Tromberg, "Frequency-domain photon migration measurements of normal and malignant tissue optical properties in a human subject," *Appl. Opt.* **36** (1), 10-20 (1997).
30. S. Fantini, S. A. Walker, M. A. Franceschini, M. Kaschke, P. M. Schlag and K. T. Moesta, "Assessment of the size, position, and optical properties of breast tumors in vivo by noninvasive optical methods," *Appl. Opt.* **37** (10), 1982-1989 (1998).
31. T. O. McBride, B. W. Pogue, E. D. Gerecht, S. B. Poplack, U. L. Osterberg and K. D. Paulsen, "Spectroscopic diffuse optical tomography for the quantitative assessment of hemoglobin concentration and oxygen saturation in breast tissue," *Appl. Opt.* **38** (25), 5480-5490 (1999).
32. D. Gosenick, H. Wabnitz, H. H. Rinneberg, K. T. Moesta and P. M. Schlag, "Development of a time-domain optical mammograph and first in vivo applications," *Appl. Opt.* **38** (13), 2927-2943 (1999).
33. O. Jarlman, R. Berg, S. Andersson-Engels, S. Svanberg and H. Pettersson, "Time-resolved white light transillumination for optical imaging," *Acta Radiologica* **38** (1), 185-189 (1997).
34. K. A. Kang, B. Chance, S. Zhao, S. Srinivasan, E. Patterson and R. Troupin, "Breast tumor characterization using near infrared spectroscopy," presented at the *Proc. SPIE*, 1993 (unpublished).
35. K. Suzuki, Y. Yamashita, K. Ohta and B. Chance, "Quantitative measurement of optical parameters in the breast using time-resolved spectroscopy. Phantom and preliminary in vivo results," *Investigative Radiology* **29** (4), 410-414 (1994).
36. K. Suzuki, Y. Yamashita, K. Ohta, M. Kaneko, M. Yoshida and B. Chance, "Quantitative measurement of optical parameters in normal breasts using time-resolved spectroscopy: In vivo results of 30 Japanese women," *J. Biomed. Opt.* **1** (3), 330-334 (1996).
37. H. Heusmann, J. Kölzer and G. Milic, "Characterization of female breasts in vivo by time-resolved and spectroscopic measurements in near infrared spectroscopy," *J. Biomed. Opt.* **1**, 425-434 (1996).
38. J. Brisson, A. S. Morrison and N. Khalid, "Mammographic parenchymal features and breast cancer in the Breast Cancer Detection Demonstration Project," *Journal of the National Cancer Institute (Bethesda)* **80** (19), 1534-1540 (1988).
39. N. F. Boyd, C. Greenberg, G. Lockwood, L. Little, L. Martin, J. Byng, M. Yaffe and D. Trichler, "Effects at two years of a low-fat, high-carbohydrate diet on radiologic features of the breast: Results from a randomized trial," *Journal of the National Cancer Institute (Bethesda)* **89** (7), 488-496. (1997).
40. N. A. Lee, H. Rusinek, J. Weinreb, R. Chandra, H. Toth, C. Singer and G. Newstead, "Fatty and fibroglandular tissue volumes in the breasts of women 20-83 years old: comparison of X-ray mammography and computer-assisted MR imaging [see comments]," *AJR: American Journal of Roentgenology* **168** (2), 501-506 (1997).
41. J. B. Fishkin and E. Gratton, "Propagation of photon-density waves in strongly scattering media containing an absorbing semi-infinite plane bounded by a straight edge," *J. Opt. Soc. Amer. A* **10** (1), 127-140 (1993).

42. L. O. Svendsen, B. J. Tromberg, R. C. Haskell, T. Tsong-Tseh and M. W. Berns, "Tissue characterization and imaging using photon density waves," *Optical Engineering* 32 (2), 258-266 (1993).
43. J. B. Fishkin, S. Fantini, M. J. van de Ven and E. Gratton, "Gigahertz photon density waves in a turbid medium: Theory and experiments," *Phys. Rev. E* 53 (3), 2307-2319 (1996).
44. J. M. Kaltenbach and M. Kaschke, "Frequency- and time-domain modeling of light transport in random media," in *Medical Optical Tomography: Functional Imaging and Monitoring*, edited by G. Müller, B. Chance, R. Alfano, S. Arridge, J. Beuthan, E. Gratton, M. Kaschke, B. Masters, S. Svanberg, P. v. d. Zee and R. F. Potter (Society of Photo-Optical Instrumentation Engineers, Bellingham, 1993), Vol. ISI1, pp. 65-86.
45. R. A. J. Groenhuis, H. A. Ferwerda and J. J. Ten Bosch, "Scattering and absorption of turbid materials determined from reflection measurements. I. Theory," *Appl. Opt.* 22 (16), 2456-2462 (1983).
46. F. P. Bolin, L. E. Preuss, R. C. Taylor and R. J. Ference, "Refractive index of some mammalian tissues using a fiber optic cladding method," *Appl. Opt.* 28 (12), 2297-2303 (1989).
47. W. H. Press, S. A. Teukolsky, W. T. Vetterling and B. P. Flannery, *Numerical Recipes in C*, 2 ed. (Cambridge University Press, Cambridge, UK, 1992).
48. S. Wray, M. Cope, D. T. Delpy, J. S. Wyatt and E. O. Reynolds, "Characterization of the near infrared absorption spectra of cytochrome aa3 and haemoglobin for the non-invasive monitoring of cerebral oxygenation," *Biochim. Biophys. Acta* 933 (1), 184-192 (1988).
49. G. M. Hale and M. R. Querry, "Optical constants of water in the 200-nm to 200- μ m wavelength region," *Appl. Opt.* 12 (3), 555-563 (1973).
50. C. Eker, "Optical characterization of tissue for medical diagnostics," Ph.D., Lund Institute of Technology, 1999.
51. L. Kou, D. Labrie and P. Chylek, "Refractive indices of water and ice in the 0.65- to 2.5- μ m spectral range," *Appl. Opt.* 32 (19), 3531-3540 (1993).
52. H. J. van Staveren, C. J. M. Moes, J. van Marle, S. A. Prahl and M. J. C. van Gemert, "Light scattering in Intralipid-10% in the wavelength range of 400-1100 nm," *Appl. Opt.* 30 (31), 4507-4514 (1991).
53. A. M. K. Nilsson, C. Stureson, D. L. Liu and S. Andersson-Engels, "Changes in spectral shape of tissue optical properties in conjunction with laser-induced thermotherapy," *Appl. Opt.* 37 (7), 1256-1267 (1998).
54. T. Pham, O. Coquoz, J. Fishkin, E. A. Anderson and B. J. Tromberg, "A Broad bandwidth frequency domain instrument for quantitative tissue optical spectroscopy," *Rev. Sci. Instrum.* 71 (6), 1-14 (2000).
55. F. Bevilacqua, A. J. Berger, A. E. Cerussi, D. Jakubowski and B. J. Tromberg, "Broadband absorption spectroscopy in turbid media by combined frequency-domain and steady-state methods," *Appl. Opt.* 39 (34), 6498-6507 (2000).
56. F. A. Duck, "Physical Properties of Tissue," (Academic Press, London, 1990), pp. 319-328.
57. "Merck Manual," edited by M. Beers and R. Berkow (Merck Research Laboratories, Whitehouse Station, NJ, 1999), pp. 14.
58. V. G. Peters, D. R. Wyman, M. S. Patterson and G. L. Frank, "Optical properties of normal and diseased human breast tissues in the visible and near infrared," *Phys. Med. Biol.* 35 (9), 1317-1334 (1990).
59. M. A. Franceschini, S. Fantini, A. Cerussi, B. Barbieri, B. Chance and E. Gratton, "Quantitative spectroscopic determination of hemoglobin concentration and saturation in a turbid medium: analysis of the effect of water absorption," *J. Biomed. Opt.* 2 (2), 147-153 (1997).
60. E. L. Hull, M. G. Nichols and T. H. Foster, "Quantitative broadband near-infrared spectroscopy of tissue-simulating phantoms containing erythrocytes," *Phys. Med. Biol.* 43 (11), 3381-3404 (1998).
61. A. M. Oza and N. F. Boyd, "Mammographic parenchymal patterns: a marker of breast cancer risk," *Epidemiol. Rev.* 15 (1), 196-208 (1993).



DEPARTMENT OF THE ARMY
US ARMY MEDICAL RESEARCH AND MATERIEL COMMAND
504 SCOTT STREET
FORT DETRICK, MARYLAND 21702-5012

REPLY TO
ATTENTION OF

MCMR-RMI-S (70-1y)

30 Sep 02


MEMORANDUM FOR Administrator, Defense Technical Information
Center (DTIC-OCA), 8725 John J. Kingman Road, Fort Belvoir,
VA 22060-6218

SUBJECT: Request Change in Distribution Statement

1. The U.S. Army Medical Research and Materiel Command has reexamined the need for the limitation assigned to technical reports written for Grant DAMD17-98-1-8186. Request the limited distribution statement for Accession Document Numbers ADB265247 and ADB281574 be changed to "Approved for public release; distribution unlimited." This report should be released to the National Technical Information Service.

2. Point of contact for this request is Ms. Judy Pawlus at DSN 343-7322 or by e-mail at judy.pawlus@det.amedd.army.mil.

FOR THE COMMANDER:


PHYLLIS M. RINEHART
Deputy Chief of Staff for
Information Management